Coordination Chemistry Reviews 386 (2019) 154–182

Contents lists available at ScienceDirect

Coordination Chemistry Reviews

journal homepage: www.elsevier.com/locate/ccr

Review

A review on strategies to LDH-based materials to improve adsorption capacity and photoreduction efficiency for CO_2

Zhong-zhu Yang [a,b], Jing-jing Wei [a,b], Guang-ming Zeng [a,b], Hua-qing Zhang [c], Xiao-fei Tan [a,b], Chi Ma [a,b], Xue-cheng Li [a,b], Zi-hao Li [a,b], Chang Zhang [a,b,*]

[a] College of Environmental Science and Engineering, Hunan University, Changsha 410082, China
[b] Key Laboratory of Environmental Biology and Pollution Control (Hunan University), Ministry of Education, Changsha 410082, China
[c] Qinglin Environmental Protection Co. Ltd., Ningbo 315000, China

ARTICLE INFO

Article history:
Received 23 April 2018
Accepted 27 January 2019

Keywords:
Carbon dioxide
LDH
Capture
Photoreduction
Strategies

ABSTRACT

There has been increasing demand for the fixation of CO_2 because the increasing atmospheric concentration of CO_2 causes the global warming. Layered double hydroxides (LDHs), known as hydrotalcite-like compounds or ionic lamellar compounds, have attracted increasing research interest because of their promising applications as CO_2 adsorbents and photocatalysts. The development of LDH-based materials used as CO_2 adsorbents and photocatalysts has been separately reviewed in previous papers. However, few of these reviews include the typical synthesis and modification strategies of LDHs to improve their adsorption capacities and photoreduction efficiencies for CO_2. Therefore, in this review we summarized some recent progress made in this field. The co-precipitation method is a simple and rapid method for fabricating the desired LDHs directly, and this synthesis method is readily scaled up for industrial production. A few methods have been used for LDHs modification, including doping LDHs with alkali metal, controlling particle characteristics, and fabrication of junctions. It is evident from the literature survey presented herein that modified LDH-based materials have exhibited good potential for the adsorption and photoreduction of CO_2. The unresolved issues and possible improvements of LDHs are also highlighted.

Contents

Abbreviations: APS, 3-aminopropyltrimethoxysilane; BC, biochar carbon; CB, conduction band; C-LDHs, calcined layered double hydroxides; CNF, carbon nanofiber; DFT, density functional theory; FBA, fix bed reactor; FTIR, Fourier transform infrared spectra; GO, graphene oxide; HMS, hollow mesoporous silica; IEP, isoelectric point; LDHs, layered double hydroxides; LDO, layered double oxide; MWCNT, multi-walled carbon nanotubes; OCN, oxygen-doped carbon nitrogen; OCNT, oxidized carbon nanotube; PBR, packed bed reactor; PFR, plug flow reactor; POM, polyoxometalate; PSA, pressure swing adsorption; r-GO, reduced graphene oxide; SEWGS, sorption-enhanced water-gas shift; TGA, thermo gravimetric analyzer; TPD, temperature programmed desorption; UV, ultraviolet; VB, valence band.

* Corresponding author at: College of Environmental Science and Engineering, Hunan University, Changsha 410082, China.
E-mail address: zhangchang@hnu.edu.cn (C. Zhang).

https://doi.org/10.1016/j.ccr.2019.01.018
0010-8545/

1. Introduction

There is a growing consensus that global climate change is occurring, and the major cause is believed to be the anthropogenic emissions of the greenhouse gas CO_2 into the atmosphere [1–4]. CO_2 is primarily produced by the combustion of fossil fuels used in power generation facilities, manufacturing industries, and transportation vehicles. The reduction of CO_2 emissions is essential to reduce the risk of future devastating effects. CO_2 capture technology is one of the most effective ways to decrease CO_2 emissions. The adsorption method, which is used for capturing CO_2, has shown great promise due to its low energy requirements and simple operation [5,6]. There are three main approaches envisaged for the capture of CO_2: (1) pre-combustion capture of the CO_2 in the synthesis gas after the conversion of CO into CO_2; (2) post-combustion capture to capture CO_2 in the exhaust gases once the fuel has been fully burned with air; and (3) oxy-fuel capture, which consists of combustion in oxygen and purification of the CO_2 flow to eliminate incondensable gases [7,8]. Both pre- and post-combustion capture are technically feasible and have the potential to reduce CO_2 emissions, while oxy-combustion options are still under development and will require significantly more effort to reach operational and commercial readiness [9]. One feasible step towards reducing CO_2 emissions is to capture the CO_2 generated during combustion and store it in a suitable location. The sorption-enhanced water-gas shift process, which is a combination of the water-gas shift reaction and CO_2 adsorption, has been widely identified as a promising pre-combustion CO_2-capture technology [10]. This approach combines a high-temperature water-gas shift catalyst and a CO_2 regenerable sorbent in the same reactor [11]. By adsorbing and removing CO_2 from the reaction mixture, the equilibrium is driven to the right-hand-side, thereby completely converting CO and maximizing the production of H_2 [1,12]. Thus, the key factor for this process is the choice of a suitable CO_2-capturing material. Hydrotalcite as a high-temperature (200–500 °C) CO_2 sorbent has attracted substantial attention because of its fast sorption/desorption kinetics and simple regenerability [13]. In the meantime, it is advantageous to capture CO_2 from the atmosphere or factories/power stations and convert it to fuel using a sustainable source of energy such as sunlight. This option simultaneously addresses the problems of global warming and sustainable energy shortages. Solid base materials are promising candidates for developing a photocatalytic system for the conversion of CO_2 [14,15]. Different kinds of materials have been studied as

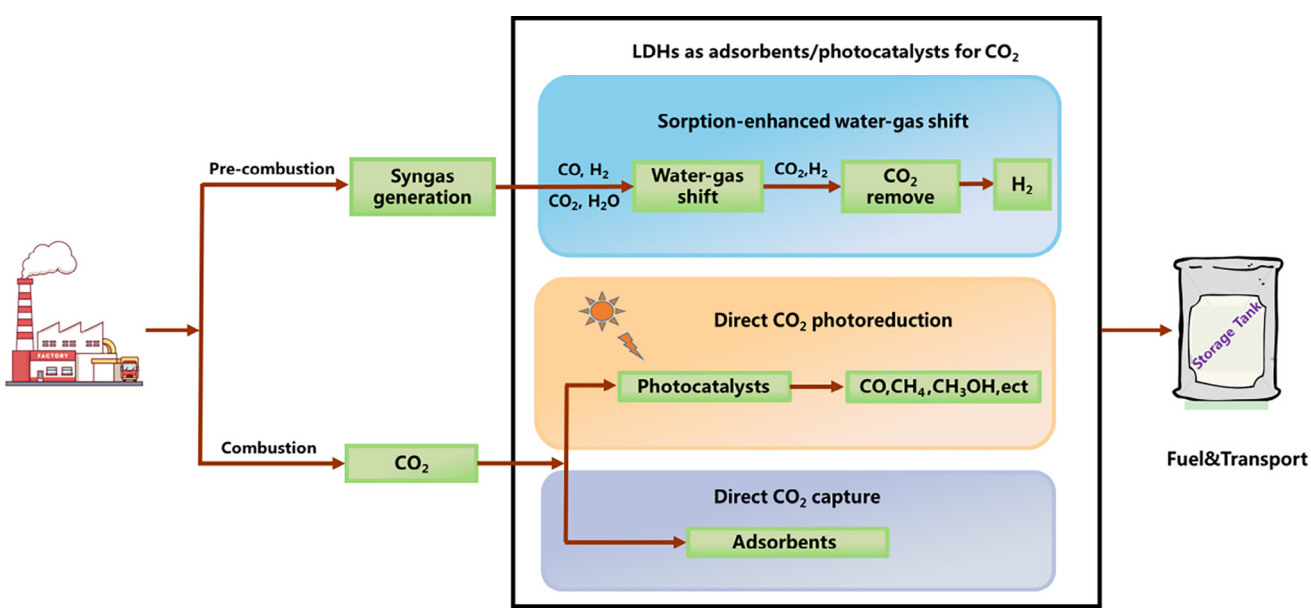

Fig. 1. Schematic of three conventional approaches using LDHs to reduce CO_2 emissions.

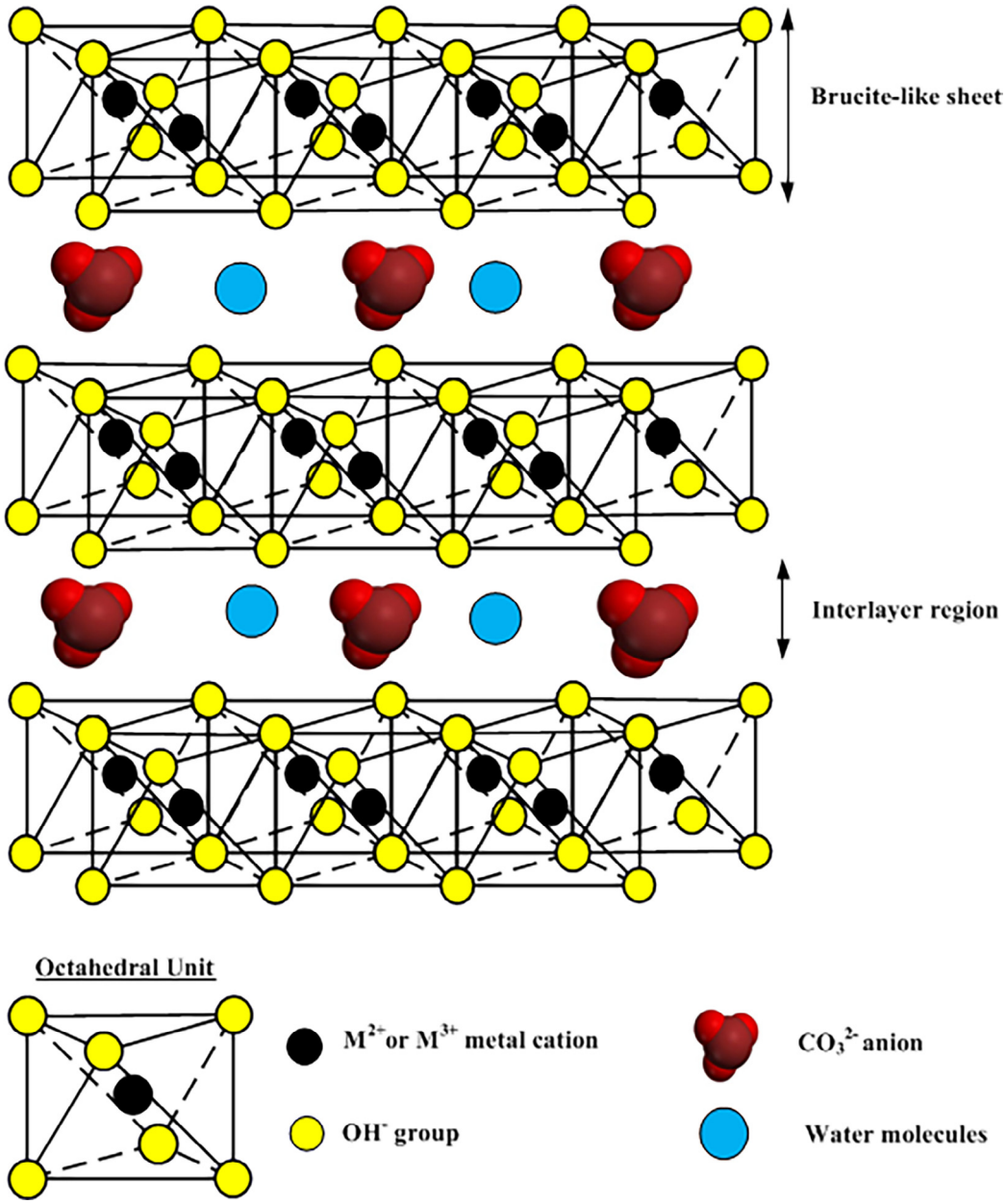

Fig. 2. The structure of a layered double hydroxide with interlayer CO_3^{2-} anions.

possible CO_2 captors and photocatalysts, such as organic sorbents [16], zeolites [17,18], activated carbon [19,20], titania nanotubes [21,22], TiO_2 [23], Bi_2WO_6 [24,25] and layered double hydroxides (LDHs). Among them, LDHs as high-temperature (200–500 °C) CO_2 sorbents have received considerable attention because of their high sorption capacities for CO_2 in the layered space and their tunable semiconductor properties [26,27]. For LDH-based materials, large specific surface areas and high affinities for CO_2 molecules facilitate the selective conversion of CO_2 under illumination. The intrinsic properties of LDHs have stimulated interest in the past ten years, and LDHs are recognized as excellent candidates for CO_2 adsorption and photoreduction applications (Fig. 1).

LDHs, which are also known as hydrotalcite-like compounds (HTlcs) or synthetic anionic clays, are a family of layered materials which comprise mono- or di- and trivalent cations represented by the general formula $[M^{2+}_{1-x}\ M^{3+}_{x}\ (OH)_2(A^{n-})_{x/n}]^{x+}\cdot mH_2O$, where M^{2+} and M^{3+} are divalent (e.g., Mg^{2+}, Ni^{2+}, Zn^{2+}, Cu^{2+}) and trivalent cations (e.g., Al^{3+}, Fe^{3+}, Ga^{3+}), respectively; x, ranging from 0.20 to 0.33, denotes the molar fraction of M^{3+} in the metallic ions; and A^{n-} is the interlayer gallery anion (e.g., CO_3^{2-}, Cl^-, NO_3^-, SO_4^{2-}) [13,28]. LDHs are composed of positively charged brucite-like metal hydroxide layers with water and charge-balancing anions located in the interlayer [29,30]. The chemical composition of the inorganic layers and the interlayer gallery anions can be precisely controlled [31,32]. The structures of LDHs and a typical octahedral unit are shown in Fig. 2. Upon thermal treatment, they are transformed into nearly amorphous metastable mixed metal oxides (MMO) with a poorly defined 3D network. The original layered structures of the calcined LDHs can be recovered through anion intercalation in solution or simply by exposure to ambient moisture; this property is known as the "memory effect" [33–36].

A few reviews have been carried out from the perspective of CO_2 capture by LDH-based materials. Yong et al. [37] first published "Hydrotalcite-like compounds as adsorbents for carbon

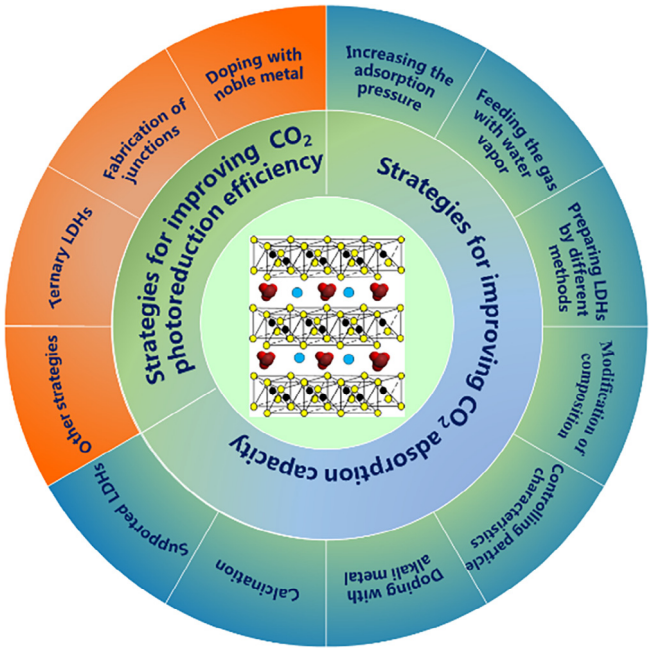

Fig. 3. Various strategies for enhancing the absorption and photoreduction of CO_2 by LDHs.

dioxide" in 2002. Bhatta et al. published the extensive "Progress in hydrotalcite like compounds and metal-based oxides for CO_2 capture: a review," covering 273 references (before 2014), which fully reviewed the removal of CO_2 from hot flue gas/syngas over LDHs and metal-based oxides materials [38]. Other review articles also covered the adsorption or photocatalytic reduction of CO_2 by LDH-based materials [2,13,39–44]. However, none of these reviews discussed the strategies for improving the adsorption capacity and photoreduction efficiency of CO_2 in detail. The rapid growth of the application of LDH adsorbents/catalysts for CO_2 requires a fresh assessment. In this review, an extensive list of various LDH-based materials from the literature has been compiled, and their adsorption capacities and photoreduction abilities for CO_2 are presented while highlighting and discussing the key advancements in the preparation of these LDH-based materials. Therefore, the present review aims to provide an overview of the efforts of the ten years of research in the synthesis of adsorptive/photoreductive LDHs for CO_2 through various strategies (Fig. 3). Such efforts are expected to bring LHD systems for adsorption/photocatalysis to the commercial level.

2. Influence of operating parameters on CO_2 adsorption

2.1. Adsorption temperature

In recent years, several reports have been published regarding the use of calcined LDHs as CO_2 sorbents in two different temperature ranges: low (30–200 °C) and moderate (200–600 °C) [45,46]. To integrate the CO_2 adsorbent into certain processes, its CO_2 adsorption performance at different temperatures is of great interest. Li-Al layered double oxide (LDO) exhibited a good CO_2 capture capacity over a wide temperature range. The maximum CO_2 capture capacity of Li-Al LDO was achieved at 60 °C, and the adsorption capacity decreased with the increase in adsorption temperature (60–400 °C). The CO_2 adsorption capacity of K_2CO_3 promoted Li-Al LDO also decreased with the increase of temperature, but the CO_2 adsorption capacity significantly increased by doping the LDHs with 20 wt% K_2CO_3 at all the tested temperatures [47]. The adsorption capacity of this novel adsorbent decreased due to losses in the physical adsorption capacity. Similar results were also observed by Qin et al. [48] and Zhu et al. [49] The equilibrium CO_2 capacity values of K_2CO_3 impregnated Mg-Al LDO were similar in the temperature range 300–400 °C, while a gradual drop in capacity was observed in the un-impregnated material when the temperature increased from 300 to 400 °C [50]. However, the maximum CO_2 sorption uptake of K_2CO_3-promoted Mg-Al LDO occurred at 400 °C in the high temperature range tested. This result implied that the equilibrium CO_2 sorption uptake on the K_2CO_3-promoted hydrotalcites was likely caused by chemisorption. The chemisorption was thought to be caused by strong basic sites of the metal oxides, and metal carbonates and the adsorbed CO_2 could be further stored as carbonate ions in the interlayer or as metal carbonate forms [51]. This behavior is quite different from that of physical adsorbents, such as activated carbon and zeolite, whose adsorption capacities decrease sharply with increasing temperatures. Similar effects of the adsorption temperature on LDHs has been reported by other researchers [52,53]. Coenen et al. [54] investigated the average measured cyclic working capacity (the cyclic working capacity is defined as the average of the adsorption and desorption capacities) for CO_2 onto Mg-Al LDO at 300, 400, and 500 °C. A nearly linear increase in cyclic working capacity in the temperature range between 300 and 500 °C was observed. The quantity of adsorbed CO_2 during the first cycle however did not seem to be significantly influenced by the temperature. This result likely occurred because of the different kinetics for adsorption and desorption. A significant influence of the temperature on the adsorption rate between 300 and 500 °C was not observed. While the desorption rate strongly depended on the temperature because the higher kinetic energy of the adsorbed molecules at increased temperatures enhanced their desorption [54].

J. Ramírez-Moreno et al. [55] analyzed the morphological evolution of pristine LDH powders after the CO_2 adsorption at different temperatures (30–350 °C). When CO_2 adsorption was performed at 30–325 °C, the particles showed a layered structure similar to platelets. The adsorbed CO_2 might inhibit the structural collapse and delay the adsorption-desorption equilibrium, as the change in the interlayer distance was a minimum. Nevertheless, the platelet particles became smaller than the original agglomerated particles. In fact, the platelets presented a more ordered distribution when the temperature was increased. The highest CO_2 adsorption was produced at 300 °C before the layered structure had completely collapsed, which might be correlated to the pore morphology changes and surface reactivity. The only significant morphology difference was observed at 350 °C, at which the platelet particles seemed to disappear and collapse. This evident change corresponded to the Mg(Al)O periclase crystallization, and these findings agreed with those of previous work [56]. Meanwhile the decarbonation process must have occurred. The adsorption temperature affects the textural properties of pristine LDH, and consequently, the CO_2 adsorption.

2.2. Adsorption pressure

The operating pressure has been proven to have a significant effect, as the CO_2 adsorption capacity increases with the increasing pressure [1,27,55,57,58]. Zhu et al. [59] studied the CO_2 capture properties of potassium-modified hydrotalcite under different CO_2 partial pressures. When the adsorption pressure increased from 0.1 to 1.0 MPa at 300 °C, the CO_2 uptake increased from 0.10 to 0.24 mmol/g. However, when the pressure continued to increase to 2.0 MPa, an increase of only 0.02 mmol/g was observed. When the pressure exceeded 1.0 MPa, the number of CO_2 active sites became the main limitation and thus decreased the adsorp-

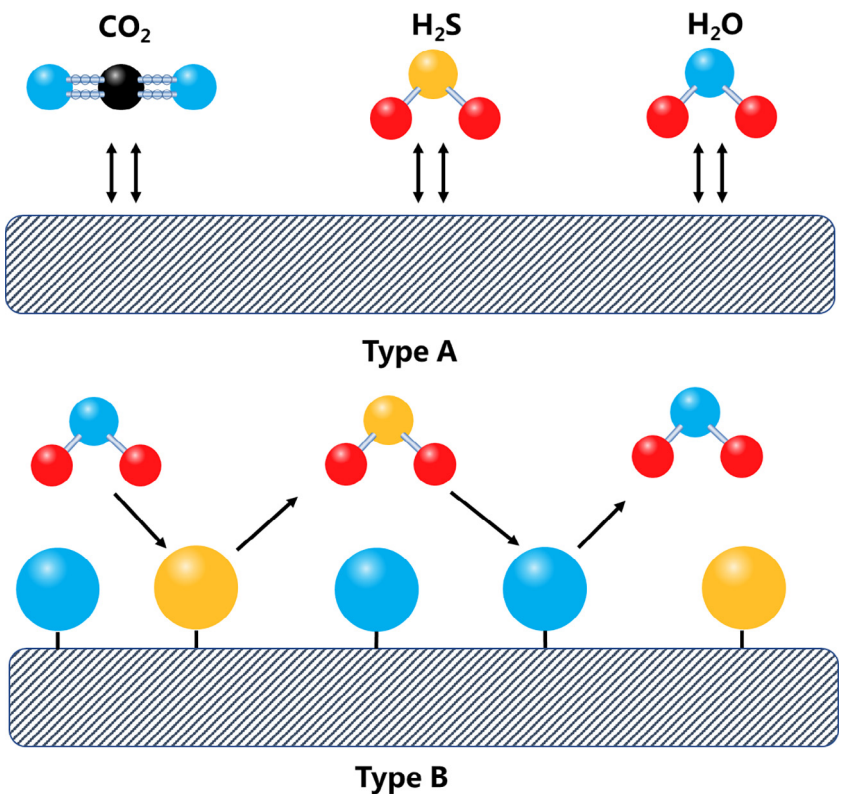

Fig. 4. Schematic representation of the proposed mechanistic model describing the interaction of CO_2 and H_2S with the sorbent.

tion rate. Moreno et al. [55] reported that the LDH sample possessed highly suitable properties as a CO_2 sorbent at elevated pressures (up to 4.35 MPa). The highest CO_2 adsorption (5.7 mmol/g) was produced at 300 °C before the layered structure had completely collapsed. The effect of the pressure on the pressure swing adsorption (PSA) process performance has also been discussed. In a study by Zheng et al., the separation of CO_2 and H_2 at elevated temperatures using the multibed PSA process was developed, and they reported that more H_2 remained in the adsorption column and less CO_2 escaped from the end of the fixed reactor when the operating pressure increased from 2 to 3 MPa. These findings are significant for guiding the elevated temperature PSA process design in pre-combustion CO_2 capture [57].

The CO_2 capacity has been reported to increase for low steam partial pressures compared to that at dry conditions [60]. However, at higher steam partial pressures, competitive adsorption has been observed [61,62]. Boon et al. [61] measured breakthrough curves for CO_2 and H_2O adsorption at 400 °C, up to 24 bar. They found that the isotherm consisted of a low partial pressure surface adsorption component and a high partial pressure nanopore adsorption component. While surface adsorption occurred at specific sites for CO_2 or H_2O up to 5 bar, CO_2 and H_2O adsorbed competitively in the nanopores at higher partial pressures. The same group additionally reported that increasing the pressure led to an increase in CO_2 cyclic working capacity only at 2 and 3 bar of total pressure, and a further increase in pressure even led to a decrease in the measured CO_2 cyclic working capacity. It was further concluded that the desorption of CO_2 seems to be hindered at higher pressures due to the stronger chemical bonding between the sorbate and sorbent [54].

2.3. SO_x, H_2S in the feeding gas

LDO has potential applications as CO_2, SO_x, H_2S sorption materials to take advantage of the acid-base interactions between the acidic gas species and basic sites on the LDO [63–66]. Several studies were performed to investigate the influence of impurities on the CO_2 capture activity. For the application of sorption-enhanced water-gas shift (SEWGS) technology to gasification processes, it must be considered that, depending on the feedstock, significant amounts of H_2S might be present in the syngas. Dijk et al. [67] determined the effect of H_2S on the CO_2 capture behavior of K_2CO_3-promoted hydrotalcite. According to the experimental results, the sorbent displayed reversible co-adsorption of CO_2 and H_2S. The CO_2 sorption capacity was not significantly affected in the multicycle experiments at 400 °C and 5 bar. The experimentally observed interactions were explained qualitatively by postulating two different sorption sites for H_2S (Fig. 4). Type A sites would display reversible competitive co-adsorption of H_2S and CO_2, likely involving surface species such as carbonates (CO_3^{2-} and HCO_3^-), –SH, and thiocarbonate (SCO_2^{2-}). The adsorption would be competitive with CO_2 and be able to push H_2S from these type A sites. Type B sites would exclusively adsorb H_2S reversibly, involving the formation of metal sulfides. The metal sulfides could be formed from the metal oxides under H_2S-rich conditions, while the presence of steam and absence of H_2S during regeneration would result in partial backformation of the metal oxide and release of H_2S. In their further study, at 30 bar pressure and a 400 °C feed temperature, a CO-, CO_2- and, H_2S-free H_2 product was obtained when feeding a syngas containing 200 ppm H_2S. Moreover, multicyclic testing at 30 bar and 400 °C for 110 cycles exhibited good sorbent stability in the presence of 200 ppm H_2S. Additionally, CO_2 was capable of replacing H_2S on the sorbent. Most importantly, H_2S did not appear to change the CO_2 sorption capacity of the sorbent materials [67]. In the most recent study, the CO_2 capture tests under 430 ppm H_2S at 15 bar also confirmed that H_2S in the feed gas did not have a significant detrimental effect on the CO_2 sorption behavior of K-promoted hydrotalcite. Competitive adsorption between CO_2 and H_2S seemed to occur, with CO_2 absorbed preferentially [68].

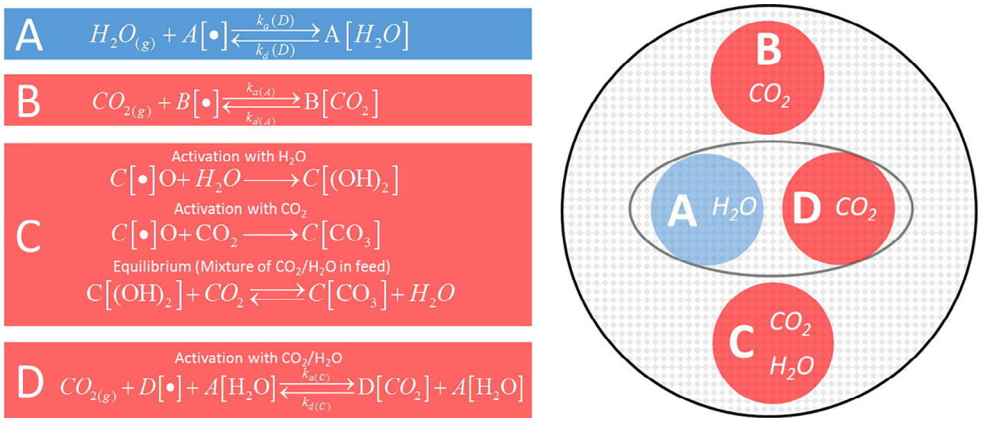

Fig. 5. Proposed model for CO_2 and H_2O adsorption on potassium-promoted Mg-Al LDH at 400 °C (adapted with permission from Ref. [71] @Copyright 2017 Elsevier).

LDH derivatives for CO_2 capture require a de-SO_x unit operating upstream. Reddy et al. [69] investigated the effect of SO_x on the performance of LDH derivatives used as adsorbents for CO_2 capture. According to the experimental results, the SO_x was found to significantly influence the CO_2 sorption on the LDO. The SO_x sorption over CO_2 was favored due to the strong acid-base interactions between SO_x and LDO. The regeneration experiments proved to some extent that SO_x replaced CO_2 via the formation of sulfites and sulfates. In a further study, the same research group subsequently reported that the presence of NH_3 did not affect CO_2 adsorption on a commercially available hydrotalcite [70].

2.4. Water vapor in the feeding gas

The effect of water as a vapor or liquid during CO_2 capture on thermally calcined LDH structures has been studied, and there is general agreement that the water seems to enhance the CO_2 capture on these materials [28,56]. The presence of water in the feed did not influence the CO_2 sorption rate but had a positive impact on the CO_2 sorption efficiency of LDOs. In the cases where CO_2 was chemisorbed, the improvements observed due to water addition were explained by a sequential reaction mechanism, in which MgO and Al_2O_3 initially react with water, producing $Mg(OH)_2$ and $Al(OH)_3$. In the presence of CO_2, they are expected to form respective bicarbonates, and this might be the reason for additional weight gain in the presence of water [60]. Marono et al. [11] reported that the presence of a different amount of steam availability during the CO_2 capture process had a strong influence on the capture process efficiency of the sorbents. According to the results, the CO_2 capture capacity of the sorbents increased with increasing partial pressure of steam. Under dry and low water content in the feed gas, the main capture mechanism identified was the formation of $KAl(CO_3)(OH)_2$. However, when the amount of steam available in the reaction system was increased to 35% v/v (P_{H2O} = 4.5 bar), the CO_2 capture capacities of the sorbents increased drastically, reaching values as high as 9 mmol/g. These high capture values were found to be due to the contributions of reconstruction of the hydrotalcite structure and the formation of hydrogen carbonate hydrate and magnesium carbonate. Recently, the mechanism of the CO_2 adsorption on a potassium-promoted hydrotalcite-based adsorbent in the presence of water was investigated in detail (Fig. 5). It was found that at least four different adsorption sites participated in the sorption/desorption of CO_2 and H_2O. Two sites, A (H_2O) and B (CO_2), could be easily regenerated with N_2. The cyclic working capacity for site B increased at higher temperatures, whereas the cyclic working capacity for site A decreased at higher temperatures. Site D was a site that could be activated if CO_2 and H_2O were present together, and its cyclic working capacity depended on the cyclic working capacity of site B and A. The experimental results proved that the main reason that steam increased the cyclic working capacity of the adsorbent was due to the regeneration of the adsorption sites (site C in particular). Regeneration of the adsorbent with steam led to a significant increase in the CO_2 cyclic working capacity from 0.30 to 0.53 mmol/g compared to the dry regeneration with N_2 using the same cycle times [71].

All the studies mentioned above were performed at temperatures >200 °C, and in several cases, using potassium or sodium as additives. The performance of CO_2 capture over the Mg-Al LDH at low temperatures (30–80 °C) and in the presence of water vapor was also investigated. If N_2 was used as the carrier gas at 70% relative humidity, the water reacted with the calcined LDH sample producing hydroxides, which promoted the LDH regeneration process. However, if CO_2 was used as the carrier gas, the calcined LDH sample behaved like MgO in the presence of CO_2 and H_2O, favoring the production of hydrated $MgCO_3$ or magnesium hydroxyl carbonate instead of the LDH regeneration. It seemed that the superficial carbonation process occurred faster than hydroxylation, so the LDH regeneration was inhibited, favoring the $MgCO_3$ formation [56]. At higher Mg/Al ratios, $MgCO_3$ may also form at high partial pressures of steam and CO_2, which can lead to mechanical stability issues [71,72].

3. Strategies for improving the CO_2 sorption capacity

As shown in Table 1, significant differences in CO_2 capture capacities are exhibited by the Mg-Al LDH-derived adsorbents. The surface basicity of the various Mg-Al LDH-derived materials can be determined using temperature programmed desorption (TPD). The basic site density of Mg-Al-CO_3 LDO was higher than those of the Mg-Al-Cl LDO and Mg-Al-ClO_4 LDO samples. Mg-Al-CO_3 LDO had two types of basic sites of increasing strength while the Mg-Al-Cl LDO was found to have two types of basic sites: weak and intermediate strength basic sites [73]. These basic sites of increasing strength have been assigned previously to the release of bicarbonates formed on the Brønsted OH^- groups, bidentate carbonates bonded to metal-oxygen pairs, and monodentate carbonates adsorbed on low-coordination oxygen anions. The Mg-Al-CO_3 LDO sample showed the highest initial rate of adsorption and the highest amount of CO_2 adsorption [73]. The memory effect of LDO also has a great influence on adsorption performance, so CO_2 adsorption tests should be performed immediately after the calcination of LDHs to prevent the influence of the memory effect. Otherwise, the experiments cannot obtain the real/effective CO_2

Table 1
Summary of different LDHs employed for CO_2 adsorption.

Adsorbent/Precursor	Synthesized conditions		Reactor	Number of cycles	CO_2 uptake capacity(mmol/g)	Refs
	Synthesized method	Calcination/Activation				
Li-AL LDH	Co-precipitation	300–500 °C, 5 h	TGA	22	0.51–0.94	[47]
Li-AL LDH	Gibbsite intercalation	300–500 °C, 5 h	TGA	22	0.30–0.45	[47]
Mg-Al LDH	Co-precipitation	400 °C, 5 h	TGA	10	0.9	[76]
Mg-Al LDH	Isoelectric point	400 °C, 5 h	TGA	–	0.83	[10]
Mg-Al LDH	Co-precipitation	400 °C, 1 or 6 h	TGA	–	0.58–0.83	[77]
Mg-Al LDH	Co-precipitation	400 °C, 1 h	TGA	–	4.521	[78]
Mg-Al LDH	Co-precipitation	400 °C, -	TGA		0.91	[79]
Mg-Al LDH	–	400 °C, 4 h	TGA	199	0.76	[53]
Mg-Al LDH	Co-precipitation	500 °C, 4 h	TGA	–	0.749–0.789	[80]
Mg-Al LDH	Co-precipitation	300–600 °C, 0–21 h	TGA	–	0.71	[27]
Mg-Al LDH	coprecipitation	400 °C, 12 h	TGA	10	0.62	[73]
Mg-Al LDH	Co-precipitation	400 °C, 5 h	TGA	–	0.85	[81]
Mg-Al LDH	Exfoliation	400 °C, 4 h	–	5	1.4	[82]
Mg-Al LDH	Co-precipitation	80 °C, 0.5 h	VBH	–	5.7	[55]
Mg-Al LDH	Co-precipitation/Rehydration	400 °C, 5 h	TGA	22	3.25	[48]
Mg-Al LDH	Co-precipitation	400 °C, 4 h	TGA	6	0.71	[60]
Mg-Al LDH	–	550 °C, 6 h	TGA	3	0.94	[51]
Mg-Al LDH	Recrystallization-impregnation	650 °C, 4 h	TGA	–	1.21	[83]
Mg-Al LDH	Urea hydrolysis	400 °C, 5 h	TGA	15	0.56	[84]
Mg-Al LDH	–	450 °C, 48 h	–	10	0.77	[85]
Mg-Al LDH	–	400 °C, 4 h	FBR	10	1.13	[86]
Mg-Al LDH	Co-precipitation	550 °C, 4 h	TA	–	2.13	[56]
Mg-Al LDH	Co-precipitation	–	TGA	6	1.25	[1]
Mg-Al-Ga LDH	Co-precipitation	400 °C, 2 h	–	–	1.82	[87]
Mg-Al-Ga LDH	Co-precipitation	400 °C, 2 h	Microbalance	–	2.09	[88]
Mg-Al-Ga LDH	Co-precipitation	400 °C, –	TGA	3	1.4	[89]
Mg-Co-Ca-Al LDH	Co-precipitation	550 °C, 4 h	FBR	–	1.39	[74]
Ca-Al LDH	Co-precipitation	500 °C, –	TGA	15	3.55	[73]
Ni-Mg-Al LDH	Co-precipitation	600 °C, 6 h	FBR	3	2.0–2.5	[90]
Cu-Al LDH	Co-precipitation	600 °C, 15 min	TGA	–	0.16	[45]
Amine/Mg-Al LDH	Exfoliation-grafting	105 °C, 30 min	TGA	–	1.76	[91]
Amine/Mg-Al LDH	Intercalation/extraction	105 °C, 30 min	TGA	30	0.18	[92]
Amine/silica@Mg-Al LDH	Grafting	105 °C, 1 h	TGA	4	1.57	[5]
APS/Mg-Al LDH	Grafting	120 °C, 1 h	TGA	5	2.02	[93]
CNF/Mg-Al LDH	Co-precipitation	500 °C, –	PFR	10	2.43	[46]
(Li-Na-K)/Mg-Al LDH	Co-precipitation/Rehydration	–	TGA	22	3.25	[48]
Na/Mg-Al LDH	Co-precipitation	–	TGA	16	9.27	[94]
(K, Na)-CNF/Mg-Al LDH	Co-precipitation	500 °C, 1 h	PFR	10	1.7–2.2	[95]
GO/Mg-Al LDH	Co-precipitation	400 °C, 4 h	TGA	20	0.54	[96]
GO/Mg-Al LDH	Co-precipitation	400 °C, 4 h	TGA	11	0.55	[97]
GO/Mg-Al LDH	Co-precipitation	400 °C, 4 h	TGA	10	0.54	[98]
GO/Mg-Al LDH	Self-assembly	400 °C, 5 h	TGA	22	0.35	[99]
GO/MWCNT/Mg-Al LDH	Deposition	400 °C, 4 h	TGA	20	0.49	[100]
(Na, K, Cs) GO/Mg-Al LDH	Impregnation	400 °C, 4 h	TGA	20	0.56–0.69	[101]
(K, Na)-CNF/Mg-Al LDH	Co-precipitation	500 °C, 1 h	PFR	10	1.7–2.2	[95]
GO/Mg-Al LDH	Co-precipitation	400 °C, 4 h	TGA	20	0.54	[96]
GO/Mg-Al LDH	Co-precipitation	400 °C, 4 h	TGA	11	0.55	[97]
GO/Mg-Al LDH	Co-precipitation	400 °C, 4 h	TGA	10	0.54	[98]
GO/Mg-Al LDH	Self-assembly	400 °C, 5 h	TGA	22	0.35	[99]
GO/MWCNT/Mg-Al LDH	Deposition	400 °C, 4 h	TGA	20	0.49	[100]
(Na, K, Cs) GO/Mg-Al LDH	Impregnation	400 °C, 4 h	TGA	20	0.56–0.69	[101]
rG-O/Mg-Al LDH	Co-hybridization	400 °C, 4 h	–	–	1.71	[102]
K_2CO_3/Mg-Al LDH	–	400 °C, 4 h	FBR	–	0.95	[103]
K_2CO_3/Mg-Al LDH	–	–	TGA	4	1.75	[58]
K_2CO_3/Mg-Al LDH	–	400 °C, 30 min	PBR	–	1.82	[57]
K_2CO_3/Mg-Al LDH	–	450 °C, 24 h	TGA	10	0.47	[54]
K_2CO_3/Mg-Al LDH	–	400 °C, –	Multicolumn		1.5	[61]
K_2CO_3/Mg-Al LDH	Co-precipitation	500 °C, 4 h	–	5	0.82	[68]
K_2CO_3-AC/Mg-Al LDH	Urea/Co-precipitation	500 °C, 1 h	TGA	10	1.741	[49]
K_2CO_3/MWNT/Mg-Al LDH	Co-precipitation	400 °C, 4 h	FBR	10	0.81	[104]
K_2CO_3/Mg-Al LDH	Hydrothermal	500 °C, –	TGA	7	1.79	[105]
MWNTs/Mg-Al LDH	Co-precipitation	400 °C, –	TGA	21	0.42	[106]
OCNT/Mg-Al LDH	Co-precipitation	400 °C, 5 h	TGA	22	0.45	[107]
OCNT/Mg-Al LDH	Exfoliation-self-assembly	400 °C, 5 h	TGA		0.54	[107]
OCNT/Mg-Al LDH	Co-precipitation	400 °C, 5 h	TGA		0.58	[107]
POM/Mg-Al-LDH	Exfoliation-reassembling	200 °C, –	–	4	0.74	[108]
Stearate/Mg-Al LDH	Anionic-exchange	450 °C, –	TGA	–	1.93	[109]
SBA-15/Mg-Al LDH	Precipitation-deposition	200 °C, 1 h	FBR	5	3.02	[110]
Urea/Zn-Al LDH	Precipitation	180 °C, 2 h	FBR	–	0.86–2.36	[111]

capture capacity. Since this memory effect can be easily ignored by researchers, it could be one of the important reasons for the significant differences in the reported CO_2 capture capacity values [27,47]. In addition, the large span of the LDH nature, composition, preparation method, promoter type and impregnation degree, pressure range, and temperature range can also be sources of the inconsistencies observed in the CO_2 sorption capacities of LDHs [74,75].

In general, LDHs do not exhibit the best CO_2 capture capacities, compared to other materials in this field. To improve the CO_2 sorption capacity of LDH materials, many efforts have been made. The effects of the synthesis conditions and adsorption performances on CO_2 adsorption over various LDH-based sorbents are summarized in Table 1.

3.1. Preparing the LDH by different methods

Currently, various synthesis approaches, including co-precipitation, urea hydrolysis, ion exchange, hydrothermal, sol-gel, and reverse-microemulsion, have been developed to prepare pristine LDHs. The synthesis method greatly affects the specific surface area, pore size, and pore volume [32,111–114]. Co-precipitation is the most frequent preparation method used by researchers. This facile and inexpensive method has been used to prepare adsorptive/photoreductive LDHs (Fig. 6). To evaluate the effect of the synthesis method on the CO_2 capture capacity, fresh Mg-Al LDHs were synthesized using a variety of methods, including co-precipitation, co-precipitation followed by hydrothermal treatment, the urea decomposition method, and the urea decomposition method followed by hydrothermal treatment or microwave heating. After being calcined, the sample prepared by co-precipitation showed the highest S_{BET} surface area and a much higher CO_2 capture capacity than those synthesized using urea hydrolysis. However, no linear relationship between the S_{BET} surface area and CO_2 capture capacity was found in this study. The difference in their CO_2 capture capacities resulted from the charge compensating anions of the LDH prepared by urea hydrolysis, which included not only CO_3^{2-} but also co-intercalated anions, such as OH^- or NCO^- [27]. In another study, Mg-Al LDH prepared by urea hydrolysis showed poor CO_2 uptake characteristics compared to those of the samples prepared by co-precipitation owing to its lower surface area [115]. For Li-Al LDH, the sample produced by co-precipitation method exhibited a slightly higher performance for CO_2 capture than that produced by the gibbsite intercalation method. This enhancement was attributed to the particle size of the Li-Al LDH synthesized by the co-precipitation method being much smaller than those synthesized by the gibbsite intercalation method. This work presented the first example of solid Li-Al LDH adsorbents for CO_2. However, the CO_2 adsorption performance by K_2CO_3/Li-Al LDH over 22 cycles of gas adsorption-desorption declined significantly (25–35%). The adsorption capacities of LDH-based materials are still too low to justify their use in practical application [47]. For practical reaction-based CO_2 separation processes, the industrial standard material is monoethanol amine (MEA), which has a CO_2 capture capacity of ca. 1.36 mmol/g [89]. Another CO_2 adsorbent was synthesized from commercially available activated carbon, which was loaded with Mg-Al LDH using the urea or co-precipitation methods. The adsorption capacity for the AC-LDH_{co} was larger than that of AC-LDH_{urea} due to the higher hydrotalcite loading on the surface [49]. Compared with other methods, the co-precipitation method has some notable features: (1) it is a simple and rapid process for fabricating the desired LDHs directly; (2) this synthesis method is easy to scale-up for industrial production; (3) the size of the LDHs can be adjusted by various conditions (not only the alkaline solution properties); and (4) sometimes the LDHs prepared by this method suffer from poor crystallinity.

Certain other methods, such as microwave irradiation and ultra-sonication of the precipitating gel, have also been used to increase the surface area of the hydrotalcites and studied to improve the high temperature CO_2 adsorption capacities of LDHs [75,78,92]. Our team also demonstrated that ultrasonic irradiation promoted the formation of a hydrotalcite-like phase [116]. Hanif et al. [50] synthesized three types of LDH-based sorbents by con-

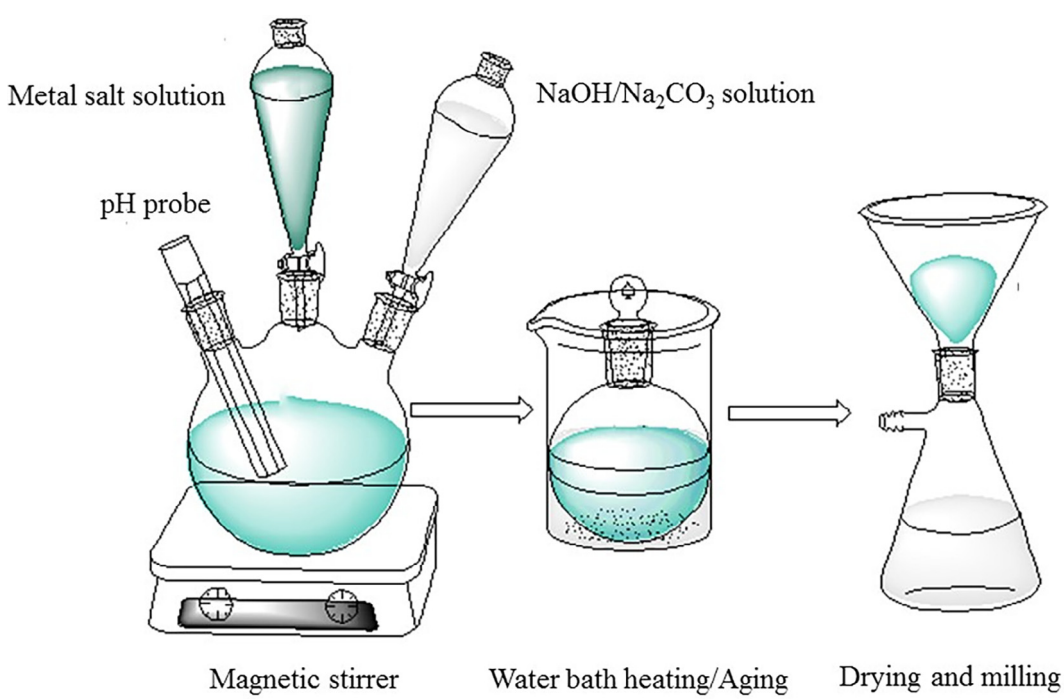

Fig. 6. The preparation process of LDHs by co-precipitation.

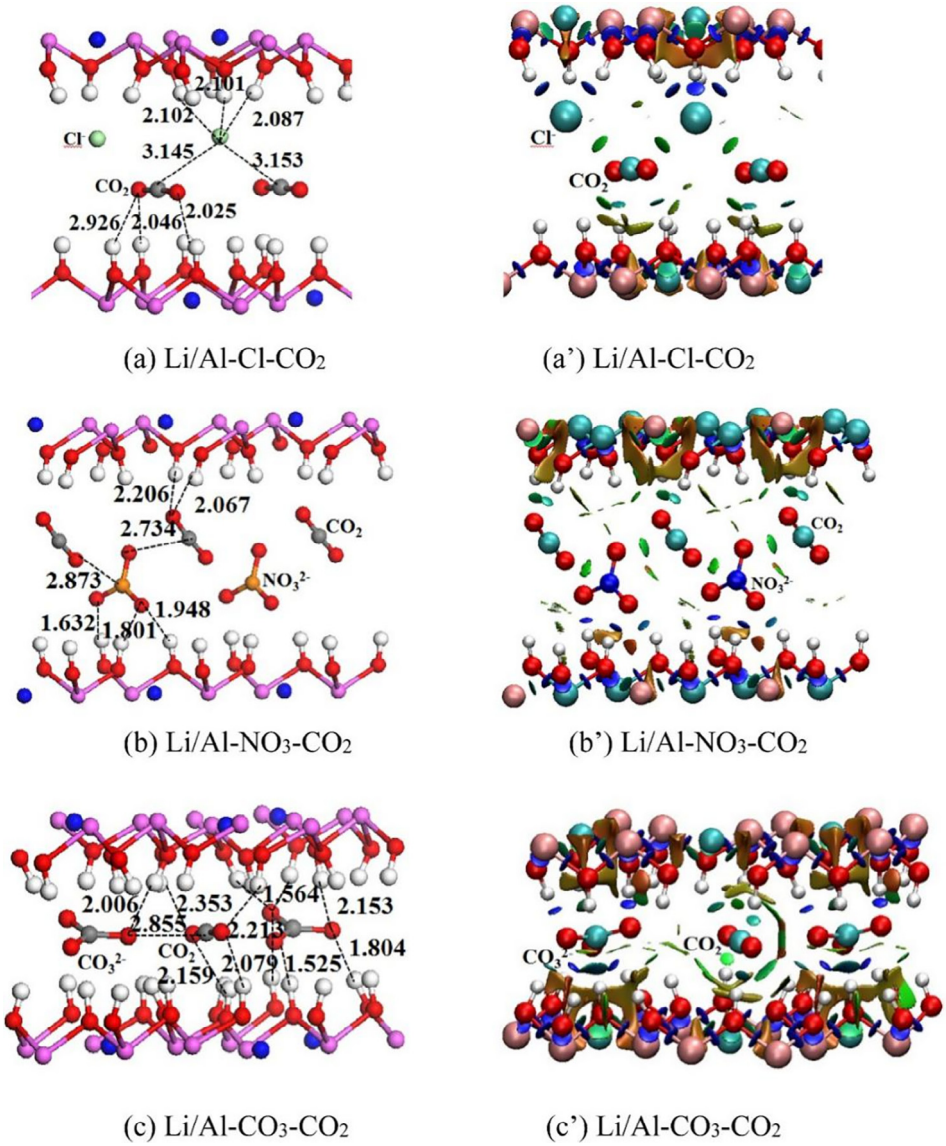

Fig. 7. Optimized structures of Li/Al-X-CO_2 (X = Cl^-, NO_3^-, CO_3^{2-}) (Al, magenta; O, red; Li, blue; H, white). (a)-(c) and corresponding gradient isosurfaces (s = 0.30 au) (a′)-(c′) (adapted with permission from Ref. [118] @Copyright 2017 Elsevier).

ventional co-precipitation, ultra-sonication assisted co-precipitation and co-precipitation prior to microwave irradiation. The cyclic CO_2 capture experiments illustrated that LDH-based sorbents prepared by the microwave- and ultrasound-assisted routes exhibited higher CO_2 sorption capacities compared to the commercial hydrotalcites in the target temperature range of 300–400 °C, because the surface areas of the microwave- and ultrasound-assisted LDHs were 2 and 5 times higher, respectively, than the conventional co-precipitated hydrotalcite. In a more recent study, LDH adsorbents were synthesized via anionic surfactant interaction and amine extraction through ultrasonic modulation. The authors reported that sonochemical modification leads to the increased pore structure and CO_2 adsorption capacity. This was attributed to the enhanced deprotonation of activated amino functional groups via the sonochemical process. However, this was dependent on the sonication intensity. Moreover, the sonochemical process improved the thermal stability of the adsorbent and reduced the irreversible CO_2 uptake [92] when compared to the results obtained by previous investigations, in which the capacity of the sonicated sample dropped to the original value of the regular HTs after the first cycle [117]. Regarding the reversibility, sonication and co-precipitation at high-supersaturation conditions in the preparation of the Mg-Al mixed oxides were found to produce materials with the strongest basic sites, leading to highly irreversible adsorption. The presence of these sites was found to be related to the formation of unidentate CO_2-adsorbent species. Preparation procedures that lead to an increase in the strength of basic sites did not lead to significant increases in the adsorption capacity, but rather led to more difficult regeneration of the saturated adsorbent [75]. Due to these benefits, parameters such as irradiation time and intensity should be further investigated.

3.2. Modification of composition

3.2.1. Changing the compensating anions

It was reported that the compensating anions have a great effect on morphologies, thermal stabilities, and the surface areas of LDHs, and they have a significant influence on the CO_2 adsorption capacity of calcined LDHs. Using CO_3^{2-} as the charge compensating anion, a spheroidal "sand rose" type of HT was synthesized and exhibited the highest S_{BET} surface area of 114.3 m^2/g. However, with other anions (NO_3^-, SO_4^{2-}, Cl^-, and HCO_3^-), "stone" type HTs were formed,

and their surface areas decreased significantly (<9 m^2/g). The Mg_3Al-CO_3 achieved the highest CO_2 capture capacity of 0.53 mmol/g, which was much higher than those of other HTs with HCO_3^-, NO_3^-, SO_4^{2-}, and Cl^- anions (~0.2 mmol/g). In addition, Mg_3-Al-SO_4 exhibited relatively higher thermal stability than the others [59]. Hou et al. [118] studied the structures of Li-Al-X LDH (X = CO_3^{2-}, NO_3^- and Cl^-) and their CO_2 adsorption performance. As shown in Fig. 7, in Li/Al-Cl-CO_2 and Li/Al-NO_3-CO_2, Cl^- and NO_3^- preferred to be located at one side of the hydroxyl layer, indicating that the hydrogen bonds between Cl^- and NO_3^- and metal hydroxyl layers were less than that of CO_3^{2-} simultaneously forming hydrogen bonds with both the upper and lower hydroxyl layers. Moreover, the adsorption energies of CO_2 in Li-Al-X LDH with X = Cl^-, NO_3^-, and CO_3^{2-} were 38.4, 8.1, and −5.4 kJ/mol, respectively, which supported another experimental finding [47] that Li/Al-CO_3 exhibited a higher CO_2 capture capacity than those of Li/Al-NO_3 and Li/Al-Cl at 200 °C. Furthermore, the relationship of the LDO crystalline structure features to the CO_2 adsorption properties has been investigated using a combination of density functional theory (DFT). A series of C-Mg-Al-LDH was prepared, and the CO_2 adsorption on the C-Mg_3Al-LDH was more energetically favorable than on the others, and the CO_2 adsorption energy and charge transfer were in the following order: C-Mg_3Al-LDH (−0.78 eV and −0.42 e) > C-Mg_5Al-LDH and C-Mg_8Al-LDH (−0.56 eV and −0.53 e). The adsorption energies from the interactions of CO_2 and the Mg-Al LDOs exceeded −0.3 eV, indicating that the CO_2 adsorbed on the surface could form carbonate species via strong chemisorption. The surface area was correlated with the adsorption capacities at small surface areas. However, at high surface areas, there was no distinct trend. The researchers also discovered that crystalline C-Mg_3Al-LDH with a relative crystallinity of about 20%, having a locally strong CO_2 adsorption strength and a large fraction of octahedral Al sites, exhibited a favorable CO_2 adsorption affinity. Furthermore, correlation between the adsorption properties and the crystallinity exhibited good agreement with experiments and could be used to predict the trends in the CO_2 adsorption capacity [119]. Most studies to date have focused on that the intercalation of CO_3^{2-} anions into the interlayers of Mg-Al LDHs. However, there is little information about how the anions affect the stability and selectivity of the material.

All the studies discussed above were limited to inorganic anions such as CO_3^{2-}, NO_3^-, SO_4^{2-}, and Cl^-. The attempted use of organo-LDHs for CO_2 capture was reported by Wang and co-workers in 2012. In their study, stearate was intercalated into the interlayer of the LDH. The inter-layer distance was enlarged from 0.78 nm for Mg-Al-CO_3 to 3.54 nm for Mg-Al-stearate. After thermal treatment, the decomposition of $C_{17}H_{35}COO^-$ anions resulted in a much lower degree of crystallinity and smaller particle size of $MgAlO_x$. These obtained mixed oxides possessed more surface basicity sites for CO_2 adsorption compared to the Mg-Al-CO_3 LDH [1]. In addition, the enlarged interlayer distance of the stearate-intercalated LDH promoted the dispersal of K ions into the LDH interlayer and, thus, create more Al(Mg)-O-K bonds to enhance the wet promotion effect on the surface and inter surface of brucite-like LDH layers [109]. A further systematic investigation on the influence of various monocarboxylate anions with different carbon chain lengths on the CO_2 capture capacities of Mg-Al LDHs was performed. Those LDHs intercalated with the long carbon chain organic anions exhibited higher specific surface areas and pore volumes. When the carbon chain was less than 10 carbon atoms long, no obvious difference in the CO_2 capture capacity was observed. However, with the increase in carbon chain length from 10 to 16 carbon atoms, the CO_2 capture capacity gradually increased, and the highest CO_2 capture capacity was achieved with the adsorbent derived from the Mg_3Al_1-C_{16} LDH. The stability of the LDOs was associated with the carbon chain length of the monocarboxylic acid counter anions. For the short carbon chain anions, all the samples reverted back to their original layered structure. However, for long carbon chain anions, they still remained in their amorphous phase even after 15 days. It is well known that a quasi-amorphous structure exhibits the highest CO_2 capture capacity, this may be a significant reason for the enhanced CO_2 capture capacities of long carbon-chain organic anion intercalated LDHs [48]. The thermal stability of the carbon chain is crucial and should be given top priority, as the adsorption temperature is always around 400 °C.

3.2.2. Changing the M^{2+} and M^{3+} structural metals

The natures of the trivalent cations in LDHs can affect the thermal stabilities of these materials, leading to different 3D networks and CO_2 capture performances after calcination at various temperatures [120]. The effects of trivalent cations on the performance of Mg-M-CO_3 (M = Al, Fe, Ga, Mn) LDHs for high-temperature CO_2 capture were comparatively investigated. The researchers demonstrated that the M^{3+} ion determined the structural evolution of LDH derivatives under thermal treatment, and finally influenced the CO_2 capture capacity [52]. In the work by Yavuz et al. [89], the effect of gallium substitution and modification with K_2CO_3 was firstly reported and a markedly improved CO_2 sorption capacity was observed at 473 K for a CO_2 partial pressure of 0.7 atm under dry conditions. Ternary LDHs modified with Fe^{3+} ions were prepared for carbon dioxide adsorption. The maximum adsorption capacity of Ni-Mg-Al LDH was reported as 1.58 mmol/g and the adsorption was found to increase by 53% compared to that of Ni-Mg-Al-Fe LDH [90].

The M^{2+}/M^{3+} ratio is one of the key parameters that determines the surface basicity of the LDH-derived mixed metal oxides. Our previous research demonstrated that for a given choice of metal cations and interlayer anions, the best crystalline LDH phase was generally obtained with an M^{2+}/M^{3+} ratio of 3:1 [41], and many other researchers used a Mg:Al ratio of 3 for CO_2 capture [48,55,75,109]. As the M^{2+}/M^{3+} ratio increased, the interlayer spacing initially increased, reaching a maximum, after which it decreased, resulting in the reduction in the number of basic sites for adsorption at higher M^{2+}/M^{3+} ratios [121]. For instance, when the Cu/Al molar ratio of the synthesized hydrotalcites was varied between 1.0 and 3.0, the hydrotalcite with Cu/Al molar ratio of 2.0 was found to be the most suitable adsorbent for high-temperature (>400 °C) CO_2 adsorption in terms of the capacity and the rate of adsorption. However, the sorbent with the Cu/Al molar ratio of 1:1 achieved the highest adsorption capacity at low temperatures up to about 400 °C [45]. Sharma et al. [122] investigated the effect of the Mg/Al ratio on CO_2 capture and concluded that an Al content of 0.37 mol% (Mg/Al molar ratio of 1.7:1) was the optimal Al content. However, it should be noted that, in their work, the maximum CO_2 adsorption was measured at 150 °C and 1 bar, not in the high temperature range (200–400 °C). Gao et al. [27] carried out a systematic investigation of the effect of the Mg/Al ratio (1.5–4.0) on the CO_2 capture capacity at 200 °C. The CO_2 capture capacity first increased from 0.51 to 0.74 mmol/g with the increase of ratio from 1.5 to 3.5, and subsequently decreased to 0.6 mmol/g when ratio was 4. According to previous studies, the typical M^{2+}/M^{3+} molar ratio of hydrotalcite used for CO_2 sorption was between 2 and 3. Kim et al. [94] prepared hydrotalcites with Mg/Al ratios between 3 and 30. For hydrotalcites having Mg/Al ratios ranging from 9 to 30, both crystalline hydrotalcite and unreacted $Mg(OH)_2$ phases were detected. When the Mg/Al molar ratio increased from 3 to 20, the CO_2 uptake at 300 min increased significantly from 0.83 to 9.27 mmol/g. When the Mg/Al molar ratio was between 12 and 30, the hydrotalcites showed a unique two-step CO_2 sorption behavior, with a low CO_2 loading initially followed by a gradual transition to very high CO_2

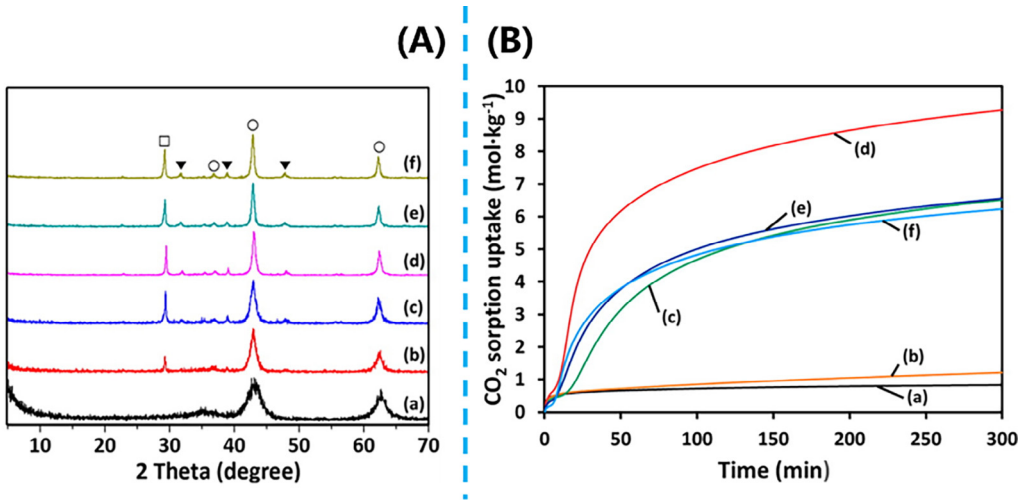

Fig. 8. (A) XRD patterns of hydrotalcites after calcination with a Mg/Al molar ratio in the feed of (a) 3, (b) 9, (c) 12, (d) 20, (e) 25, and (f) 30. ●, hydrotalcite; ♦, $Mg(OH)_2$; □, $NaNO_3$; ▼, Na_2CO_3; ○, MgO. (B) CO_2 sorption behavior at 240 °C and 1 atm CO_2 for hydrotalcite with a Mg/Al molar ratio in the feed of (a) 3, (b) 9, (c) 12, (d) 20, (e) 25, and (f) 30 (adapted with permission from Ref. [94] @Copyright 2011 American Chemical Society).

loading. It was noteworthy that the hydrotalcites with higher Mg/Al molar ratios exhibited completely different two-step CO_2 sorption behaviors compared with the normal single-step CO_2 sorption of the hydrotalcite with a Mg/Al molar ratio of 3 (Fig. 8). When the Mg/Al ratio was further increased to 25 or 30, the sorbents developed from nitrate-based precursors exhibited smaller CO_2 capture capacities due to the loss of pores and reduction of surface area resulting from pore blockage caused by the deposition of excess $NaNO_3$.

The well-known, Mg-based Mg-Al LDH powders always exhibited low CO_2 capture capacities, and CaO-based solid adsorbents have been widely used for high-temperature CO_2 capture [123–126]. Ca-Al LDH as the precursor was prepared through co-precipitation [127] and sol-gel [128] methods by the same research group. Upon thermal treatment, the Ca-Al LDH structure with a Ca^{2+}/Al^{3+} ratio of less than three was disrupted to form a weakly crystalline Ca-Al-O oxide. However, Ca^{2+}/Al^{3+} ratios larger than three tended to produce CaO particles that were dispersed in an LDO matrix. In this structure, the CaO showed a high CO_2 adsorption capacity at mid-to-high temperatures, and the LDO matrix provided stability at high temperatures to allow higher residual conversion after many cycles [127]. The LDHs synthesized by the sol-gel method exhibited scaffold-like porous structure morphologies rather than platelet-like particles. The samples with $Ca^{2+}/Al^{3+} = 7$ exhibited greater absorption of CO_2, although the surface areas, pore volumes, and pore sizes for the samples decreased with increasing Ca^{2+} content. In addition, the sorbents not only maintained long-term stabilities in the cyclic tests, but also displayed excellent rapid absorption and high capacities. These were strongly related to the scaffold-like structures with large pore volumes and pore sizes, which provided a stable framework to successfully separate the CaO particles and inhibit partial sintering of the CaO particles [128]. Furthermore, an appropriate amount of Al was necessary, as the homogeneous distribution of Al_2O_3 among the CaO particles effectively prevented the aggregation and sintering of CaO crystallites. When Al_2O_3 was dispersed into the CaO particles, Al_2O_3 particles surrounded the CaO particles and hindered their mutual contact. Ensuring that the Al_2O_3 and CaO particles were mixed well increased the anti-aggregation effect of CaO particles [129]. The CaO in the Ca-Al-O mixed oxide phase plays a key role in the adsorption of CO_2, as the CaO has a high CO_2 sorption capacity. All the efforts have focused on preventing the aggregation and sintering of CaO crystallite to separate the CaO particles successfully. It is worth noting that the Ca-Al LDHs exhibited the better adsorption capacity than the fresh Mg-Al LDHs. This is a new trend for CO_2 adsorption, and the selectivity should be further studied in the future.

Fabricating pristine LDHs with different metal cations and anions offers unique advantages, including simplicity and flexibility of the preparation procedure. Determining the appropriate M^{2+}/M^{3+} ratio and compensating anions to synthesize the LDHs for a particular CO_2 removal system is also a prerequisite for scale-up.

3.3. Controlling particle characteristics

3.3.1. Controlling particle size

In addition to changing the composition of LDHs, another effective method of improving the CO_2 capture capacities is to control the particle sizes of the LDHs. Generally, decreasing the particle sizes or improving the specific surface areas of adsorbents can improve the surface adsorption activity sites [130–132], which then improves the CO_2 capture capacities [99]. Wang et al. [10] found that the CO_2 capture capacity was increased by the nano-sized spherical Mg-Al LDHs with an average particle size of ca. 20 nm compared to the "sand rose" LDH. However, due to the layered feature of LDHs, it is difficult to further reduce the particle size lower than 20 nm. The exfoliation of a pristine LDH into individual nanosheets may be the most effective method to overcome this problem [82,108]. Exfoliated LDH nanosheets with thicknesses of 2–3 nm were synthesized by Manohara et al. [82] by exfoliating the precursor LDH layers. The enhanced surface area (275 m^2/g) in the HTlc structure resulted in a high CO_2 sorption (1.4 mmol/g) at room temperature compared to that of the pristine LDH (0.63 mmol/g). To further enhance the CO_2 adsorption functionality of the LDO material, Sidek et al. [102] developed an efficient CO_2 adsorbent by the electrostatically derived self-assembly between cationic Mg-Al LDH nanosheets and anionic grapheme oxide/layered titanate nanosheets (Fig. 9). The obtained nanocomposites exhibited mesopores with an average size of ~3.5 nm and the LDO material exhibited a much greater pore size of ~6.5 nm, which was attributable to the formation of mesopores by the agglomeration of spherical nanoparticles. The resulting LDO-rG-O-layered titanate nanocomposite exhibited a promising CO_2 adsorption capability of 1.71 mmol/g at 273 K, which was much greater than those of LDO (0.79 mmol/g) and LDO-rG-O nanocomposites (1.19 mmol/g).

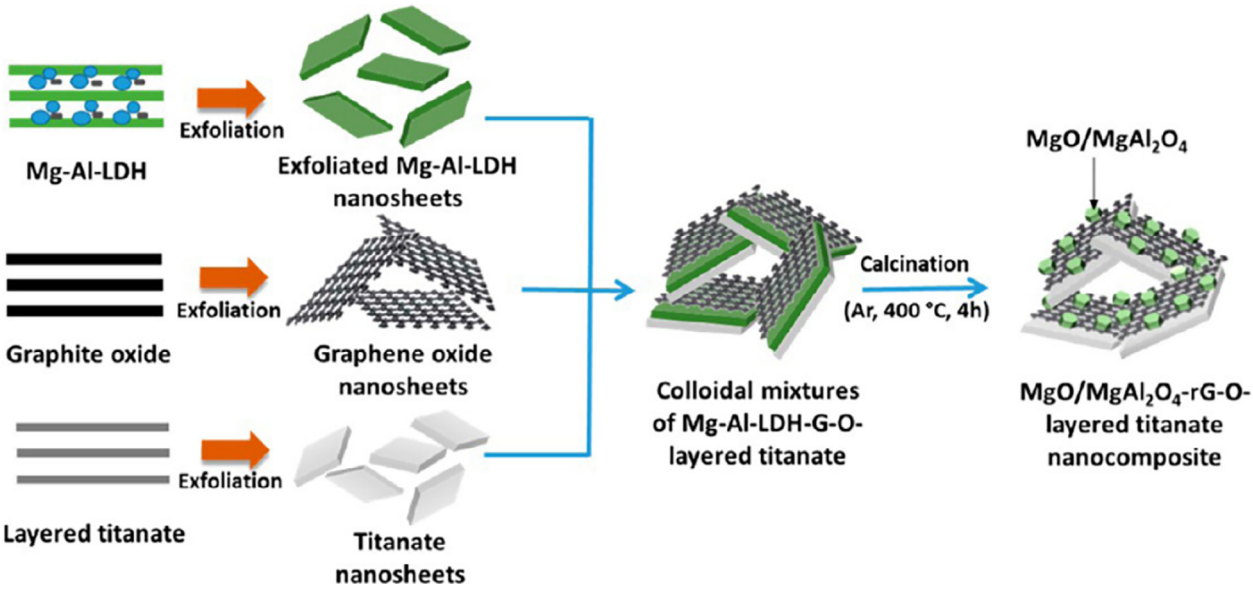

Fig. 9. Schematic diagram of the stabilization of LDO crystallites in the hybrid matrix of exfoliated rG-O and layered titanate nanosheets (adapted with permission from Ref. [102] @Copyright 2011 American Chemical Society).

There are contradictory results on the effect of particle size during adsorption. Dadwhal et al. [80] assessed the adsorption performance of LDH materials of four different particle sizes (53–75, 75–90, 90–180, and 180–300 μm) at 500 °C. Surprisingly, the adsorption capacity at saturation was found to be independent of the particle size. Before a CO_2 molecule is adsorbed in the microparticles, it must diffuse through the intercrystalline porous region. In a similar work, no relation was found between the CO_2 sorption properties of activated HTs and their specific surface areas. The researchers revealed that the CO_2 sorption capacities of LDHs were determined by the amounts of low-coordination oxygen sites in $Mg(Al)O_x$ nanoparticles. The amounts of low-coordinated oxygen in the activated samples were identical on a weight basis for all the samples [46]. These controversial findings proved the need for a comprehensive investigation of the material structure and the corresponding sorption mechanisms. For instance, theoretical infrared frequencies could be calculated to verify the dentate configuration in the LDH structure. In addition, the structural changes during thermal treatment should also been carried out using in-situ X-ray diffraction and solid state nuclear magnetic resonance analyses.

3.3.2. Controlling particle morphology

Due to their layered structures, LDHs generally prefer to form either "sand-rose-like" or "platelet-like" morphologies [10,78]. The "sand-rose-like" HT possesses abundant pores between "petals", and thus, it favors CO_2 diffusion as well as adsorption [81]. Several other studies have indicated that the adsorption capacities of LDHs can be increased by changing the morphologies and microstructures of the individual crystallites. Chang et al. [133] employed the reverse microemulsion technique to synthesize Ca-Al LDH nanoparticles. They found that different structural morphologies, including platelets, regular hexagons and, hydrangea-like hierarchical structures, could be produced by changing the concentration, reaction time and temperature during the synthesis process. When calcined at 700 °C, additional Ca-Al LDH layers in the hierarchical structure were exfoliated and transformed into separated individual nanoplatelets, leading to homogeneous nano-scale Ca-Al-O mixed oxides. Based on the experimental results, most of the calcinated hexagon LDH nanocrystallites exhibited higher CO_2 sorption capabilities and stabilities during multi-cyclic carbonation/calcination operation, which was attributed to the highest specific surface area of the sorbents, and the formation of a small amount of nano-scale calcium aluminum oxide. Wang et al. [77] revealed that the synthesis pH played a crucial role on the morphologies, pore structures, and chemical compositions of the final products. When the synthesis pH equaled the isoelectric point (IEP) of Mg-Al LDH, a "rosette" morphology was formed, while when the pH was higher than the IEP, mesoporous LDHs were synthesized (Fig. 10). All the HTs synthesized at pH 10–14 showed much better performances for capturing CO_2, which might have been attributed to the formation of mesoporous LDHs. The same researchers subsequently presented the successful synthesis of nano-sized spherical Mg_3Al-CO_3 LDHs using a facile IEP method. It was apparent that the nano-spherical LDH had a slightly enhanced CO_2 capture capacity compared to the "sand-rose-like" LDH. Furthermore, the K_2CO_3-LDH (IEP) exhibited a much higher CO_2 capture capacity, and it was believed that the mesopores within the LDH (IEP) may have favored the dispersion of K_2CO_3 and led to its superior CO_2 capture capacity [10]. Another spherical HMS@Mg-Al LDH was successfully prepared to evaluate its CO_2 adsorption capacity. At every temperature, pure hollow mesoporous silica (HMS) and Mg-Al LDH always exhibited the lowest CO_2 adsorption capacities. However, the CO_2 uptake capacity of the HMS@Mg-Al LDH illustrated that they had no direct relation with the S_{BET} or pore volume. Although HMS had higher S_{BET} and pore volume than the others, it was found to have the lowest adsorption capacity. The higher CO_2 adsorption capacities resulted from the synergistic effect of the hollow mesoporous silica and LDH [5]. Our team also prepared a shell-core Ni/Mg-Al LDH catalyst by the structural "memory effect" of MMO [14]. We tentatively suggest that more attempts to apply core@LDH or LDH@shell nanocomposites as CO_2 adsorbents should be encouraged. Until now, no study has focused on the utilization of LDH@shell materials as the CO_2 adsorbents, while these core@shell materials have been wildly used for energy storage and water purification [134]. Because 3-dimensional (3D) hierarchical structures possess appealing and unique properties, we have

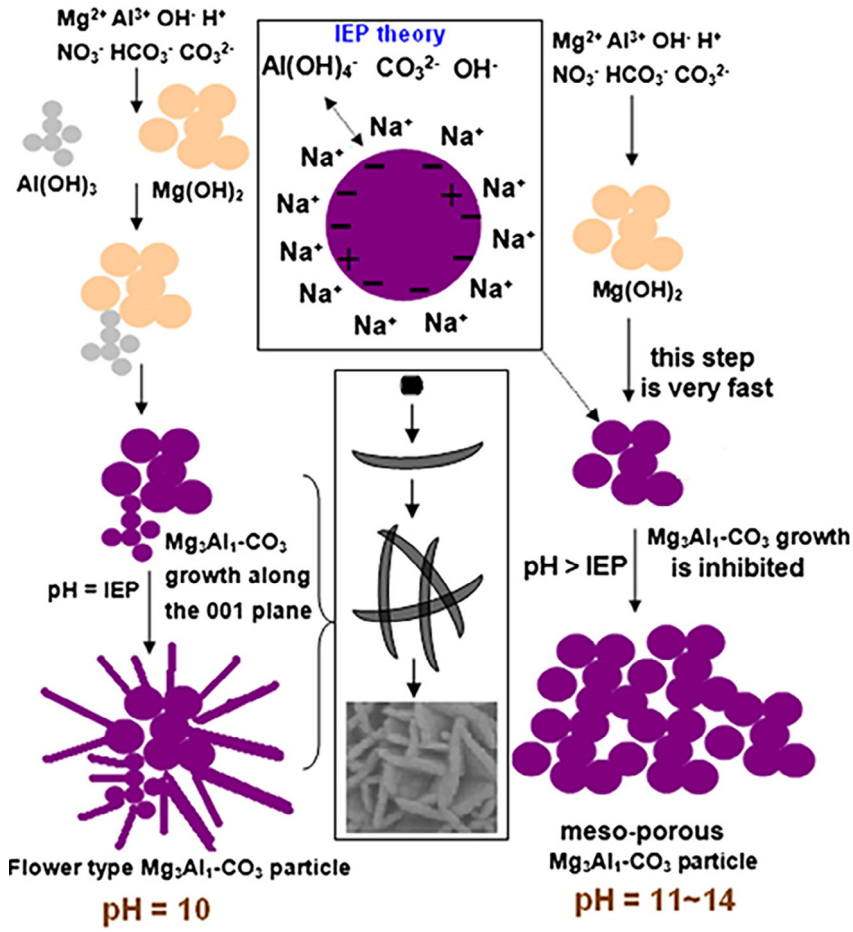

Fig. 10. Proposed synthesis mechanism for Mg-Al LDH at pH 10–14 (adapted with permission from Ref. [77] @Copyright 2013 The Royal Society of Chemistry).

reasons to believe that the field of CO_2 removal is one particular potential application of hierarchical structures.

3.4. Calcination at an appropriate temperature

The basic nature of LDH materials affects the suitability of these promising candidates as CO_2 adsorbents. The CO_2 adsorption capabilities of LDHs can be further improved by calcination at elevated temperatures, leading to the formation of LDO nanocomposites with high concentrations of surface basic sites. The precursor seems to have only a limited effect on the crystallinity of the mixed oxides, and the calcination temperature is the main parameter affecting the crystallinity [75]. Significantly different calcination temperatures are required for different LDHs to obtain their maximum CO_2 capture capacities [27]. As shown in Table 1, the typical calcination temperatures in air are between 400 and 500 °C [71]. After thermal treatment, LDHs gradually lose their interlayer water and subsequently dehydroxylate and decarbonate to a large extent, leading to the formation of a mixed oxide with a poorly defined 3D network. The S_{BET} values of all samples significantly improved, with relatively smaller pore sizes and larger pore volumes. The effect of the pre-calcination temperature (300–700 °C) on the CO_2 capture capacity of Mg-Al LDH was investigated. At 400 °C, Mg-Al LDH reached its highest CO_2 adsorption capacity of 0.71 mmol/g. If the calcination temperature was too low, the Mg-OH and Al-OH bonds could not be broken, and the hydroxide phase remained. However, if the calcination temperature was too high, the Mg and Al started to react and form the $MgAl_2O_4$ spinel oxide. The researchers further proposed two mechanisms for the formation of active Mg-O species when the LDH was optimally calcined. The substitution of Mg^{2+} by Al^{3+} in the periclase MgO lattice leads to the formation of coordinatively unsaturated oxygen anions and consequently produces two active Mg-O species, as shown in Fig. 11 (A). The other mechanism is that a part of the inserted Al^{3+} might diffuse out of the octahedral sites and the site formerly occupied by Al^{3+} is left vacant, which consequently produces three active Mg-O species around it, as shown in Fig. 11 (B). Therefore, the calcination temperature is one of the key parameters that determines the number of active Mg-O species [27].

A series of Mg-M (M = Al^{3+}, Fe^{3+}, Ga^{3+}, Mn^{3+}) LDH derivatives was prepared, and the CO_2 capture capacities were measured at 200, 300, and 400 °C. It was found that low temperatures favored CO_2 adsorption, and maximum CO_2 capture occurred at 200 °C for all LDHs. The low-temperature calcination of LDHs led to amorphous phases on which the CO_2 was mainly adsorbed physically. The adsorption strength is weak and only a small amount of CO_2 can be adsorbed at high temperatures. This phenomenon is similar to that of the Li-Al LDHs, for which it was subsequently suggested by Huang et al. [47,48] that the quasi-amorphous phase obtained by the thermal treatment of LDHs at the lowest temperature possessed the highest CO_2 capture capacity. However, when the pre-calcination temperature was sufficiently high, the CO_2 capture capacities of Mg-Ga LDH, Mg-Fe LDH, and Mg-Mn LDH increased with increasing adsorption temperature. The samples calcined at high temperatures transformed into the MgO phase and chemical adsorption of CO_2 mainly occurred. As a result, a high temperature facilitates this adsorption process [45,52].

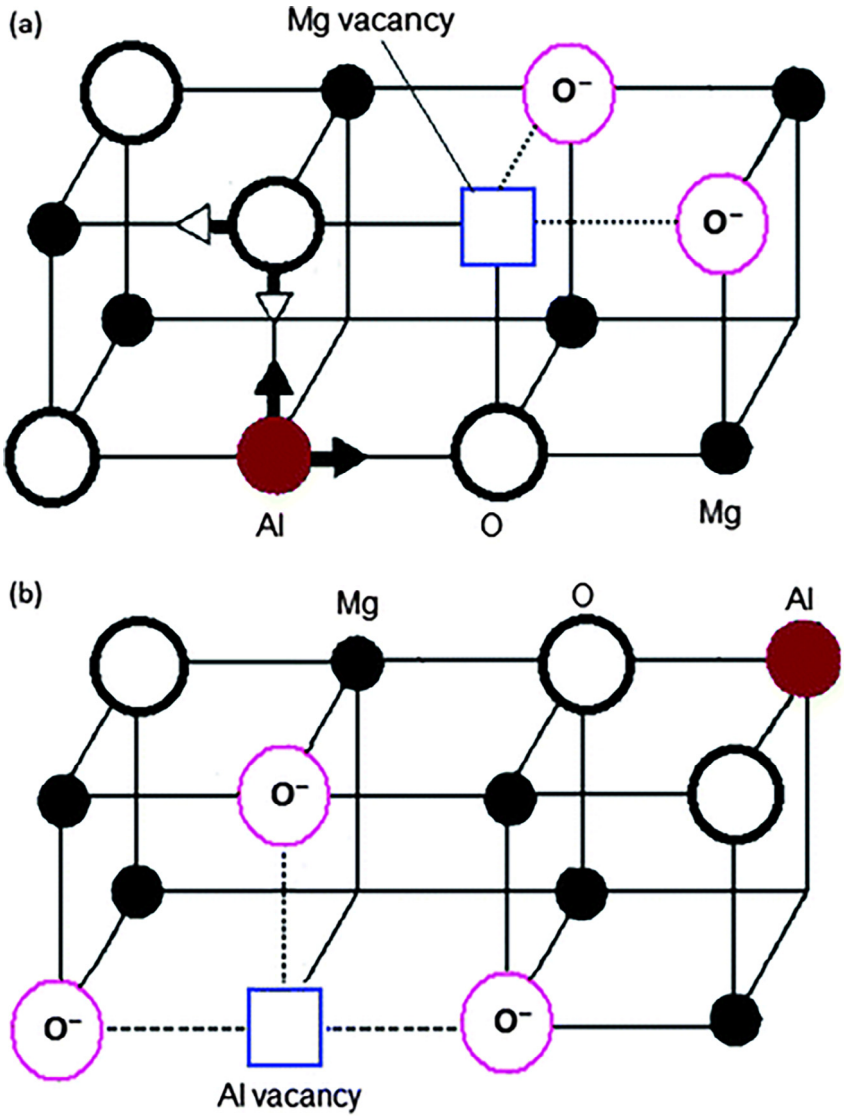

Fig. 11. The proposed mechanisms for the formation of active Mg-O species induced by (A) the substitution of Mg by Al and (B) the diffusion of Al atoms out of the octahedral brucite layers (adapted with permission from Ref. [27] @Copyright 2013 The Royal Society of Chemistry).

Because the pre-calcination model also has a great effect on the CO_2 capture, Gao et al. [27] investigated the effect of the adsorption temperature with in-situ calcination and ex-situ calcination followed by in-situ calcination. For the in-situ pretreated sample, the CO_2 capture capacity decreased with the increase in adsorption temperature, while for the ex-situ pretreated sample, the CO_2 capture capacity remained almost constant over the temperature range of 200–400 °C. Unfortunately, they did not provide an explanation for this phenomenon. Furthermore, the pre-calcination times were mostly 4–6 h (Table 1) and only two papers have discussed the effect of pre-calcination time [27,77]. More in-depth investigations could be performed in this area.

3.5. Doping LDHs with alkali metal

The basicity can be improved by impregnation with alkaline anions. It has been frequently reported in the literature that promotion of hydrotalcites with K_2CO_3 can increase the sorption capacity of CO_2 [95,103,135]. There is an optimal amount of K_2CO_3 for the maximum equilibrium CO_2 sorption uptake, which is caused by the two conflicting effects: enhanced basicity and reduced surface area with increasing K_2CO_3 amount [51]. Higher loading tends to block some small active pores for CO_2 adsorption; therefore the capacity is negatively affected [103]. The sorption capacity is more likely to be related to the chemical nature of the exposed surface [51,103] and this content is typically found in other works [53,87,136]. Lee et al. [51] reported that the incorporation of Mg-Al LDH and K_2CO_3 increased the thermal stability of K_2CO_3 without changing the structure of hydrotalcite, resulting in both enhanced equilibrium CO_2 sorption uptake and fast CO_2 sorption kinetics. However, in another study, it was also confirmed that CO_2 was adsorbed faster on Mg-Al-Ga LDH than on the potassium-loaded samples, which suggested that impregnation with potassium slowed the sorption process, despite it enhanced CO_2 sorption capacity [88]. Previous studies focused heavily on the use of K_2CO_3 as the precursor for K. Wu et al. [86] reported novel results employing KNO_3 as the K precursor, with a new impregnation method to obtain a K-promoted HTlc for CO_2 sorption. Recently, Qin and coworkers have reported that the (Li-Na-K)NO_3 molten salt promoted LDH intercalated with carboxylic

anions and achieved a high CO_2 capture capacity. After being coated with 55 mol% (Li-Na-K)NO_3 molten salt, the CO_2 uptake of palmitate acid/LDH sample with high Mg/Al ratios can be increased up to 3.25 mmol/g. The results confirmed that there was no deterioration in the CO_2 uptake over 22 cycles. In contrast, the CO_2 uptake gradually increased within the first few cycles, and eventually became stable thereafter [48].

Oliveira et al. [53] compared the effects of impregnation with two alkali metals (K and Cs) and found that CO_2 adsorption capacities of commercial hydrotalcites modified by K_2CO_3 were better than that of the material modified by Cs_2CO_3. A bi-Langmuir isotherm was derived to describe the CO_2 sorption capacity over the different samples up to a CO_2 pressure of 0.5 bar. Miguel et al. [87] reported that adding K provided higher sorption values when compared to Cs and this was related to its higher basicity. However, the sorption capacity decreased for the sample modified with Sr. The CO_2-TPD measurements were further conducted using Na-, K-, and Cs-promoted LDO samples. The amount of CO_2 released from the bicarbonates that formed on the Brønsted OH^- groups was maintained with respect to the unpromoted LDO, whereas the evolution in the intermediate temperature state decreased. Additionally, the number of monodentate carbonates adsorbed on low coordinated oxygen anions was significantly higher for the alkali promoted samples [101]. The doped alkali metal may have blocked the pores of the LDH derivatives and consequently lowered their adsorption capacities. Therefore, in order to improve the CO_2 capture capacities of LDHs, decreasing the particle size and fabricating mesoporous-type LDH samples are proposed for a better dispersion of doped K_2CO_3 species. Most of the former studies focused on the effect of cations of the alkali metal salt, while the effect of the anions of the salt was unknown.

The influence and role of alkali metals on modified LDHs for CO_2 sorption were also studied [95,101,109]. Meis et al. [95] attempted to increase the sorption capacity of the carbon nanofiber (CNF) supported LDHs by adding alkali carbonates to reach their full capacities. The increase in capture capacity on alkali-loaded CNF-supported LDHs was attributed to a higher concentration of defects (low-coordination oxygen sites) on the surface of the alkali-loaded LDHs formed by the partial substitution of Mg^{2+} by K^+ or Na^+ (Fig. 12). Li et al. [109] claimed that the smaller-sized K ions were more easily promoted not only on the brucite-like layer surface but also possibly into the interlayer of a much spatial stearate-pillared LDH, facilitating a better promotion effect of K^+ by forming weak surface chemical bonds. The stability of K-stearate-Mg-Al LDH was evaluated, and it retained a 1.2 mmol/g CO_2 capacity after 10 cycles of regeneration at 400 °C. The randomly dispersed K_2CO_3 promotion in an enlarged basal distance markedly improved the K_2CO_3 promotion effect of the adsorption capacity from 0.71 to 1.11 mmol/g (1.7 times higher), as well as the adsorption kinetics. More recently, Iruretagoyena and co-workers [101] found that the enhancement in the adsorption capacity achieved by alkali promotion was higher for the LDO than for the graphene oxide (GO)/LDO. It was likely that the impregnated alkali carbonates did not interact with the magnesium and aluminum oxides as efficiently as in the unsupported LDO. This effect could be ascribed to strong interactions between the alkali cations and the oxygen groups of the support that occurred during impregnation, preventing the optimal incorporation of the promoter on the LDO.

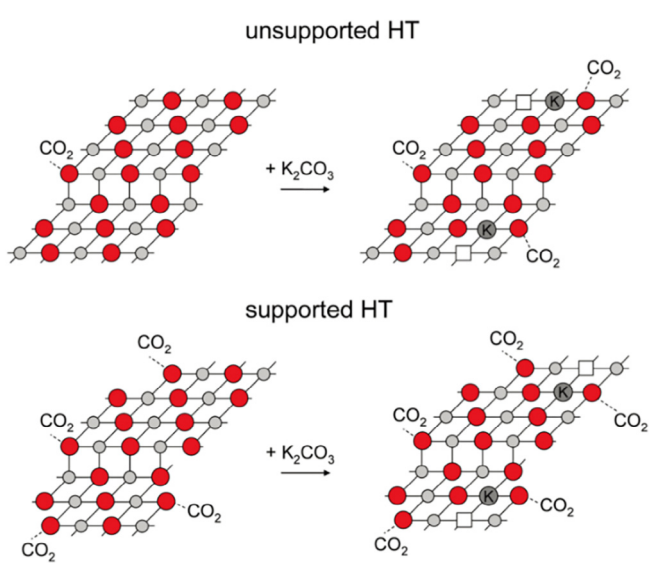

Fig. 12. Schematic representation of addition of K_2CO_3. More low coordinated sites (edges and corners), which are important for CO_2 adsorption, are formed. Light gray spheres are magnesium; red spheres are oxygen, and dark gray spheres are potassium (adapted with permission from Ref. [135] @Copyright 2010 American Chemical Society).

3.6. Supported LDHs

Recently, the dispersion of LDO particles over high-surface-area materials has been shown to increase the intrinsic capacity of the LDOs and their thermal stabilities. These materials included AC/LDH, CNT/LDH, MWNTs/LDH, and GO/LDH hybrids. Our findings suggested that LDHs and C-LDHs particles can also be loaded onto high surface area carbonaceous materials to further improve the dispersion of the LDHs and C-LDHs particles, improving the performance and reducing the cost of LDHs and C-LDHs [137,138]. In general, the synthesis methods can be divided into three general strategies (Fig. 13).

One is the direct co-precipitation method. Garcia-Gallastegui et al. [106] used MWCNT as a support to synthesize a MWCNTs/Mg-Al LDH hybrid as a CO_2 adsorbent. The use of a MWNT support was found to improve the absolute capacity and cycle stability of the hybrid adsorbent under dry conditions. However, the 2D geometry of the GO was more obviously compatible with the LDHs, while the surface chemistry was expected to be similarly favorable. They also prepared a GO/Mg-Al LDH hybrid by the direct precipitation of the LDH nanoparticles onto GO to improve CO_2 adsorption capacity and recyclability. The absolute capacity of the LDH increased by over 60% using only 7 wt% GO as a support. GO appeared to be especially effective at supporting LDH compared to oxidized MWNTs with similar surface chemistries, an effect that can be attributed to the obvious morphological compatibility [97]. The use of wet gas mixtures was found to have a positive effect on the CO_2 adsorption capacity of the GO-LDH [98]. Sodium ions incorporated by residual sodium from the synthesis greatly enhanced the adsorption capacity of the GO/LDH hybrid. The improved thermal stability achieved by the use of GO in the GO/LDO hybrids was not affected significantly by the presence of residual sodium [96]. SBA-15-supported Mg-Al LDH composite materials with varied hydrotalcite loadings were prepared by precipitation-deposition method for CO_2 adsorption studies at 70 °C and the experiments revealed that 50 wt% of LDH loading led to the best performance. Beyond 50% loading of hydrotalcite, LDH attained a bulk nature and exhibited decreased CO_2 uptake. The improvement in performance was observed only with high loadings of the supports, which may result in large sorption units [110]. Small LDH platelets were obtained by deposition onto a carbon nanofiber (CNF) supports. The C of CO_2 adsorbed on low-coordinated oxygen (oxygen surrounded by fewer than five atoms) of unsupported LDO, and the amounts of low-coordinated oxygen in the activated unsupported samples were identical on a weight basis for all the samples. The large increase in CO_2 capacities of the activated CNF-supported LDHs was due to the greater number

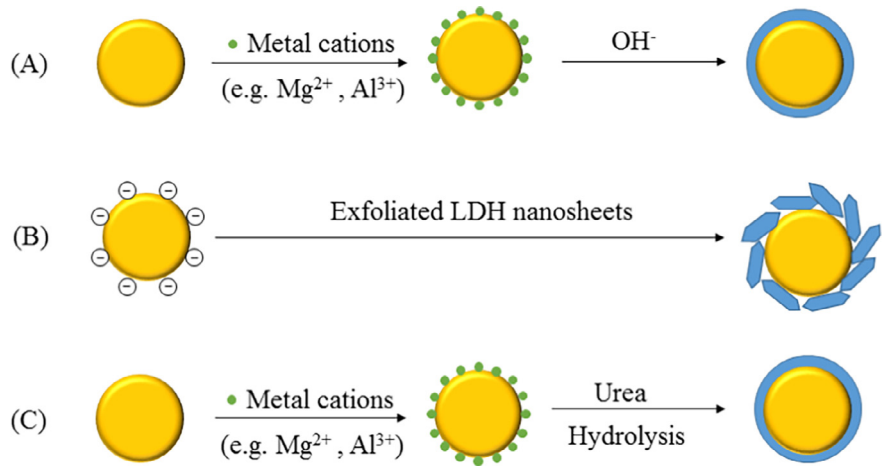

Fig. 13. Schematic illustration of the fabrication of supported LDH composites by (A) co-precipitation, (B) electrostatic self-assembly, and (C) hydrothermal urea.

of defects on the small $Mg(Al)O_x$ crystals. The individual crystals were anchored on the CNF and thus had lower flexibilities, which may have contributed to the greater numbers of defects and low-coordinated oxygen [46].

The second synthesis method is based on the electrostatically driven self-assembly between a delaminated positively charged LDH single sheet and a negatively charged monolayer. The substrate materials and LDH nanoparticles or nanosheets are prepared separately, and subsequent combination of these building blocks generates the mixture. Wang et al. [99] synthesized a GO/Mg-Al LDH hybrid for CO_2 capture. The GO/Mg-Al LDH nanocomposites with 6.54 wt% GO exhibited the maximum adsorption capacity, which was more than twice larger than that of the pure Mg-Al LDH. The enhancement can be attributed to the LDH single sheets and their dispersion and stabilization on the support. They subsequently prepared OCNT/Mg-Al LDH nanocomposites using the "electrostatic self-assembly" and "direct co-precipitation" methods. Both the CO_2 adsorption capacities and the multicycle stabilities of LDH derived adsorbents were improved by the introduction of OCNT. The characterization results revealed that the synthesis method had little influence on the morphology and structure of the formed nanocomposites [107].

The third method is the hydrothermal urea reaction and obtained high-temperature CO_2 adsorbent. The novel hybrid solid sorbent offers practical advantages such as higher thermal and mechanical stability. The group of Chang and Chen prepared the mesoporous AlOOH/Ca-Al LDH by using a hydrothermal urea reaction [139]. Some previous studies reported that the CO_2 molecules were adsorbed into the active sites of the calcined metal oxide and four species of adsorbed CO_2 were detected by the FTIR spectroscopy. Bicarbonates require surface hydroxyl groups (OH^-, weak base sites), whereas carbonates are formed on surface oxygen atoms with different coordination degrees, leading to unidentate and bidentate, chelating or bridging, carbonates. Unidentate species are formed on oxygen ions showing the lowest coordination number (O^{2-}, strong base sites), whereas chelating and bridging bidentate carbonates require the participation of an adjacent cationic site (Mn^+-O^{2-} pairs, medium-strength base sites) (Fig. 14) [75,139,140]. The FTIR spectra of AlOOH/Ca-Al LDH after adsorption indicated that the strongest active sites were correlated with the unidentate-type adsorption and were chiefly responsible for the irreversibility of the adsorption. At this point, infrared spectroscopy of the chemisorbed species was a powerful technique for understanding the adsorption mechanisms, allowing for discrimination between different basic sites and also providing information about the reversibility of the interactions.

During the CO_2 adsorption/desorption cycles, LDH granules gradually changed to a slurry (LDH pasting issue) due to the sintering at high operating temperatures and the presence of steam. To overcome these problems, a multilayer Mg-Al LDH-based thin film on an aluminum foil/mesh substrate was fabricated by the urea hydrolysis method. The anchoring effect combined with the

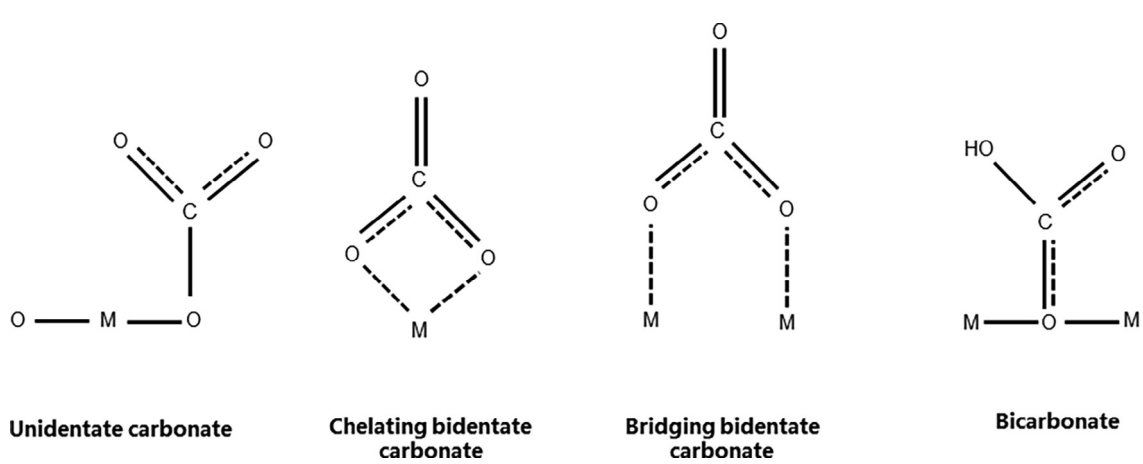

Fig. 14. Species formed upon CO_2 adsorption (adapted with permission from Ref. [75] @Copyright 2010 American Chemical Society.)

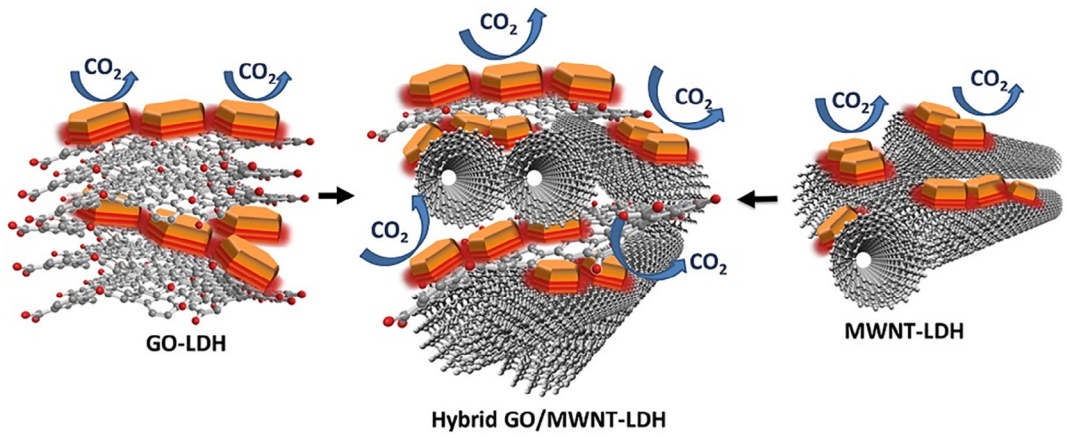

Fig. 15. Schematic representation of the hybrid GO/MNWT-LDH (adapted with permission from Ref. [100] @Copyright 2017 Elsevier).

vertical alignment of the LDH platelets in the LDH thin film could prevent the sintering and pasting issues of the LDHs. In addition, these uniformly aligned 3-D arrays of LDHs should produce a high surface area [84].

Above all, it is a priority to consider whether the supported-LDHs make full use of the LDH and substrate materials. The strong tendency of graphene for self-agglomeration hinders the gas adsorption function of the calcined graphene-LDO nanocomposites [102]. Activated carbon also tends to have relatively inaccessible slit micropores that are readily blocked by LDH deposition [141]. In addition, the multicycle stability of the GO/LDH and MWCNT/LDH subjected to temperature-swing adsorption cycles could still be improved considerably. Inspired by the synergistic effects of hybrid GO/MWCNT systems, Martina De Marco et al. [100] promoted the thermal stability LDH over twenty cycles of CO_2 adsorption-desorption (96% of retention of the initial sorption capacity at the 20th cycle) by the incorporation of a robust and thoroughly hybridized carbon network (Fig. 15). The primary role of the MWCNT was to form a compatible, robust network, preventing restacking of the GO. The optimum carbon loading for the GO/MWCNT-LDH hybrid was between 10 and 20 wt%, higher than previously used support fractions (about 7% for GO) [97,99]. In principle, the synthesis and application of hybridized GO/MWCNT-LDH is a new and emerging area and worthy of further investigation, as lower loadings of the inert supports are more appealing from an industrial perspective.

4. LDHs in photocatalytic CO_2 reduction

Photocatalysis is a promising technology that can contribute to the environmental remediation field [142–158] and energy conversion [159–171]. Inspired by successful examples of LDH-based photocatalysts for water splitting, LDH nanohybrids should be excellent alternatives for creating efficient catalysts for CO_2 photoreduction [172–177]. Photocatalytic reduction of CO_2 into value-added fuels (e.g., CO and CH_4) is a promising approach for storing solar energy and mitigating greenhouse gas emissions simultaneously [178]. Among the various efficient and stable semiconductor photocatalysts used for this purpose, LDHs have attracted attention as catalysts for CO_2 photoconversion into CO and/or methanol [179].

4.1. Basic principle of photocatalytic CO_2 reduction on LDHs

Fig. 16 highlights the typical process of photocatalytic CO_2 photoreduction by the LDH-based materials. As illustrated, the basic

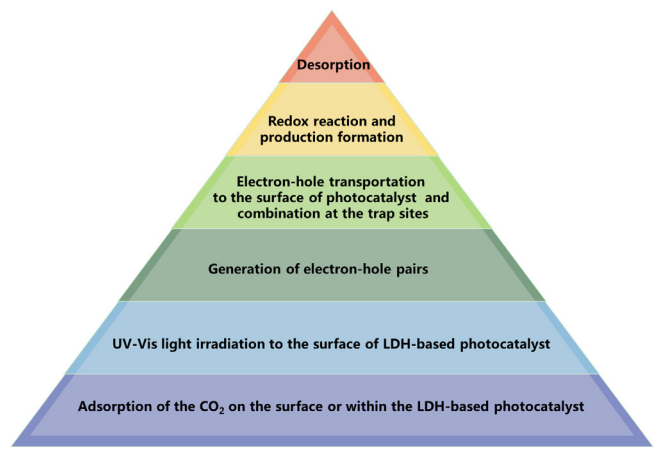

Fig. 16. Illustration of propagation of photocatalytic CO_2 reduction.

process can be summarized as four steps. The first step is the adsorption of CO_2 molecules on the surface or within the LDHs [172,180]. The intrinsic basicity of the LDH can enhance CO_2 adsorption at the composite photocatalyst surface, and the CO_2 species in the LDH-based photocatalytic reduction system have been well-understood with possible forms including (1) residual CO_3^{2-} as charge compensating anions in the interlayer of LDH, (2) captured CO_2 (as CO_3^{2-}) in the interlayer of LDH, (3) dissolved CO_2 in water, and (4) the linear/nonlinear CO_2 molecules on the surface [181–183]. Adding $^{13}CO_2$ would be the best method to demonstrate the source of the reduced products, and some ^{12}CO was generated from the residual CO_3^{2-} ions in the interlayer after the heat treatment [181,184]. The nonlinear CO_2 molecules generated on the surface of solid bases were more destabilized than the linear CO_2 molecules, which indicated that the distorted CO_2 molecules could be easily activated under photo irradiation during the conversion of CO_2 [182,185]. In addition, the interlayer CO_3^{2-} was reduced more efficiently to CH_4 compared to the surrounding free CO_2 or CO_3^{2-}. It is expected that the consumed interlayer CO_3^{2-} can be replaced readily by the surrounding free CO_2 [25]. Thus, increasing the adsorption capacity is crucial for photo-catalytically converting CO_2. The intrinsic basicity of the active sites on the surface of photocatalyst can be enhanced by changing the ratio of metal components [185] and fluorination [181]. The surface basicity site density [73] and base strength [186] of LDHs can be determined using TPD of CO_2. It was concluded that the basicity and base strength of the adsorbents played important roles in

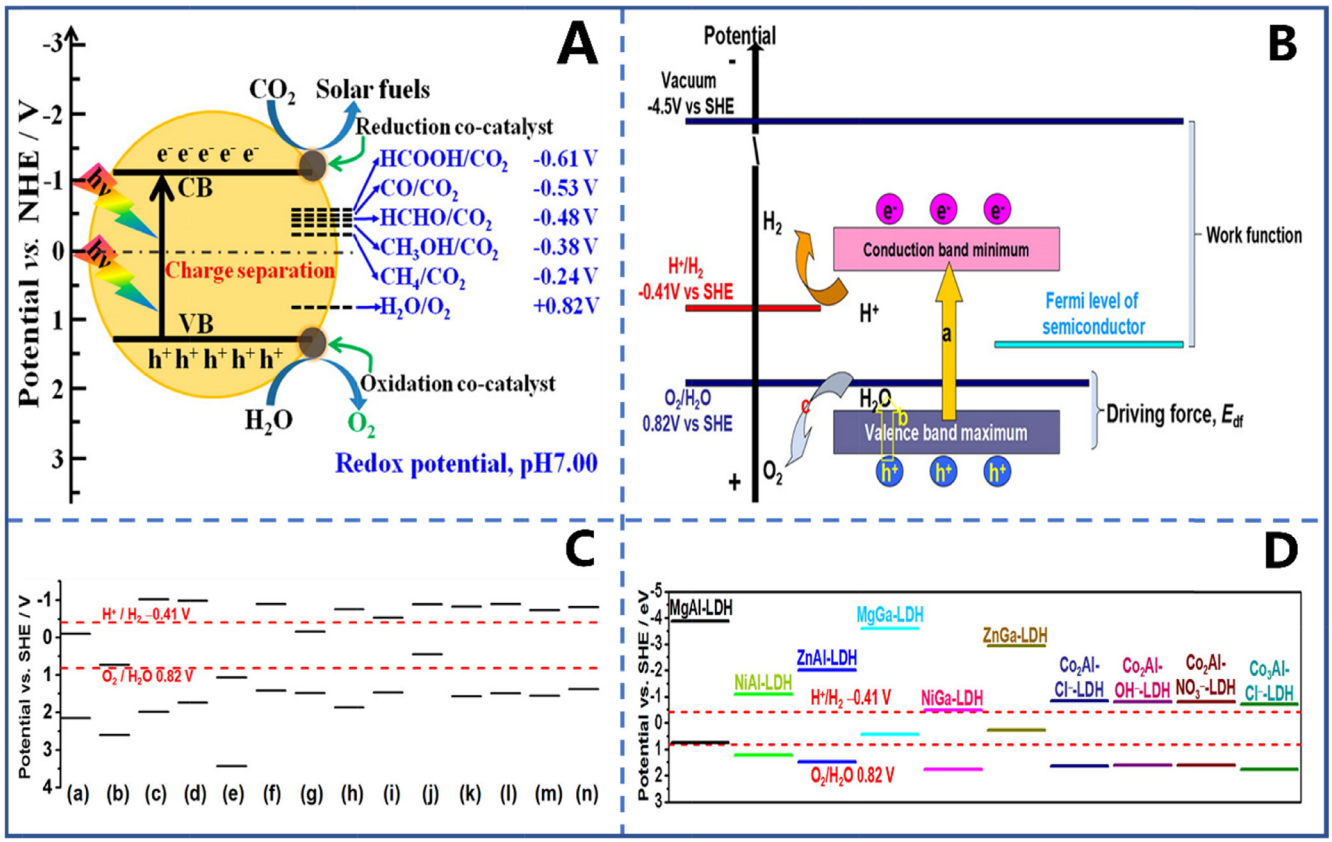

Fig. 17. (A) Schematic illustration of probable mechanism of photocatalytic CO_2 conversion over a semiconducting photocatalyst for solar fuel production mediated by suitable redox cocatalysts; (adapted with permission from Ref. [192] @Copyright 2016 American Chemical Society). (B) Schematic diagram of photocatalytic water splitting to produce H_2 and O_2 when pH is 7; (adapted with permission from Ref. [193] @Copyright 2015 American Chemical Society). (C) Band edge placements of Ni_2Ti-Cl-LDH (a), Cu_2Ti-Cl-LDH (b), Zn_2Ti-Cl-LDH (c), Mg_2Cr-Cl-LDH (d), Co_2Cr-Cl-LDH (e), Ni_2Cr-Cl-LDH (f), Cu_2Cr-Cl-LDH (g), Zn_2Cr-Cl-LDH (h), Co_2Fe-Cl-LDH (i), Ni_2Fe-Cl-LDH (j), Ni_2Cr-NO_3-LDH (k), Ni_2Cr-CO_3-LDH (l), Ni_3Cr-Cl-LDH (m), and Ni_4Cr-Cl-LDH (n); (adapted with permission from Ref. [194] @Copyright 2017 American Chemical Society). (D) Band edge placements of $M^{II}M^{III}$-LDHs (M^{II} = Mg, Co, Ni, and Zn; M^{III} = Al and Ga) (adapted with permission from Ref. [193] @Copyright 2015 American Chemical Society).

determining the CO_2 adsorptive performance, depending on the operating temperature [73,186]. Furthermore, the number of active sites is also a crucial factor that affects the adsorption activity [187]. The higher surface areas of certain LDHs correspond to more active sites for CO_2 adsorption [188]. Increasing the interlayer distance (characterized by XRD) is another procedure to improve the adsorption capacity of CO_2. The increased interlayer reaction space is expected to facilitate the diffusion of more CO_2 into the reaction space and the reaction with the hydroxyl groups to form hydrogen carbonate intermediates [180,182,189]. These strategies can be simultaneously combined to greatly improve the adsorption activity of the LDH photocatalyst. Hong et al. [25] assembled Mg-Al LDH nanosheets with a carbon nitride photocatalyst, which was demonstrated to yield more CH_4 from photoreduction of CO_2 than C_3N_4 alone in an aqueous solution with Pd as the co-catalyst. The main reason was identified to be the enrichment of CO_2 adsorption on the catalyst surface by Mg-Al-LDH. Other LDHs like Zn-Al LDH, Zn-Cr LDH, and Ni-Al-LDH did not yield significant improvements of CH_4 production since they had very limited CO_2 adsorption capacities [25]. The increased amounts of CO_2 adsorbed on LDHs also significantly influence the selectivity toward CO_2 reduction products. S. Iguchi et al. reported that the modification of the Ga_2O_3 photocatalyst with Mg-Al LDH drastically enhanced not only the amount of CO evolved but also the selectivity toward CO evolution [190].

The second step is the generation of charge carriers (electron-hole pairs) upon absorption of photons with energies equal to or exceeding the band gap of the LDH-based photocatalyst. For LDHs with different bandgap energies, the position of the conduction band (CB) and valence band (VB) are correlated with possible solar fuel and standard reduction potentials as demonstrated in Fig. 17 (A, C, and D). As shown in Table 2, the UV light is preferred as UV light with lower wavelength, which encompasses high energy photons and can generate the electrons-holes pairs in large band-gap LDHs. For example, the Co-Al LDH with a narrow band gap of 2.1 eV, the electrons were photoexcited from the valence band to the conduction band of the Co-Al LDH upon visible light irradiation [191].

The third step is charge carrier separation and transportation. The generated electrons and holes undergo intra-band transitions, migrate to the surface and get trapped at the trap sites. The rate of charge transfer depends on the band edge position of the band gap and redox potential of the adsorbate species. Undesirable electron-hole recombination prevents them from transferring to the surface, and the recombination occurs within the semiconductor volume or on the surface [195]. Thus, suppressing the recombination is a paramount step for controlling the reactions for higher yields. However, pristine LDHs generally exhibit slow charge carrier mobilities and high rates of electron-hole recombination [40]. The loaded nanoparticles on the LDHs can function as effective electron traps, promoting charge separation and providing active sites for CO_2 reduction [196].

The last step is the chemical reactions between the adsorbed CO_2 and charge carriers. When electrons migrate to the surface and after they are trapped at the edge of the CB, they serve as reduction centers, the semiconductor donates electrons to

Table 2
Summary of different LDHs employed for CO_2 photoreduction.

Photocatalyst	Synthesized method	Light source	Reducing agent	Isotope labeling	Scavenger	Major oxidation products/ μmol h^{-1} $g_{cat.}^{-1}$	Major reduction products/ μmol h^{-1} $g_{cat.}^{-1}$	Refs
Mg-Al LDH	Co-precipitation	UV/400 W Hg lamp	Water solution	$^{13}CO_2$	Cl^-	ClO^- = 7.58	9.33 (^{13}CO = 8.8, ^{12}CO = 0.53)	[181]
Mg-In LDH	Hydrothermal	200 W Hg-Xe lamp	Water solution	$^{13}CO_2$	–	O_2 = 17.0	^{13}CO = 3.21	[182]
Mg-Al-Ti LDH	Co-precipitation	UV/400 W lamp (Oriel)	Water vapor	–	–	O_2	CO = 10.2	[178]
Co-Al LDH	Co-precipitation	Solar light	Water vapor	–	–	O_2	CH_4 = 4.3	[183]
Ni-V LDH	Co-precipitation	UV/400 W Hg lamp	Water solution	–	Cl^-	ClO^-	CO = 58.84	[14]
Ni-Al LDH	Co-precipitation	Hg lamp	Water solution	$^{13}CO_2$	Cl^-	ClO^-, ClO_3^-, ClO_4^-	^{13}CO = 5.25	[185]
Ni-Al LDH	Co-precipitation	UV/400 W Hg lamp	Water solution	–	Cl^-	ClO^-=7.6	CO = 9.33	[181]
Ni-Al LDH	Nano-crystallization	400 W Hg lamp	Water solution	$^{13}CO_2$	Cl^-	ClO^-, ClO_4^-	50 (^{13}CO = 37.5, ^{12}CO = 12.5)	[184]
Zn-Al LDH	Co-precipitation	UV/500-W xenon arc lamp	Hydrogen	–	–	H_2O	0.64 (CH_3OH = 0.04, CO = 0.62)	[208]
Zn-Al LDH	Microemulsion hydrolysis	UV–visible light	Water vapor.	$^{13}CO_2$	–	O_2	^{13}CO = 7.6	[209]
Zn-Ga LDH	Co-precipitation	UV–visible light	Hydrogen	–	–	H_2O	0.13 (CH_3OH = 0.05, CO = 0.08)	[208]
Zn-Ga LDH	Co-precipitation	UV	Hydrogen	–	–	H_2O	0.13 (CH_3OH = 0.05, CO = 0.08)	[189]
Zn-Cu-Ga LDH	Co-precipitation	UV	Hydrogen	–	–	H_2O	0.56 (CH_3OH = 0.49, CO = 0.07)	[189]
Zn-Cu-Ga LDH	Co-precipitation	UV–visible light	Water solution	–	–	O_2	CH_3OH = 0.05	[210]
Zn-Cu-Ga LDH	Co-precipitation	UV/500-w xenon arc lamp	Hydrogen	–	–	H_2O	CH_3OH = 0.17	[208]
Cd-Al LDH	Self-assembly	Solar Light	Hydrogen	$^{13}CO_2$	–	O_2	^{13}CO = 0.214	[180]
TiO_2/Mg-Al LDH	Co-precipitation	UV	Water vapor	–	–	O_2	CO = 1.5	[211]
Pd-C_3N_4/Mg-Al LDH	Self-assembled	500 W Hg (Xe) lamp	Water solution	$^{13}CO_2$	–	O_2	$^{13}CH_4$ = 0.77	[25]
Ru@Mg-Al LDH	Impregnation	Visible-light/300 W Xenon lamp	Hydrogen	–	–	H_2O	CH_4 = 2.7 × 10^5	[172]
TiO_2@Co-Al LDH	One-pot hydrothermal	UV–visible light/ 300 W Xe light	Water solution	–	–	O_2 = 1.1	CO = 2.21	[191]
TiO_2@Co-Al LDH	One-pot hydrothermal	UV–visible light/ 300 W Xe light	Water solution	–	2-propanol	CH_4, C_2H_6, CH_3OH, C_2H_5OH	–	[191]
ZnO@Cu-Zn-Al LDH	Deposition precipitation	UV–visible light/ 450 W Xe lamp	Water vapor	–	–	O_2	CH_4 = 11.4	[26]
Cu_2O@Zn-Cr LDH	In situ reduction	200-W Hg-Xe lamp	Water solution	$^{13}CO_2$	–	O_2	5.25 (^{13}CO = 2.67, ^{12}CO = 2.58)	[196]
M/Zn-Cr LDH (M = Pt Pd Au)	Photochemical deposition	UV	Water vapor	–	–	O_2	CO = 7.6, 4.7, 3.4	[25]
Ag/Zn-Ga LDH	Ion exchange	UV–visible light	Hydrogen	–	–	H_2O = 94	94 (CH_3OH = 30, CO = 64)	[207]
Au/Zn-Ga LDH	Ion exchange	UV–visible light	Hydrogen	–	–	H_2O = 231	231 (CH_3OH = 30, CO = 201)	[207]
Monometallic cerium LDH	Alkalization-calcination	300-W xenon lamp	Water vapor	–	–	O_2 = 8.5	CO = 1.68	[188]

acceptors. Similarly, the holes trapped at the VB edges serve as oxidizing sites, where they combine with electrons from donor species. To reduce CO_2 into carbon monoxide or hydrocarbons, electrons in the semiconductor are required to have more negative chemical potentials, while for water oxidation, holes need to reside on more positive potential levels [197]. For example, for Co-Al LDH nanosheets, with CB and VB potentials of −1.14 and 0.96 eV, respectively, the more negative conduction band maximum of −1.14 eV is sufficient to drive CO_2/CH_4 (−0.24 eV at pH = 7). The conduction band edge and the valence band edge straddle the redox potentials of CO_2 reduction and water oxidation, indicating the feasibility of CO_2 photoreduction. The adsorbed CO_2 is further converted into CH_4 via a proton-assisted multi-electron transfer mechanism, while some H_2 is generated by the direct combination of two protons and two electrons [183]. Importantly, the yields of products from CO_2 reduction increase as the CB becomes more negative, and photocatalysts with more negative CB levels seem to be better choices for the photocatalytic reduction of CO_2 [197,198]. The Co-Al LDH produced appreciable CO and O_2, reflecting its higher conduction band maximum of −0.75 eV and longer average charge carrier lifetime. The P25 reference by comparison exhibited a poorer photoactivity for CO_2 reduction or water oxidation, presumably reflecting its conduction band maximum potential of −0.37 eV, which is too low to drive CO_2/CO (−0.53 eV at pH 7) but sufficient to drive significant proton reduction to hydrogen [191].

Because the CB potential of the LDH catalyst is more negative than the reduction potential of H^+/H_2 and the VB edge is more positive than the redox potential of O_2/H_2O, the overall or half reaction of water splitting may occur during the photocatalytic conversion of CO_2 in water. The water molecules are oxidized by the valence band holes to form oxygen gas and are reduced by the conductance band electrons to form hydrogen gas (Fig. 17 (B)). The more positive VB position has a better oxidation capacity [199] and the more

negative CB position is conducive for water splitting to hydrogen [200]. According to Fig. 17 (D), the photogenerated holes of Zn-Ga LDH, Mg-Ga LDH, and Mg-Al LDH cannot proceed with water oxidization because their VB are not more positive than the oxidation potential of water to O_2 [193]. However, a total of 2–8 electrons are required to reduce CO_2 into potential hydrocarbon fuels, which is a much more challenging process compared with water splitting [44]. In addition to the CB values of the catalysts, the photocatalytic performance can be influenced by other factors, such as the band gap [201], specific surface area [25], crystallinity [184], and crystallite size [178].

4.2. Selectivity of photoreduction products

If the CO_2 photoreduction reaction is purely under thermodynamic control, the order of the expected product yields is $CH_4 > CH_3OH > HCHO > CO > HCOOH$. However, as shown in Table 2, photoreduction products are primarily CO, indicating that the reaction is kinetically controlled. This is because the numbers of electrons required for the formation of one molecule of the products from CO_2 are eight for methane and two for CO. Therefore, more proton and electron transfer steps are required for methane, compared to just two proton and electron transfers for the formation of CO [199].

The overall water splitting occurs together with the photocatalytic conversion of CO_2 with H_2O as a reductant, resulting in H_2 as the by-products [202–204]. Thus, it is very important to control the reduction of protons in the presence of both CO_2 and H_2O to achieve the reduction of CO_2 by H_2O. Mg-In LDH and Ni-In LDH, which contain indium as trivalent cations in the hydroxide sheet, exhibited high efficiencies for H_2 production, but the amount of CO evolved was small. For the Ni-Al LDH, the amount of H_2 evolved was much lower than those of other LDHs. The Ni species in Ni-Al LDH, which functioned as a co-catalyst, caused the selective formation of CO. These results proved that the selectivity for CO obviously depended on the metal components of the hydroxide sheets of LDHs [185]. Simultaneously, the addition of NaCl suppressed the formation of H_2 as a reduction product of H^+, and the selectivity toward CO evolution was advanced. It was believed that chloride ions in solution acted as hole scavengers in the photocatalytic reaction as chloride ions can be oxidized by holes [185,205]. However, the addition of carbonate ions or hydrocarbonate ions to an aqueous solution enhanced the evolution of H_2 for the photocatalytic conversion of CO_2 in an aqueous solution. Another attempt was made to modify the chemical/physical properties of LDHs. The incorporation of fluorine into the hydroxide sheets greatly influenced the basicity of the LDHs. The fluorination led to an enhancement in the amount of CO_2 adsorbed and the selectivity toward CO formation [181].

Generally, both electrons and holes are consumed during the photocatalytic reaction and the oxidation products are shown in Table 2. Some of the photocatalytic experiments for CO_2 were performed in an aqueous solution without the sacrificial agent and the oxidation products were mainly O_2. When CO was found to be the sole product of CO_2 reduction, the amount of O_2 in a stoichiometric ratio ($CO:O_2 = 2:1$ in a molar ratio) can be detected because the CO_2 reduction to CO is a $2e^-$ process, unlike water oxidation, which is a $4e^-$ process. Kumar et al. [191] reported that the stoichiometric ratio of $CO:O_2$ was between 1.78:1 and 1.96:1 for P25@ Co-Al LDH and Co-Al LDH, which were very close to the stoichiometric ratio of 2:1 for O_2 production during CO_2 conversion, as CO, H_2, and O_2 were the only three products in the study. In another study, CO was also found to be the only carbon-based product of CO_2 reduction, but the total amount of O_2 was much larger than that of CO. This may have been because the CO_2 photoreduction and water photo-oxidation were involved in two half-reactions: H_2O molecules were oxidized by h^+ to generate O_2 and H^+ at the VB of CeO_{2-x}, and the rate-determining step of the CO_2 reduction was driven by electrons on the bottom of the CB of CeO_{2-x}. Meanwhile, active sites on the LDHs for CO_2 reduction reaction may have been covered by CO and/or intermediate products with prolonged irradiation, resulting in the reduced increment for CO [188,206]. The effect of chloride ions as hole scavengers in the photocatalytic conversion of CO_2 in an aqueous solution has been studied. The oxidation products of chloride ions, such as ClO^-, ClO^{3-}, and ClO^{4-}, were evolved instead of O_2 as the oxidation product of H_2O [14,181,184,185]. The stoichiometric formation of the oxidation products of Cl^- was achieved in the photocatalytic conversion of CO_2 using Ni-Al LDH, as the ratio of total amounts of reduction products ($H_2 + CO$) to the amount of oxidation products (HClO) was approximately 1.0 [205]. While in the other LDH systems, the amount of HClO produced in the reaction solution was less than the stoichiometric amount, which indicated that the HClO produced in the reaction solution was continuously consumed by metal cations present in the hydroxide sheets and/or in the reaction solution [14] or that some of the photogenerated holes were scavenged by another process [181]. In a more recent study, the generation of HClO was not confirmed when nano-Ni-Al LDH was used as the catalyst. A possible explanation was that a series of disproportionation reactions of ClO^- yielded ClO^{4-} with high stability and that was less oxidative than ClO^- [184]. Conversely, excessive water was obtained when using the H_2 as the reductant. This discrepancy was due to the desorption of interlayer water molecules of the LDHs [189,207,208].

4.3. Strategies for improving the CO_2 photoreduction efficiency

As shown in Table 2, for the photoreduction of carbon dioxide, two types-based photocatalysts have been created hitherto: (1) direct photocatalysts/pristine LDH and (2) nanoparticles/support co-catalytic systems. Many attempts have been made to modify the chemical and/or physical properties of LDHs to improve their photocatalytic activities.

4.3.1. Fabrication of junctions

Our team recently fabricated a novel oxygen-doped carbon nitrogen/Co-Al LDH heterojunction photocatalyst. The strong electronic coupling effect in the heterostructured interface induced photogenerated charge to transfer from Co-Al LDH to OCN and made for the construction of an interfacial internal electric field between the Co-Al LDH and OCN [142]. Matching of the semiconductor band structures and strong donor-acceptor coupling improved the photoinduced charge carrier separation and transfer via the heterojunction. In addition, LDH species can increase the surface areas and the solid basicities of catalysts effectively, which means that more active/available sites for CO_2 adsorption can be provided. Current efforts are mainly focused on two aspects (1) combining commercially available UV light-responsive nanoparticles and a visible-light-responsive LDH and (2) maximizing the heterojunction interface contact area between the LDHs and other different semiconductors.

Typically, the hierarchical TiO_2@CoAl-LDH nanocomposites were prepared for photocatalytic CO_2 reduction. The weakly chemisorbed CO_2 molecules at the titania surface or that spilled over onto titania facets were reduced to CO via the CO_2^- anion radical in a proton-coupled process [191]. In a more recent study, the Co-Al-DS LDH@TiO_2-NT nanocomposites were prepared, and the CO productivities for the hybrids exhibited fivefold increases over those obtained for the delaminated Co-Al LDH components. The superior photocatalytic reduction of the Co-Al-LDH-DS@TiO_2-NT nanocomposites indicated the formation of a staggered type-II heterojunction across the interface between these high aspect ratio

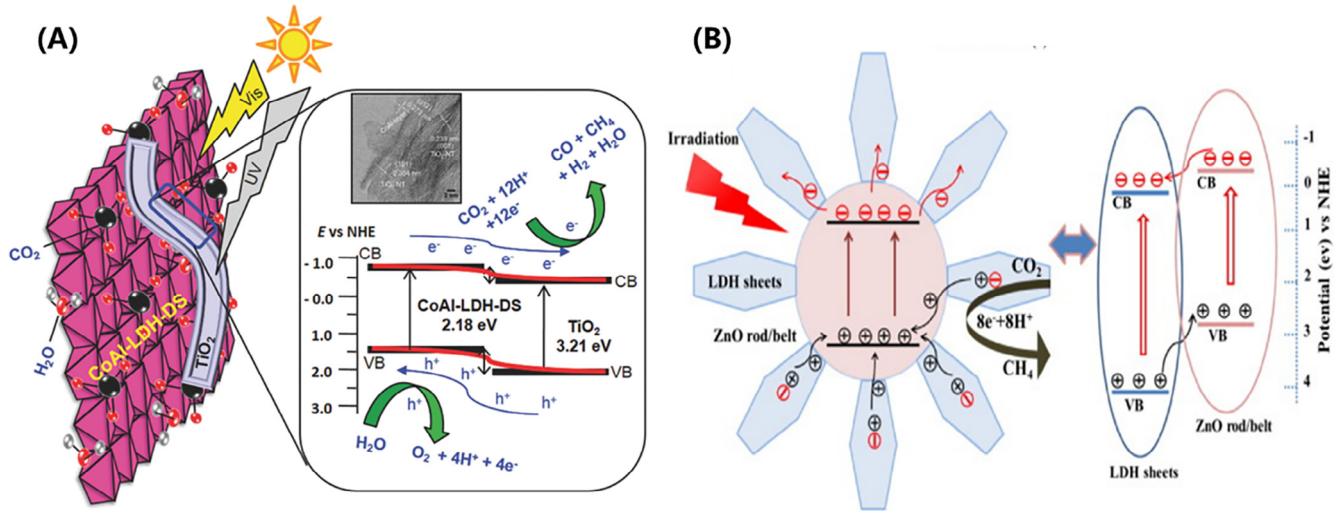

Fig. 18. (A) Proposed mechanism of CO_2 photoreduction due to heterojunction formation over the Co-Al LDH-DS@TiO_2-NT heterojunction (adapted with permission from Ref. [212] @Copyright 2017 Wiley Online Library). (B) The photocatalytic conversion of CO_2 over ZnO, LDHs, and ZnO@LDHs catalysts under visible light (adapted with permission from Ref. [26] @Copyright 2016 Elsevier).

semiconductors. The CO_2 was first adsorbed at the LDH surface, and the type-II band alignment between the LDH and titania permitted efficient photoexcited charge separation, which resulted from the transfer of the electrons from the Co-Al LDH to the titania and the transfer of holes from the titania into the Co-Al-LDH nanostructure. The photoexcited holes oxidized H_2O to liberate O_2 and release protons that migrated to the interface with titania, where they combined with electrons and/or molecular carbon species to form H_2, CO, or CH_4 (Fig. 18 (A)) [212]. It was noteworthy that CH_4 was only produced over the Co-Al-LDH-DS@TiO_2-NT photocatalyst and not over the parent Co-Al-LDH and delaminated Co-Al-LDH-DS nanosheets. The production of CH_4 could be explained by the longest charge carrier lifetimes and slower kinetics induced by a larger heterojunction interface that favored the multielectron process of CH_4 formation.

Interestingly, the transfer of the photogenerated electrons or holes was opposite in another study. Guo et al. synthesized hierarchical ZnO@Cu-Zn-Al LDH heterostructures and used the catalysts for the photoreduction of CO_2 to hydrocarbons. The LDHs accepted photogenerated electrons transferred from ZnO because it had a more positive CB (+0.05 eV) than ZnO (−0.33 eV), while the photogenerated holes of the LDHs migrated to the VB of ZnO due to the more negative VB of ZnO (Fig. 18 (B)) [191]. The charge carrier transfer between the ZnO core to the LDH shell effectively depressed the recombination and was in favorable for CO_2 reduction [26].

The above examples represent two different types depending on the charge carrier separation mechanism: type-II [26] and p-n [191]. Proper control of the morphology of ZnO is also important for enhancing the efficiency of ZnO-based type-II heterojunction photocatalysts for CO_2 reduction. Compared to the conventional type-II heterojunction, the separation of the photogenerated electron-hole pairs on the surface can be accelerated by an electric field within the photocatalytic systems by forming p-n heterojunctions.

4.3.2. Doping with noble metal

Another effective way to synthesize visible-light-driven photocatalysts is noble metal doping. We have explored the application of Pd/Au bimetallic nanoparticle-loaded nanosheets in the catalytic reduction process [213]. To enhance the visible-light-induced photocatalytic activities, nanoparticles/LDH co-catalytic systems have been recently reported as the metal nanoparticles manifest the surface plasmon resonance (SPR) effect [172,207,214]. The morphologies and sizes of metal nanoparticles supported on the LDHs can substantially influence the catalytic activity. Therefore, the design of metal nanoparticles is very important. In addition, preparing a noble-metal-loaded three-component co-catalyst system has been used to enhance photocatalytic efficiency recently [25,215,216].

To date, a number of methods, including self-redox process, cathodic reduction, liquid phase reduction and photochemical deposition, have been studied for the fabrication of noble-metal-doped LDH nanocomposites [214,217,218]. $[Zn_3Ga(OH)_8]_2CO_3 \cdot mH_2O$ was combined with a sensitizer of silver or gold nanoparticles that were responsive to visible light. The rate of CO_2 photoreduction on Ag/Zn-Ga LDH increased by a factor of 1.69 compared to that of Zn-Ga LDH, while the methanol selectivity also increased from 39 to 54 mol%. On Au/Zn-Ga LDH, the reduction rate of CO_2 was 1.78 times higher than on Zn-Ga LDH, whereas the methanol selectivity decreased from 39 to 13 mol%. The electrons created by the SPR of Au were not able to photoreduce CO_2 under visible light, whereas the electrons in the LDH that were Eg-excited by UV light were trapped in Au and subsequently transferred to CO_2-derived species. As the potentials of the excited electrons at Au were lower (more positive) than those of the excited electrons at the CB of the Zn-Ga LDH, energetically favorable CO formation would have priority over methanol formation in the presence of UV light [207]. The results confirmed that for Ag/Zn-Ga LDH catalysts, CO_2 photoreduction by H_2 under visible light was promoted by the SPR effect of the Ag nanoparticles, while for the Au/Zn-Ga LDH catalysts, the Au nanoparticles may have acted as electron-trapping active sites (Fig. 19 (A)) [207]. Pt, Pd, and Au have also been identified as efficient co-catalysts for the photoreduction of CO_2 by Zn-Cr LDH. Among them, the 0.1 mass% Pt-loaded LDH exhibited the highest performance. This was attributed to the fact that noble metals can act as the co-catalysts not only for the reduction of recombination of electrons and holes but also for the enhancement of multi-electron reductive reactions (Fig. 19 (B)) [14]. Well-dispersed Ru nanoparticles embedded on exfoliated LDHs were prepared and used as highly active catalysts for CO_2 methanation under light irradiation. The high-efficiency photothermal conversion of CO_2 over Ru@FL-LDHs was ascribed to targeting and simultaneous activation of CO_2 and H_2 over ultrathin LDHs and Ru nanoparticles, respectively [172].

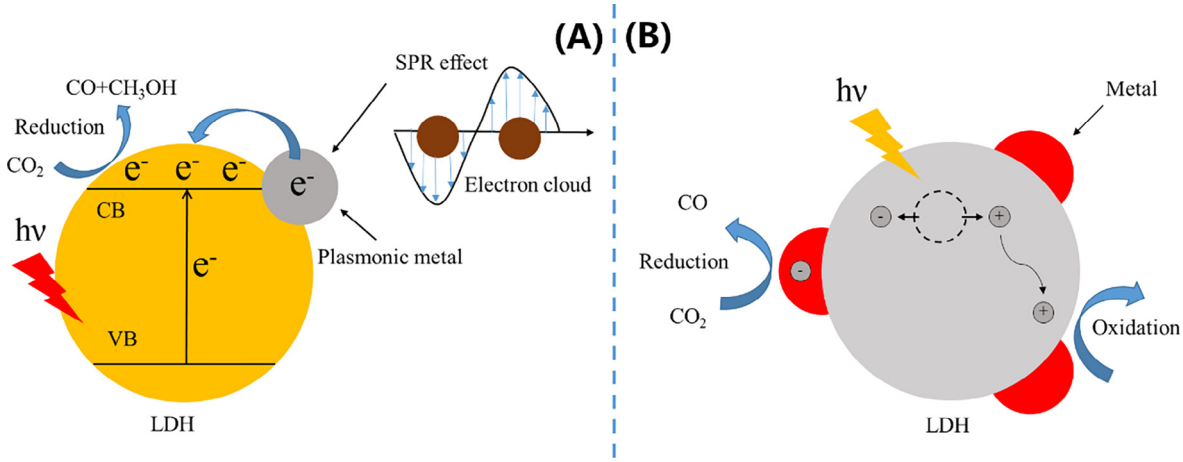

Fig. 19. Proposed electron flows in Ag/Zn-Ga LDH (A) and Pt/Zn-Cr LDH (B) during photocatalytic reduction of CO_2.

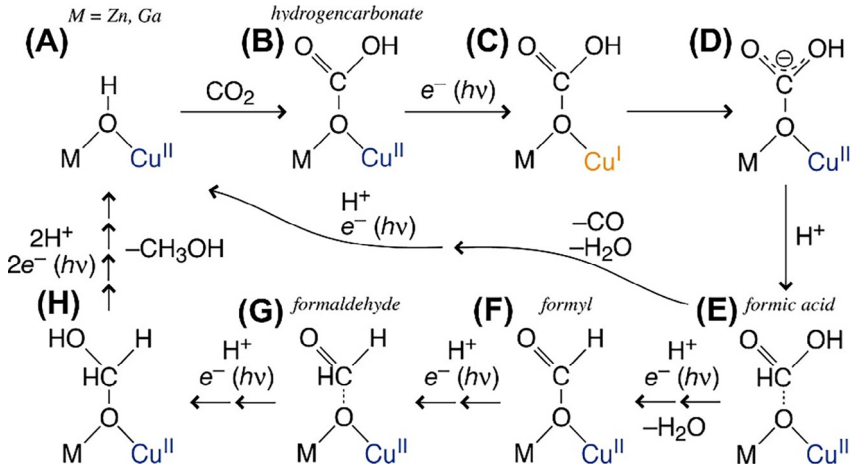

Fig. 20. Proposed photocatalytic catalytic cycle of CO_2 reduction to methanol or CO over Zn-Cu-Ga LDH catalysts (adapted with permission from Ref. [189] @Copyright 2011 Elsevier).

4.3.3. Ternary LDHs

In addition to binary LDHs, a series of ternary LDHs have also been used as photocatalysts for the photoreduction of CO_2. Recently, the photoreduction of CO_2 and H_2 into methanol was reported using semiconductor layered double hydroxide photocatalysts that were formulated as $[Zn^{II}_{1-x-y}Cu^{II}_{y}M^{III}_{x}(OH)_2]^{x+}_{2/x}(CO_3)^{2-}\cdot mH_2O$ (M = Ga, Al; $0 \le x \le 1/3$; $0 \le y \le 1/2$; m∼1/x). The inclusion of Cu sites in the LDH layers improved the methanol selectivity. The methanol selectivity (39 mol%) obtained using Zn-Cu LDH catalysts was improved to 68 mol% using Zn-Cu-Ga LDH catalysts under UV–visible light using hydrogen. Specific interaction of Cu sites with CO_2 was spectroscopically suggested to enable coupling with protons and photogenerated electrons to form methanol (Fig. 20). The key factor for determining the selectivity to methanol vs CO was suggested to be the binding of CO_2 at the Cu sites as hydrogen carbonate species Cu-O(-Zn)-C(OH)=O and Cu-O(-Ga)-C(OH)=O. Under UV–visible light, the Cu ions in the cationic layer facilitated charge separation utilizing the reduction-oxidation (redox) of $Cu^{II} \leftrightarrow Cu^{I}$. Hydrogen carbonate species were gradually reduced to formic acid, formaldehyde, and finally to methanol by utilizing the trapped photogenerated electrons as Cu^{I} ions [208]. Therefore, the interlayer spaces of these LDH photocatalysts served as active pockets for the reduction of CO_2 to methanol. The photoactive $[Cu(OH)_4]^{2-}$ sites could also be accommodated as anion species of the LDHs between the cationic layers, and the photocatalytic rates per unit amount of the Zn-Cu-Ga-$[Cu(OH)_4]^{2-}$ LDH were further optimized. The effects of the interlayer $[Cu(OH)_4]^{2-}$ were greater than those of the in-layer octahedral Cu sites because of its steric availability (accessibility) and semiconductivity (Eg values of 3.0–4.2 eV) [189]. In a more recent study, the same research group reported that if the Zn-Cu-Ga LDHs were preheated in vacuum and never in contact with air prior to the photoreduction tests, methanol was produced exclusively. This selectivity to methanol was attributed to the liberation of interlayer spaces by removing 31% of the interlayer water [219]. A series of Cu_2O-loaded Zn-Cr LDHs were prepared via an in-situ reduction process from Cu-Zn-Cr ternary LDHs. The Cu_2O could serve as an electron trap, reducing the recombination of photogenerated electrons and holes and increasing the photocatalytic efficiency. The photogenerated electrons reduced CO_2 to CO and the holes oxidized water to oxygen simultaneously. Almost 80% of the CO production was assigned to the reduction of CO_2 but not the incomplete oxidation products of the surface-adsorbed organic contaminants [196].

4.3.4. Other strategies

Recently, layered materials with thicknesses approaching atomic length scales have been fabricated, these structures can possess abundant coordinatively unsaturated metal cations, which serve as active centers for catalytic chemistry. Ultrathin Zn-Al LDH

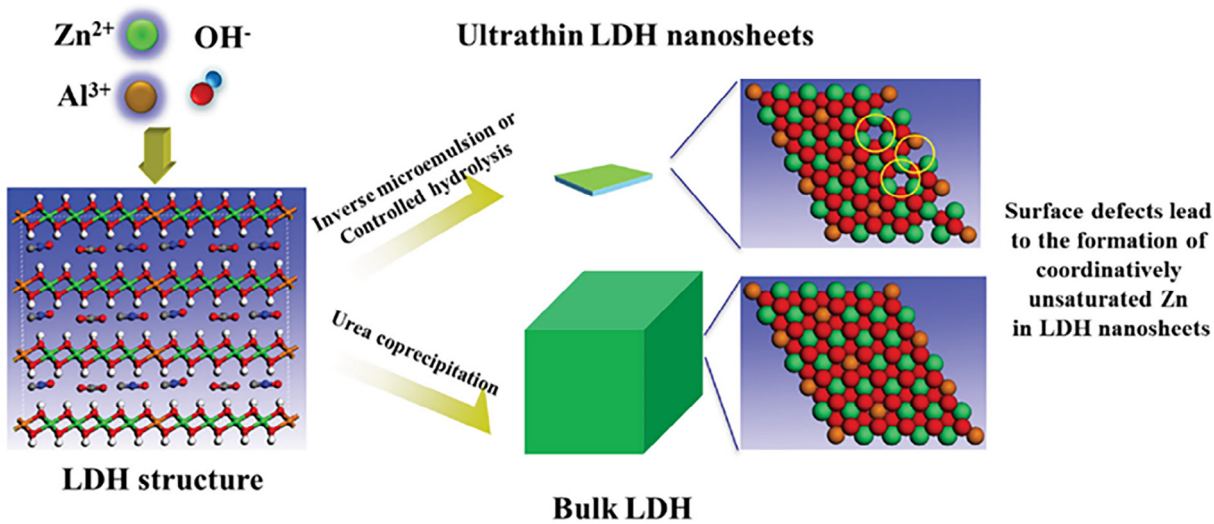

Fig. 21. Schematic showing the formation of coordinatively unsaturated ZnAl-LDH nanosheets (adapted with permission from Ref. [209] @Copyright 2015 Wiley Online Library).

nanosheets were synthesized, and these nanosheets exhibited extraordinarily high activities for the photoreduction of CO_2 to CO in the presence of water vapor. In comparison, the nano-sized Zn-Al LDH exhibited far superior CO_2 reduction photo catalytic activity than that of the equivalent bulk LDH. This was partially due to the formation of coordinatively unsaturated Zn structures that promoted the photoinduced charge separation (Fig. 21) [209]. In addition, the ultrathin LDH matrices provide considerable numbers of active sites for the chemical adsorption and activation of CO_2. Meanwhile, the Ru nanoparticles can dramatically increase the local temperature under light irradiation to activate H_2 and subsequently initiate the generation of CH_4 [172]. Cd-Al LDH microspheres exhibited a promising performance in the photoreduction of carbon dioxide using solar light. The abundance of OH groups on the surface of the microspheres increased the material's affinity toward carbon dioxide molecules [180].

Above all, pristine or functionalized LDHs are alternative and promising candidates for CO_2 reduction [172]. In general, their suitable surface properties and high water tolerance properties enable these LDHs to be ideal agents for the photocatalytic conversion of CO_2 in H_2O [181,185]. Therefore, finding novel functional groups and special material structures may give rise to unprecedented material properties, e.g., specific catalytic functionalities [188].

5. Strategies and future recommendations

In this paper, the current research progress in the CO_2 capture and photoreduction by the LDH-based materials over the last ten years (2009–2018) has been thoroughly reviewed. In order to improve their CO_2 capture capacities and selectivities, many attempts have been made, such as morphology control, doping the LDHs with alkali metal, modification of composition, and the formation of hybrid materials. LDH materials clearly demonstrate the great potential in this regard. Although considerable progress has been achieved in the field of adsorption and photoreduction of CO_2 by LDHs, studies still must be further developed, and at least the following aspects should be considered:

(1) For practical reaction-based CO_2 separation processes, the industrial standard is monoethanol amine (MEA), which has a CO_2 capture capacity of ca. 1.36 mmol/g. In comparison, the reported sorption capacities of LDH-based systems are still not high enough for industrial standards (seen from Table 1). Strategies for improving cyclical performance of new types of LDO could be extensively developed in the near future. Further development of hydrotalcites could focus on the intercalation of brucite layers with carbon dioxide accepting organic molecules, such as calixarenes, or the attachment of functional groups, such as amines, to their surfaces, to further enhance their capabilities for carbon dioxide desorption. The optimization of the synthesis methods and development of interesting composites offer a huge scope for future research.

(2) It is important to consider the pre-calcination time, the heating rate, cost analysis, and lifetime of the sorbent under actual regeneration conditions, which are crucial for industrial applications. Besides the co-adsorption of CO_2 and water, limited data on the co-adsorption of CO_2 and other gases in LDHs has been reported. When other acid gases exist in the feed gas, the adsorption performance of these new prepared materials is unknown. When considering LDHs for industrial separations of CO_2 from other gases, information on the reproducibility of the separation performance after long-term exposure to gas streams and the response of the materials to repetitive circulation are also needed. Therefore, parameters relevant to industrial operating conditions deserve systematic investigations for rational design of the adsorbents.

(3) Many LDH-based adsorbents have been produced from the waste for the removal of pollutant in aqueous systems [220–223]. Fabricating functional materials from the waste has become a trend in materials science. Until 2018, Gil et al. [224] first used hydrotalcite-like compounds prepared from aluminum saline slag wastes for the adsorption of CO_2. The CO_2 adsorption capacities of the synthesized hydrotalcites were even higher than the results reported by other authors in the literature. The development of LDH materials from the waste creates promising prospects for the CO_2 adsorption. More detailed studies on these LDHs should be conducted in the near future.

(4) It is highly desirable to prepare visible-light-driven photocatalysts that predominantly take advantage of solar energy. Insights into the active sites and structure-property correlations have been revealed in the field of using Co-Al LDH for

aldol condensation [225]. However, roles about the CO_2 reduction sites and the mechanisms between the structure-basic and site-ability in LDH-based materials have rarely been revealed and remain a challenge. Combined studies including XPS, XAFS, FTIR, TPD, and isotope monitoring can be applied to determine the LDH active site structures and the source of C used to produce the fuels. A thorough understanding of the reaction pathways, active sites, electron transfer dynamics, and reaction intermediates are keys for the design of photocatalysts.

(5) As shown in Table 2, research of modified materials has heavily focused on the binary hybrid systems, while the multi-hybrid LDH-based photocatalysts may also provide high photoreduction efficiencies. In addition, the exfoliated nanosheet LDHs have been widely used in the field of water splitting [226,227], which provide a new direction for further enhancing the photoreduction efficiency of CO_2. Moreover, the nanosheets of LDHs can be combined with organic and inorganic components to achieve long-term photocatalyst stability or high photoreduction efficiency. The high photoconversion efficiencies and improved light harvesting abilities can also be achieved through the combined use of optimized photoreactor and photocatalyst configurations. In particular, the combination of water photosplitting to form hydrogen (or protons and electrons) and CO_2 photoreduction with the formed hydrogen (or the formed protons and electrons) can potentially boost the efficiency of CO_2 conversion [228]. Studies on the performances of current photoreactor designs have been rarely reported. In order to achieve high conversion efficiencies, photoreactor designs must account for the material of construction, the thickness, the mass of catalyst, the reactor geometry (length, volume etc.), the flow rate, and the relationship between the reactor and irradiation source.

(6) Direct modification methods are usually preferred because the synthesis pathways are shorter and the consumption of chemicals is lower. Although many reports are available on the topic of LDH-based adsorbents and photocatalysts, the majority of the studies are limited to batch-scale only and are not fully developed at a commercial level to any extent, and therefore, more research is needed in this area. A comparison of the costs of LDHs relative to other CO_2 sorbents should be encouraged.

Acknowledgement

We thank the National Natural Science Foundation of China (51179068, 51679086, 51521006, 51879102). The authors also thank Miss sisi Cao for her help in the English writing.

References

[1] Q. Wang, H.H. Tay, Z. Zhong, J. Luo, A. Borgna, Synthesis of high-temperature CO_2 adsorbents from organo-layered double hydroxides with markedly improved CO_2 capture capacity, Energy Environ. Sci. 5 (2012) 7526, https://doi.org/10.1039/c2ee21409a.

[2] S. Wang, S. Yan, X. Ma, J. Gong, Recent advances in capture of carbon dioxide using alkali-metal-based oxides, Energy Environ. Sci. 4 (2011) 3805, https://doi.org/10.1039/c1ee01116b.

[3] X. Chen, Z. Wang, D.D. Wu, Modeling the price mechanism of carbon emission exchange in the European union emission trading system, Hum. Ecol. Risk Assess. Int. J. 19 (2013) 1309–1323, https://doi.org/10.1080/10807039.2012.719389.

[4] B. Yuan, X. Wu, Y. Chen, J. Huang, H. Luo, S. Deng, Adsorption of CO_2, CH_4, and N_2 on ordered mesoporous carbon: approach for greenhouse gases capture and biogas upgrading, Environ. Sci. Technol. 47 (2013) 5474–5480, https://doi.org/10.1021/es4000643.

[5] M. Sari Yilmaz, Synthesis of novel amine modified hollow mesoporous silica@Mg-Al layered double hydroxide composite and its application in CO2 adsorption, Microporous Mesoporous Mater. 245 (2017) 109–117, https://doi.org/10.1016/j.micromeso.2017.02.077.

[6] J. Wang, L. Huang, Y. Gao, R. Yang, Z. Zhang, Z. Guo, Q. Wang, A simple and reliable method for determining the delamination degree of nitrate and glycine intercalated LDHs in formamide, Chem. Commun. 50 (2014) 10130, https://doi.org/10.1039/C4CC05015K.

[7] N. MacDowell, N. Florin, A. Buchard, J. Hallett, A. Galindo, G. Jackson, C.S. Adjiman, C.K. Williams, N. Shah, P. Fennell, An overview of CO_2 capture technologies, Energy Environ. Sci. 3 (2010) 1645, https://doi.org/10.1039/c004106h.

[8] S. Kumar, J.de A. e Silva, M.Y. Wani, J.M. Gil, A.J.F.N. Sobral, Carbon dioxide capture and conversion by an environmentally friendly chitosan based meso-tetrakis(4-sulfonatophenyl) porphyrin, Carbohydr. Polym. 175 (2017) 575–583, https://doi.org/10.1016/j.carbpol.2017.08.031.

[9] R. Balasubramanian, S. Chowdhury, Recent advances and progress in the development of graphene-based adsorbents for CO_2 capture, J. Mater. Chem. A 3 (2015) 21968–21989, https://doi.org/10.1039/c5ta04822b.

[10] Q. Wang, Y. Gao, J. Luo, Z. Zhong, A. Borgna, Z. Guo, D. O'Hare, Synthesis of nano-sized spherical $Mg_3Al–CO_3$ layered double hydroxide as a high-temperature CO_2 adsorbent, RSC Adv. 3 (2013) 3414, https://doi.org/10.1039/c2ra22607c.

[11] M. Maroño, Y. Torreiro, L. Gutierrez, Influence of steam partial pressures in the CO_2 capture capacity of K-doped hydrotalcite-based sorbents for their application to SEWGS processes, Int. J. Greenh. Gas Control. 14 (2013) 183–192, https://doi.org/10.1016/j.ijggc.2013.01.024.

[12] Q. Wang, D. O'Hare, Recent advances in the synthesis and application of layered double hydroxide (LDH) nanosheets, Chem. Rev. 112 (2012) 4124–4155, https://doi.org/10.1021/cr200434v.

[13] M.R. Othman, Z. Helwani, Martunus, W.J.N. Fernando, Synthetic hydrotalcites from different routes and their application as catalysts and gas adsorbents: a review, Appl Organomet. Chem. 23 (2009) 335–346, https://doi.org/10.1002/aoc.1517.

[14] S. Iguchi, Y. Hasegawa, K. Teramura, S. Hosokawa, T. Tanaka, Preparation of transition metal-containing layered double hydroxides and application to the photocatalytic conversion of CO_2 in water, J. CO_2 Util. 15 (2016) 6–14, https://doi.org/10.1016/j.jcou.2016.04.001.

[15] S. Das, W.M.A. Wan Daud, A review on advances in photocatalysts towards CO_2 conversion, RSC Adv. 4 (2014) 20856, https://doi.org/10.1039/c4ra01769b.

[16] F.N. Ridha, V. Manovic, A. Macchi, M.A. Anthony, E.J. Anthony, Assessment of limestone treatment with organic acids for CO_2 capture in Ca-looping cycles, Fuel Process. Technol. 116 (2013) 284–291, https://doi.org/10.1016/j.fuproc.2013.07.007.

[17] Z. Zhang, Y. Xiao, B. Wang, Q. Sun, H. Liu, Waste is a misplayed resource: synthesis of zeolites from fly ash for CO_2 capture, Energy Procedia. 114 (2017) 2537–2544, https://doi.org/10.1016/j.egypro.2017.08.036.

[18] A. Arefi Pour, S. Sharifnia, R. NeishaboriSalehi, M. Ghodrati, Performance evaluation of clinoptilolite and 13X zeolites in CO_2 separation from CO_2/CH_4 mixture, J. Nat. Gas Sci. Eng. 26 (2015) 1246–1253, https://doi.org/10.1016/j.jngse.2015.08.033.

[19] M. Wei, Q. Yu, H. Xie, Z. Zuo, L. Hou, F. Yang, Kinetics studies of CO_2 adsorption and desorption on waste ion-exchange resin-based activated carbon, Int. J. Hydrogen Energy 42 (2017) 27122–27129, https://doi.org/10.1016/j.ijhydene.2017.09.102.

[20] A. Silvestre-Albero, J. Silvestre-Albero, M. Martínez-Escandell, F. Rodríguez-Reinoso, Micro/mesoporous activated carbons derived from polyaniline: promising candidates for CO_2 adsorption, Ind. Eng. Chem. Res. 53 (2014) 15398–15405, https://doi.org/10.1021/ie5013129.

[21] L.K.G. Bhatta, S. Subramanyam, M.D. Chengala, U.M. Bhatta, K. Venkatesh, Low-temperature CO_2 adsorption on Titania nanotubes (TNTs), Surf. Interfaces 8 (2017) 158–162, https://doi.org/10.1016/j.surfin.2017.06.001.

[22] S. Delavari, N.A.S. Amin, M. Ghaedi, Photocatalytic conversion and kinetic study of CO_2 and CH_4 over nitrogen-doped titania nanotube arrays, J. Clean. Prod. 111 (2016) 143–154, https://doi.org/10.1016/j.jclepro.2015.07.077.

[23] Z. Xiong, Z. Lei, S. Ma, X. Chen, B. Gong, Y. Zhao, J. Zhang, C. Zheng, J.C.S. Wu, Photocatalytic CO_2 reduction over V and W codoped TiO_2 catalyst in an internal-illuminated honeycomb photoreactor under simulated sunlight irradiation, Appl. Catal. B Environ. 219 (2017) 412–424, https://doi.org/10.1016/j.apcatb.2017.07.078.

[24] W. Dai, J. Yu, Y. Deng, X. Hu, T. Wang, X. Luo, Facile synthesis of MoS_2/Bi_2WO_6 nanocomposites for enhanced CO_2 photoreduction activity under visible light irradiation, Appl. Surf. Sci. 403 (2017) 230–239, https://doi.org/10.1016/j.apsusc.2017.01.171.

[25] J. Hong, W. Zhang, Y. Wang, T. Zhou, R. Xu, Photocatalytic reduction of carbon dioxide over self-assembled carbon nitride and layered double hydroxide: the role of carbon dioxide enrichment, ChemCatChem 6 (2014) 2315–2321, https://doi.org/10.1002/cctc.201402195.

[26] Q. Guo, Q. Zhang, H. Wang, Z. Liu, Z. Zhao, Core-shell structured ZnO@Cu-Zn–Al layered double hydroxides with enhanced photocatalytic efficiency for CO_2 reduction, Catal. Commun. 77 (2016) 118–122, https://doi.org/10.1016/j.catcom.2016.01.019.

[27] Y. Gao, Z. Zhang, J. Wu, X. Yi, A. Zheng, A. Umar, D. O'Hare, Q. Wang, Comprehensive investigation of CO2 adsorption on Mg–Al–CO3 LDH-derived

mixed metal oxides, J. Mater. Chem. A 1 (2013) 12782, https://doi.org/10.1039/c3ta13039h.
[28] H. Pfeiffer, E. Lima, V. Lara, J.S. Valente, Thermokinetic study of the rehydration process of a calcined MgAl-layered double hydroxide, Langmuir 26 (2010) 4074–4079, https://doi.org/10.1021/la9035248.
[29] J.S. Valente, H. Pfeiffer, E. Lima, J. Prince, J. Flores, Cyanoethylation of alcohols by activated Mg–Al layered double hydroxides: Influence of rehydration conditions and Mg/Al molar ratio on Brönsted basicity, J. Catal. 279 (2011) 196–204, https://doi.org/10.1016/j.jcat.2011.01.018.
[30] Q. Yang, Y. Zhong, X. Li, X. Li, K. Luo, X. Wu, H. Chen, Y. Liu, G. Zeng, Adsorption-coupled reduction of bromate by Fe(II)–Al(III) layered double hydroxide in fixed-bed column: experimental and breakthrough curves analysis, J. Ind. Eng. Chem. 28 (2015) 54–59, https://doi.org/10.1016/j.jiec.2015.01.022.
[31] Q. Xinhong, K. Sasaki, Removal mechanism of polymeric borate by calcined layered double hydroxides containing different divalent metals, Colloids Surf. Physicochem. Eng. Asp. 482 (2015) 702–709, https://doi.org/10.1016/j.colsurfa.2015.07.036.
[32] C. Gong, F. Chen, Q. Yang, K. Luo, F. Yao, S. Wang, X. Wang, J. Wu, X. Li, D. Wang, G. Zeng, Heterogeneous activation of peroxymonosulfate by Fe-Co layered doubled hydroxide for efficient catalytic degradation of Rhoadmine B, Chem. Eng. J. 321 (2017) 222–232, https://doi.org/10.1016/j.cej.2017.03.117.
[33] G. Mascolo, M.C. Mascolo, On the synthesis of layered double hydroxides (LDHs) by reconstruction method based on the "memory effect ", Microporous Mesoporous Mater. 214 (2015) 246–248, https://doi.org/10.1016/j.micromeso.2015.03.024.
[34] X. Yuan, Y. Wang, J. Wang, C. Zhou, Q. Tang, X. Rao, Calcined graphene/MgAl-layered double hydroxides for enhanced Cr(VI) removal, Chem. Eng. J. 221 (2013) 204–213, https://doi.org/10.1016/j.cej.2013.01.090.
[35] Y. Guo, Z. Zhu, Y. Qiu, J. Zhao, Enhanced adsorption of acid brown 14 dye on calcined Mg/Fe layered double hydroxide with memory effect, Chem. Eng. J. 219 (2013) 69–77, https://doi.org/10.1016/j.cej.2012.12.084.
[36] K.H. Goh, T.T. Lim, Z. Dong, Application of layered double hydroxides for removal of oxyanions: a review, Water Res. 42 (2008) 1343–1368, https://doi.org/10.1016/j.watres.2007.10.043.
[37] Z. Yong, A.E. Rodrigues, Hydrotalcite-like compounds as adsorbents for carbon dioxide, Energy Convers.Manag. 43 (2002) 1865–1876, https://doi.org/10.1016/S0196-8904(01)00125-X.
[38] L.K.G. Bhatta, S. Subramanyam, M.D. Chengala, S. Olivera, K. Venkatesh, Progress in hydrotalcite like compounds and metal-based oxides for CO_2 capture: a review, J. Clean. Prod. 103 (2015) 171–196, https://doi.org/10.1016/j.jclepro.2014.12.059.
[39] F. Cavani, F. Trifirò, A. Vaccari, Hydrotalcite-type anionic clays: preparation, properties and applications, Catal. Today 11 (1991) 173–301, https://doi.org/10.1016/0920-5861(91)80068-K.
[40] Y. Zhao, X. Jia, G.I.N. Waterhouse, L.Z. Wu, C.H. Tung, D. O'Hare, T. Zhang, Layered double hydroxide nanostructured photocatalysts for renewable energy production, Adv. Energy Mater. 6 (2016) 1501974, https://doi.org/10.1002/aenm.201501974.
[41] Z. Yang, F. Wang, C. Zhang, G. Zeng, X. Tan, Z. Yu, Y. Zhong, H. Wang, F. Cui, Utilization of LDH-based materials as potential adsorbents and photocatalysts for the decontamination of dyes wastewater: a review, RSC Adv. 6 (2016) 79415–79436, https://doi.org/10.1039/C6RA12727D.
[42] R. Dębek, M. Motak, T. Grzybek, M. Galvez, P. Da Costa, A short review on the catalytic activity of hydrotalcite-derived materials for dry reforming of methane, Catalysts 7 (2017) 32, https://doi.org/10.3390/catal7010032.
[43] J. Wang, L. Huang, R. Yang, Z. Zhang, J. Wu, Y. Gao, Q. Wang, D. O'Hare, Z. Zhong, Recent advances in solid sorbents for CO_2 capture and new development trends, Energy Env. Sci. 7 (2014) 3478–3518, https://doi.org/10.1039/C4EE01647E.
[44] L. Mohapatra, K. Parida, A review on the recent progress, challenges and perspective of layered double hydroxides as promising photocatalysts, J. Mater. Chem. A 4 (2016) 10744–10766, https://doi.org/10.1039/C6TA01668E.
[45] Y. Lwin, F. Abdullah, High temperature adsorption of carbon dioxide on Cu–Al hydrotalcite-derived mixed oxides: kinetics and equilibria by thermogravimetry, J. Therm. Anal. Calorim. 97 (2009) 885–889, https://doi.org/10.1007/s10973-009-0156-7.
[46] N.N.A.H. Meis, J.H. Bitter, K.P. de Jong, Support and size effects of activated hydrotalcites for precombustion CO_2 capture, Ind. Eng. Chem. Res. 49 (2010) 1229–1235, https://doi.org/10.1021/ie901114d.
[47] L. Huang, J. Wang, Y. Gao, Y. Qiao, Q. Zheng, Z. Guo, Y. Zhao, D. O'Hare, Q. Wang, Synthesis of $LiAl_2$-layered double hydroxides for CO_2 capture over a wide temperature range, J. Mater. Chem. A 2 (2014) 18454–18462, https://doi.org/10.1039/C4TA04065A.
[48] Q. Qin, J. Wang, T. Zhou, Q. Zheng, L. Huang, Y. Zhang, P. Lu, A. Umar, B. Louis, Q. Wang, Impact of organic interlayer anions on the CO_2 adsorption performance of Mg-Al layered double hydroxides derived mixed oxides, J. Energy Chem. 26 (2017) 346–353, https://doi.org/10.1016/j.jechem.2017.01.003.
[49] X. Zhu, Q. Wang, Y. Shi, N. Cai, Layered double oxide/activated carbon-based composite adsorbent for elevated temperature H_2/CO_2 separation Int, J. Hydrogen Energy. 40 (2015) 9244–9253, https://doi.org/10.1016/j.ijhydene.2015.05.116.
[50] A. Hanif, S. Dasgupta, S. Divekar, A. Arya, M.O. Garg, A. Nanoti, A study on high temperature CO_2 capture by improved hydrotalcite sorbents, Chem. Eng., J. 236 (2014) 91–99, https://doi.org/10.1016/j.cej.2013.09.076.
[51] J.M. Lee, Y.J. Min, K.B. Lee, S.G. Jeon, J.G. Na, H.J. Ryu, Enhancement of CO_2 sorption uptake on hydrotalcite by impregnation with K_2CO_3, Langmuir 26 (2010) 18788–18797, https://doi.org/10.1021/la102974s.
[52] Q. Wang, H.H. Tay, D.J.W. Ng, L. Chen, Y. Liu, J. Chang, Z. Zhong, J. Luo, A. Borgna, The effect of trivalent cations on the performance of Mg-M-CO_3 layered double hydroxides for high-temperature CO_2 capture, ChemSusChem 3 (2010) 965–973, https://doi.org/10.1002/cssc.201000099.
[53] E.L.G. Oliveira, C.A. Grande, A.E. Rodrigues, CO_2 sorption on hydrotalcite and alkali-modified (K and Cs) hydrotalcites at high temperatures, Sep. Purif. Technol. 62 (2008) 137–147, https://doi.org/10.1016/j.seppur.2008.01.011.
[54] K. Coenen, F. Gallucci, P. Cobden, E. van Dijk, E. Hensen, M. van Sint Annaland, Chemisorption working capacity and kinetics of CO_2 and H_2O of hydrotalcite-based adsorbents for sorption-enhanced water-gas-shift applications, Chem. Eng. J. 293 (2016) 9–23, https://doi.org/10.1016/j.cej.2016.02.050.
[55] M.J. Ramírez-Moreno, I.C. Romero-Ibarra, M.A. Hernández-Pérez, H. Pfeiffer, CO_2 adsorption at elevated pressure and temperature on Mg–Al layered double hydroxide, Ind. Eng. Chem. Res. 53 (2014) 8087–8094, https://doi.org/10.1021/ie5010515.
[56] D.A. Torres-Rodríguez, E. Lima, J.S. Valente, H. Pfeiffer, CO_2 capture at low temperatures (30–80°C) and in the presence of water vapor over a thermally activated Mg–Al layered double hydroxide, J. Phys. Chem. A 115 (2011) 12243–12250, https://doi.org/10.1021/jp207836m.
[57] Y. Zheng, Y. Shi, S. Li, Y. Yang, N. Cai, Elevated temperature hydrogen/carbon dioxide separation process simulation by integrating elementary reaction model of hydrotalcite adsorbent, Int. J. Hydrogen Energy 39 (2014) 3771–3779, https://doi.org/10.1016/j.ijhydene.2013.12.167.
[58] H. Du, A.D. Ebner, J.A. Ritter, Pressure dependence of the nonequilibrium kinetic model that describes the adsorption and desorption behavior of CO_2 in K-promoted hydrotalcite like compound, Ind. Eng. Chem. Res. 50 (2011) 412–418, https://doi.org/10.1021/ie100965b.
[59] X. Zhu, Y. Shi, N. Cai, High-pressure carbon dioxide adsorption kinetics of potassium-modified hydrotalcite at elevated temperature, Fuel 207 (2017) 579–590, https://doi.org/10.1016/j.fuel.2017.06.137.
[60] M.K. Ram Reddy, Z.P. Xu, J.C. Diniz da Costa, Influence of water on high-temperature CO_2 capture using layered double hydroxide derivatives, Ind. Eng. Chem. Res. 47 (2008) 2630–2635, https://doi.org/10.1021/ie0716060.
[61] J. Boon, P.D. Cobden, H.A.J. van Dijk, C. Hoogland, E.R. van Selow, M. van Sint Annaland, Isotherm model for high-temperature, high-pressure adsorption of and on K-promoted hydrotalcite, Chem. Eng. J. 248 (2014) 406–414, https://doi.org/10.1016/j.cej.2014.03.056.
[62] E.R. van Selow, P.D. Cobden, H.A.J. van Dijk, S. Walspurger, P.A. Verbraeken, D. Jansen, Qualification of the ALKASORB sorbent for the sorption-enhanced water-gas shift process, Energy Procedia 37 (2013) 180–189, https://doi.org/10.1016/j.egypro.2013.05.100.
[63] M.A. Othman, W.M. Zahid, A.E. Abasaeed, Selectivity of layered double hydroxides and their derivative mixed metal oxides as sorbents of hydrogen sulfide, J. Hazard. Mater. 254–255 (2013) 221–227, https://doi.org/10.1016/j.jhazmat.2013.03.030.
[64] J. Li, F.P. Chen, G.P. Jin, X.S. Feng, X.X. Li, Removals of aqueous sulfur dioxide and hydrogen sulfide using CeO_2-NiAl-LDHs coating activated carbon and its mix with carbon nano-tubes, Colloids Surf. Physicochem. Eng. Asp. 476 (2015) 90–97, https://doi.org/10.1016/j.colsurfa.2015.03.026.
[65] T. Kameda, A. Kodama, Y. Fubasami, S. Kumagai, T. Yoshioka, Removal of SO_2 with a Mg−Al oxide slurry via reconstruction of a Mg−Al layered double hydroxide, Chemosphere 88 (2012) 250–254, https://doi.org/10.1016/j.chemosphere.2012.03.045.
[66] T. Kameda, N. Uchiyama, T. Yoshioka, Removal of HCl, SO_2, and NO by treatment of acid gas with Mg–Al oxide slurry, Chemosphere 82 (2011) 587–591, https://doi.org/10.1016/j.chemosphere.2010.11.020.
[67] H.A.J. van Dijk, S. Walspurger, P.D. Cobden, R.W. van den Brink, F.G. de Vos, Testing of hydrotalcite-based sorbents for CO_2 and H_2S capture for use in sorption enhanced water gas shift, Int. J. Greenh. Gas Control 5 (2011) 505–511, https://doi.org/10.1016/j.ijggc.2010.04.011.
[68] Y. Torreiro, M. Maroño, J.M. Sánchez, Study of sour water gas shift using hydrotalcite based sorbents, Fuel 187 (2017) 58–67, https://doi.org/10.1016/j.fuel.2016.09.038.
[69] M.K.R. Reddy, Z.P. Xu, G.Q. (Max) Lu, J.C. Diniz da Costa, Effect of SO_x adsorption on layered double hydroxides for CO_2 capture, Ind. Eng. Chem. Res. 47 (2008) 7357–7360, https://doi.org/10.1021/ie8004226.
[70] R. Singh, M.K. Ram Reddy, S. Wilson, K. Joshi, J.C. Diniz da Costa, P. Webley, High temperature materials for CO_2 capture, Energy Procedia. 1 (2009) 623–630, https://doi.org/10.1016/j.egypro.2009.01.082.
[71] K. Coenen, F. Gallucci, G. Pio, P. Cobden, E. van Dijk, E. Hensen, M. van Sint, Annaland On the influence of steam on the CO_2 chemisorption capacity of a hydrotalcite-based adsorbent for SEWGS applications, Chem. Eng. J. 314 (2017) 554–569, https://doi.org/10.1016/j.cej.2016.12.013.
[72] E.R. van Selow, P.D. Cobden, A.D. Wright, R.W. van den Brink, D. Jansen, Improved sorbent for the sorption-enhanced water-gas shift process, Energy Procedia. 4 (2011) 1090–1095, https://doi.org/10.1016/j.egypro.2011.01.159.
[73] N.D. Hutson, B.C. Attwood, High temperature adsorption of CO_2 on various hydrotalcite-like compounds, Adsorption 14 (2008) 781–789, https://doi.org/10.1007/s10450-007-9085-6.
[74] X.P. Wang, J.J. Yu, J. Cheng, Z.P. Hao, Z.P. Xu, High-temperature adsorption of carbon dioxide on mixed oxides derived from hydrotalcite-like compounds, Environ. Sci. Technol. 42 (2008) 614–618, https://doi.org/10.1021/es072085a.

[75] M. León, E. Díaz, S. Bennici, A. Vega, S. Ordóñez, A. Auroux, Adsorption of CO_2 on hydrotalcite-derived mixed oxides: sorption mechanisms and consequences for adsorption irreversibility, Ind. Eng. Chem. Res. 49 (2010) 3663–3671, https://doi.org/10.1021/ie902072a.
[76] X. Kou, H. Guo, E.G. Ayele, S. Li, Y. Zhao, S. Wang, X. Ma, Adsorption of CO_2 on MgAl-CO_3 LDHs-derived sorbents with 3D nanoflower-like structure, Energy Fuels 32 (2018) 5313–5320, https://doi.org/10.1021/acs.energyfuels.8b00024.
[77] Q. Wang, H.H. Tay, Z. Guo, L. Chen, Y. Liu, J. Chang, Z. Zhong, J. Luo, A. Borgna, Morphology and composition controllable synthesis of Mg–Al–CO_3 hydrotalcites by tuning the synthesis pH and the CO_2 capture capacity, Appl. Clay Sci. 55 (2012) 18–26, https://doi.org/10.1016/j.clay.2011.07.024.
[78] S. Zeng, X. Xu, S. Wang, Q. Gong, R. Liu, Y. Yu, Sand flower layered double hydroxides synthesized by co-precipitation for CO_2 capture: morphology evolution mechanism, agitation effect and stability, Mater. Chem. Phys. 140 (2013) 159–167, https://doi.org/10.1016/j.matchemphys.2013.03.015.
[79] T.M. Rossi, J.C. Campos, M.M.V.M. Souza, CO_2 capture by Mg–Al and Zn–Al hydrotalcite-like compounds, Adsorption 22 (2016) 151–158, https://doi.org/10.1007/s10450-015-9732-2.
[80] M. Dadwhal, T.W. Kim, M. Sahimi, T.T. Tsotsis, Study of CO_2 diffusion and adsorption on calcined layered double hydroxides: the effect of particle size Ind, Eng. Chem. Res. 47 (2008) 6150–6157, https://doi.org/10.1021/ie701701d.
[81] Q. Wang, Z. Wu, H.H. Tay, L. Chen, Y. Liu, J. Chang, Z. Zhong, J. Luo, A. Borgna, High temperature adsorption of CO_2 on Mg–Al hydrotalcite: effect of the charge compensating anions and the synthesis pH, Catal. Today 164 (2011) 198–203, https://doi.org/10.1016/j.cattod.2010.10.042.
[82] G.V. Manohara, Exfoliation of layered double hydroxides (LDHs): a new route to mineralize atmospheric CO_2, RSC Adv. 4 (2014) 46126–46132, https://doi.org/10.1039/C4RA08865D.
[83] M.R. Martunus, W.J.N. Othman, Fernando Elevated temperature carbon dioxide capture via reinforced metal hydrotalcite, Microporous Mesoporous Mater. 138 (2011) 110–117, https://doi.org/10.1016/j.micromeso.2010.09.023.
[84] Y. Qiao, J. Wang, L. Huang, Q. Zheng, D. O'Hare, Q. Wang, LDH/$MgCO_3$ hybrid multilayer on an aluminium substrate as a novel high-temperature CO_2 adsorbent, RSC Adv. 5 (2015) 82777–82780, https://doi.org/10.1039/C5RA19170J.
[85] E. van Dijk, S. Walspurger, P. Cobden, R. van den Brink, Testing of hydrotalcite based sorbents for CO_2 and H_2S capture for use in sorption enhanced water gas shift, Energy Procedia 4 (2011) 1110–1117, https://doi.org/10.1016/j.egypro.2011.01.162.
[86] Y.J. Wu, P. Li, J.G. Yu, A.F. Cunha, A.E. Rodrigues, K-promoted hydrotalcites for CO_2 capture in sorption enhanced reactions, Chem. Eng. Technol. 36 (2013) 567–574, https://doi.org/10.1002/ceat.201200694.
[87] C.V. Miguel, R. Trujillano, V. Rives, M.A. Vicente, A.F.P. Ferreira, A.E. Rodrigues, A. Mendes, L.M. Madeira, High temperature CO_2 sorption with gallium-substituted and promoted hydrotalcites, Sep. Purif. Technol. 127 (2014) 202–211, https://doi.org/10.1016/j.seppur.2014.03.007.
[88] J.M. Silva, R. Trujillano, V. Rives, M.A. Soria, L.M. Madeira, High temperature CO_2 sorption over modified hydrotalcites, Chem. Eng. J. 325 (2017) 25–34, https://doi.org/10.1016/j.cej.2017.05.032.
[89] C.T. Yavuz, B.D. Shinall, A.V. Iretskii, M.G. White, T. Golden, M. Atilhan, P.C. Ford, G.D. Stucky, Markedly improved CO_2 capture efficiency and stability of gallium substituted hydrotalcites at elevated temperatures, Chem. Mater. 21 (2009) 3473–3475, https://doi.org/10.1021/cm900834g.
[90] O. Aschenbrenner, P. McGuire, S. Alsamaq, J. Wang, S. Supasitmongkol, B. Al-Duri, P. Styring, J. Wood, Adsorption of carbon dioxide on hydrotalcite-like compounds of different compositions, Chem. Eng. Res. Des. 89 (2011) 1711–1721, https://doi.org/10.1016/j.cherd.2010.09.019.
[91] J. Wang, L.A. Stevens, T.C. Drage, J. Wood, Preparation and CO_2 adsorption of amine modified Mg–Al LDH via exfoliation route, Chem. Eng. Sci. 68 (2012) 424–431, https://doi.org/10.1016/j.ces.2011.09.052.
[92] C.I. Ezeh, X. Huang, X. Yang, C. Sun, J. Wang, Sonochemical surface functionalization of exfoliated LDH: Effect on textural properties, CO_2 adsorption, cyclic regeneration capacities and subsequent gas uptake for simultaneous methanol synthesis, Ultrason. Sonochem. 39 (2017) 330–343, https://doi.org/10.1016/j.ultsonch.2017.04.041.
[93] N. Tang, T. He, J. Liu, L. Li, H. Shi, W. Cen, Z. Ye, New insights into CO_2 adsorption on layered double hydroxide (LDH)-based nanomaterials, Nanoscale Res. Lett. 13 (2018), https://doi.org/10.1186/s11671-018-2471-z.
[94] S. Kim, S.G. Jeon, K.B. Lee, High-temperature CO_2 sorption on hydrotalcite having a high Mg/Al molar ratio, ACS Appl. Mater. Interfaces 8 (2016) 5763–5767, https://doi.org/10.1021/acsami.5b12598.
[95] N.N.A.H. Meis, J.H. Bitter, K.P. de Jong, On the influence and role of alkali metals on supported and unsupported activated hydrotalcites for CO_2 sorption, Ind. Eng. Chem. Res. 49 (2010) 8086–8093, https://doi.org/10.1021/ie902016f.
[96] D. Iruretagoyena, M.S.P. Shaffer, D. Chadwick, Layered double oxides supported on graphene oxide for CO_2 adsorption: effect of support and residual sodium, Ind. Eng. Chem. Res. 54 (2015) 6781–6792, https://doi.org/10.1021/acs.iecr.5b01215.
[97] A. Garcia-Gallastegui, D. Iruretagoyena, V. Gouvea, M. Mokhtar, A.M. Asiri, S. N. Basahel, S.A. Al-Thabaiti, A.O. Alyoubi, D. Chadwick, M.S.P. Shaffer, Graphene oxide as support for layered double hydroxides: enhancing the CO_2 adsorption capacity, Chem. Mater. 24 (2012) 4531–4539, https://doi.org/10.1021/cm3018264.
[98] D. Iruretagoyena, M.S.P. Shaffer, D. Chadwick, Adsorption of carbon dioxide on graphene oxide supported layered double oxides, Adsorption 20 (2014) 321–330, https://doi.org/10.1007/s10450-013-9595-3.
[99] J. Wang, X. Mei, L. Huang, Q. Zheng, Y. Qiao, K. Zang, S. Mao, R. Yang, Z. Zhang, Y. Gao, Z. Guo, Z. Huang, Q. Wang, Synthesis of layered double hydroxides/graphene oxide nanocomposite as a novel high-temperature CO_2 adsorbent, J. Energy Chem. 24 (2015) 127–137, https://doi.org/10.1016/S2095-4956(15)60293-5.
[100] M. De Marco, R. Menzel, S.M. Bawaked, M. Mokhtar, A.Y. Obaid, S.N. Basahel, M.S.P. Shaffer, Hybrid effects in graphene oxide/carbon nanotube-supported layered double hydroxides: enhancing the CO_2 sorption properties, Carbon 123 (2017) 616–627, https://doi.org/10.1016/j.carbon.2017.07.094.
[101] D. Iruretagoyena, X. Huang, M.S.P. Shaffer, D. Chadwick, Influence of alkali metals (Na, K, and Cs) on CO_2 adsorption by layered double oxides supported on graphene oxide, Ind. Eng. Chem. Res. 54 (2015) 11610–11618, https://doi.org/10.1021/acs.iecr.5b02762.
[102] H.B. Mohd Sidek, Y.K. Jo, I.Y. Kim, S.J. Hwang, Stabilization of layered double oxide in hybrid matrix of graphene and layered metal oxide nanosheets: an effective way to explore efficient CO_2 adsorbent, J. Phys. Chem. C 120 (2016) 23421–23429, https://doi.org/10.1021/acs.jpcc.6b08065.
[103] M.H. Halabi, M.H.J.M. de Croon, J. van der Schaaf, P.D. Cobden, J.C. Schouten, High capacity potassium-promoted hydrotalcite for CO_2 capture in H_2 production, Int. J. Hydrogen Energy 37 (2012) 4516–4525, https://doi.org/10.1016/j.ijhydene.2011.12.003.
[104] L.K.G. Bhatta, S. Subramanyam, M.D. Chengala, U.M. Bhatta, P. Guha, R.P.H. Dinakar, K. Venkatesh, Layered double hydroxides/multiwalled carbon nanotubes-based composite for high-temperature CO_2 adsorption, Energy Fuels 30 (2016) 4244–4250, https://doi.org/10.1021/acs.energyfuels.6b00141.
[105] H.J. Jang, C.H. Lee, S. Kim, S.H. Kim, K.B. Lee, Hydrothermal synthesis of K_2CO_3-promoted hydrotalcite from hydroxide-form precursors for novel high-temperature CO_2 sorbent, ACS Appl. Mater. Interfaces 6 (2014) 6914–6919, https://doi.org/10.1021/am500720f.
[106] A. Garcia-Gallastegui, D. Iruretagoyena, M. Mokhtar, A.M. Asiri, S.N. Basahel, S.A. Al-Thabaiti, A.O. Alyoubi, D. Chadwick, M.S.P. Shaffer, Layered double hydroxides supported on multi-walled carbon nanotubes: preparation and CO_2 adsorption characteristics, J. Mater. Chem. 22 (2012) 13932, https://doi.org/10.1039/c2jm00059h.
[107] J. Wang, L. Huang, Q. Zheng, Y. Qiao, Q. Wang, Layered double hydroxides/oxidized carbon nanotube nanocomposites for CO_2 capture, J. Ind. Eng. Chem. 36 (2016) 255–262, https://doi.org/10.1016/j.jiec.2016.02.010.
[108] J.L. Gunjakar, I.Y. Kim, S.J. Hwang, Efficient hybrid-type CO_2 adsorbents of reassembled layered double hydroxide 2d nanosheets with polyoxometalate 0d nanoclusters: efficient hybrid-type CO_2 adsorbents, Eur. J. Inorg. Chem. 2015 (2015) 1198–1202, https://doi.org/10.1002/ejic.201402480.
[109] S. Li, Y. Shi, Y. Yang, Y. Zheng, N. Cai, High-performance CO_2 adsorbent from interlayer potassium-promoted stearate-pillared hydrotalcite precursors 130819124454008 Energy Fuels (2013), https://doi.org/10.1021/ef400914r.
[110] C.V. Pramod, K. Upendar, V. Mohan, D.S. Sarma, G.M. Dhar, P.S.S. Prasad, B.D. Raju, K.S.R. Rao, Hydrotalcite-SBA-15 composite material for efficient carbondioxide capture, J. CO_2 Util. 12 (2015) 109–115, https://doi.org/10.1016/j.jcou.2015.05.002.
[111] A.A.E. Sakr, T. Zaki, O. Saber, S.A. Hassan, A.K. Aboul-Gheit, S. Faramawy, Synthesis of Zn–Al LDHs intercalated with urea derived anions for capturing carbon dioxide from natural gas, J. Taiwan Inst. Chem. Eng. 44 (2013) 957–962, https://doi.org/10.1016/j.jtice.2013.02.003.
[112] C. Ma, F. Wang, C. Zhang, Z. Yu, J. Wei, Z. Yang, Y. Li, Z. Li, M. Zhu, L. Shen, G. Zeng, Photocatalytic decomposition of Congo red under visible light irradiation using MgZnCr-TiO_2 layered double hydroxide, Chemosphere 168 (2017) 80–90, https://doi.org/10.1016/j.chemosphere.2016.10.063.
[113] M. Yu, C. Li, G. Zeng, Y. Zhou, X. Zhang, Y. Xie, The selective catalytic reduction of NO with NH_3 over a novel Ce–Sn–Ti mixed oxides catalyst: promotional effect of SnO_2, Appl. Surf. Sci. 342 (2015) 174–182, https://doi.org/10.1016/j.apsusc.2015.03.052.
[114] C. Zhang, Y. Li, F. Wang, Z. Yu, J. Wei, Z. Yang, C. Ma, Z. Li, Z. Xu, G. Zeng, Performance of magnetic zirconium-iron oxide nanoparticle in the removal of phosphate from aqueous solution, Appl. Surf. Sci. 396 (2017) 1783–1792, https://doi.org/10.1016/j.apsusc.2016.11.214.
[115] S. Radha, A. Navrotsky, Energetics of CO_2 adsorption on Mg–Al layered double hydroxides and related mixed metal oxides, J. Phys. Chem. C 118 (2014) 29836–29844, https://doi.org/10.1021/jp508678k.
[116] Y. Zhong, Q. Yang, K. Luo, X. Wu, X. Li, Y. Liu, W. Tang, G. Zeng, B. Peng, Fe(II)–Al(III) layered double hydroxides prepared by ultrasound-assisted co-precipitation method for the reduction of bromate, J. Hazard. Mater. 250–251 (2013) 345–353, https://doi.org/10.1016/j.jhazmat.2013.01.081.
[117] R. Chimentao, S. Abello, F. Medina, J. Llorca, J. Sueiras, Y. Cesteros, P. Salagre, Defect-induced strategies for the creation of highly active hydrotalcites in base-catalyzed reactions, J. Catal. 252 (2007) 249–257, https://doi.org/10.1016/j.jcat.2007.09.015.
[118] X.J. Hou, H. Li, P. He, Z. Sun, S. Li, Structural and electronic analysis of Li/Al layered double hydroxides and their adsorption for CO_2, Appl. Surf. Sci. 416 (2017) 411–423, https://doi.org/10.1016/j.apsusc.2017.04.187.
[119] H.J. Kwon, S. Kwon, J.G. Seo, I.S. Jung, Y.H. Son, C.H. Lee, K.B. Lee, H.C. Lee, Predictive guide for collective CO_2 adsorption properties of Mg−Al mixed

oxides, ChemSusChem 10 (2017) 1701–1709, https://doi.org/10.1002/cssc.201601581.
[120] S. Paikaray, M.J. Hendry, The role of trivalent cations and interlayer anions on the formation of layered double hydroxides in an oxic-CO_2 medium, Appl. Surf. Sci. 263 (2012) 633–639, https://doi.org/10.1016/j.apsusc.2012.09.125.
[121] S.J. Palmer, H.J. Spratt, R.L. Frost, Thermal decomposition of hydrotalcites with variable cationic ratios, J. Therm. Anal. Calorim. 95 (2009) 123–129, https://doi.org/10.1007/s10973-008-8992-4.
[122] U. Sharma, B. Tyagi, R.V. Jasra, Synthesis and characterization of Mg–Al–CO_3 layered double hydroxide for CO_2 adsorption, Ind. Eng. Chem. Res. 47 (2008) 9588–9595, https://doi.org/10.1021/ie800365t.
[123] A. Akgsornpeak, T. Witoon, T. Mungcharoen, J. Limtrakul, Development of synthetic CaO sorbents via CTAB-assisted sol–gel method for CO_2 capture at high temperature, Chem. Eng. J. 237 (2014) 189–198, https://doi.org/10.1016/j.cej.2013.10.023.
[124] A. Prathap, M.M. Shaijumon, K.M. Sureshan, CaO nanocrystals grown over SiO_2 microtubes for efficient CO_2 capture: organogel sets the platform, Chem. Commun. 52 (2016) 1342–1345, https://doi.org/10.1039/C5CC07636F.
[125] C. Luo, Y. Zheng, J. Guo, B. Feng, Effect of sulfation on CO_2 capture of CaO-based sorbents during calcium looping cycle, Fuel 127 (2014) 124–130, https://doi.org/10.1016/j.fuel.2013.09.063.
[126] N.J. Amos, M. Widyawati, S. Kureti, D. Trimis, A.I. Minett, A.T. Harris, T.L. Church, Design and synthesis of stable supported-CaO sorbents for CO_2 capture, J. Mater. Chem. A 2 (2014) 4332, https://doi.org/10.1039/c3ta14953f.
[127] P.H. Chang, Y.P. Chang, S.Y. Chen, C.T. Yu, Y.P. Chyou, Ca-rich Ca-Al-oxide, high-temperature-stable sorbents prepared from hydrotalcite precursors: synthesis, characterization, and CO_2 capture capacity, ChemSusChem 4 (2011) 1844–1851, https://doi.org/10.1002/cssc.201100357.
[128] P.H. Chang, T.J. Lee, Y.P. Chang, S.Y. Chen, CO_2 sorbents with scaffold-like Ca-Al layered double hydroxides as precursors for CO_2 capture at high temperatures, ChemSusChem 6 (2013) 1076–1083, https://doi.org/10.1002/cssc.201200910.
[129] S. Wang, C. Li, S. Yan, Y. Zhao, X. Ma, Adsorption of CO_2 on mixed oxides derived from Ca–Al–ClO_4-layered double hydroxide, Energy Fuels (2016), https://doi.org/10.1021/acs.energyfuels.5b02506.
[130] G. Chen, B. Yi, G. Zeng, Q. Niu, M. Yan, A. Chen, J. Du, J. Huang, Q. Zhang, Facile green extracellular biosynthesis of CdS quantum dots by white rot fungus phanerochaete chrysosporium, Colloids Surf. B Biointerfaces 117 (2014) 199–205, https://doi.org/10.1016/j.colsurfb.2014.02.027.
[131] W. Guo, H. Xiao, X. Yao, J. Liu, J. Liang, P. Gao, G. Zeng, Tuning pore structure of corrosion resistant solid-state-sintered SiC porous ceramics by particle size distribution and phase transformation, Mater. Des. 100 (2016) 1–7, https://doi.org/10.1016/j.matdes.2016.03.105.
[132] H. Zhong, Y. Tian, Q. Yang, M.L. Brusseau, L. Yang, G. Zeng, Degradation of landfill leachate compounds by persulfate for groundwater remediation, Chem. Eng. J. 307 (2017) 399–407, https://doi.org/10.1016/j.cej.2016.08.069.
[133] P.H. Chang, Y.P. Chang, Y.H. Lai, S.Y. Chen, C.T. Yu, Y.P. Chyou, Synthesis, characterization and high temperature CO_2 capture capacity of nanoscale Ca-based layered double hydroxides via reverse microemulsion, J. Alloys Compd. 586 (2014) S498–S505, https://doi.org/10.1016/j.jallcom.2013.05.213.
[134] Z. Gu, J.J. Atherton, Z.P. Xu, Hierarchical layered double hydroxide nanocomposites: structure, synthesis and applications, Chem. Commun. 51 (2015) 3024–3036, https://doi.org/10.1039/C4CC07715F.
[135] S. Walspurger, L. Boels, P.D. Cobden, G.D. Elzinga, W.G. Haije, R.W. van den Brink, The crucial role of the K^+–aluminium oxide interaction in K^+ promoted alumina and hydrotalcite-based materials for CO_2 sorption at high temperatures, ChemSusChem 1 (2008) 643–650, https://doi.org/10.1002/cssc.200800085.
[136] E. Dvininov, H. Stephenson, H. Krutka, M. Lindsay, Improved hydrotalcite-type compounds for post-combustion CO_2 abatement, Energy Procedia 37 (2013) 1658–1669, https://doi.org/10.1016/j.egypro.2013.06.041.
[137] X. Tan, Y. Liu, Y. Gu, S. Liu, G. Zeng, X. Cai, X. Hu, H. Wang, S. Liu, L. Jiang, Biochar pyrolyzed from MgAl-layered double hydroxides pre-coated ramie biomass (Boehmeria nivea (L.) Gaud.): characterization and application for crystal violet removal, J. Environ. Manage. 184 (2016) 85–93, https://doi.org/10.1016/j.jenvman.2016.08.070.
[138] X. Tan, S. Liu, Y. Liu, Y. Gu, G. Zeng, X. Cai, Z. Yan, C. Yang, X. Hu, B. Chen, One-pot synthesis of carbon supported calcined-Mg/Al layered double hydroxides for antibiotic removal by slow pyrolysis of biomass waste, Sci. Rep. 6 (2016), https://doi.org/10.1038/srep39691.
[139] Y.P. Chang, Y.C. Chen, P.H. Chang, S.Y. Chen, Synthesis characterization, and, CO_2 adsorptive behavior of mesoporous AlOOH-Supported layered hydroxides, ChemSusChem 5 (2012) 1249–1257, https://doi.org/10.1002/cssc.201100617.
[140] Z. Sun, L. Jin, S. He, Y. Zhao, M. Wei, D.G. Evans, X. Duan, A structured catalyst based on cobalt phthalocyanine/calcined Mg–Al hydrotalcite film for the oxidation of mercaptan, Green Chem. 14 (2012) 1909, https://doi.org/10.1039/c2gc16462k.
[141] A. Malak-Polaczyk, C. Vix-Guterl, E. Frackowiak, Carbon/layered double hydroxide (LDH) composites for supercapacitor application, Energy Fuels 24 (2010) 3346–3351, https://doi.org/10.1021/ef901505c.
[142] Y. Wu, H. Wang, Y. Sun, T. Xiao, W. Tu, X. Yuan, G. Zeng, S. Li, J.W. Chew, Photogenerated charge transfer via interfacial internal electric field for significantly improved photocatalysis in direct Z-scheme oxygen-doped carbon nitrogen/CoAl-layered double hydroxide heterojunction, Appl. Catal. B Environ. 227 (2018) 530–540, https://doi.org/10.1016/j.apcatb.2018.01.069.
[143] L. Jiang, X. Yuan, G. Zeng, X. Chen, Z. Wu, J. Liang, J. Zhang, H. Wang, H. Wang, Phosphorus- and sulfur-codoped g-C_3N_4: facile preparation, mechanism insight, and application as efficient photocatalyst for tetracycline and methyl orange degradation under visible light irradiation, ACS Sustain. Chem. Eng. 5 (2017) 5831–5841, https://doi.org/10.1021/acssuschemeng.7b00559.
[144] L. Jiang, X. Yuan, Y. Pan, J. Liang, G. Zeng, Z. Wu, H. Wang, Doping of graphitic carbon nitride for photocatalysis: a review, Appl. Catal. B Environ. 217 (2017) 388–406, https://doi.org/10.1016/j.apcatb.2017.06.003.
[145] Z. Wu, X. Yuan, J. Zhang, H. Wang, L. Jiang, G. Zeng, Photocatalytic decontamination of wastewater containing organic dyes by metal-organic frameworks and their derivatives, ChemCatChem 9 (2017) 41–64, https://doi.org/10.1002/cctc.201600808.
[146] X. Yuan, L. Jiang, X. Chen, L. Leng, H. Wang, Z. Wu, T. Xiong, J. Liang, G. Zeng, Highly efficient visible-light-induced photoactivity of Z-scheme Ag_2CO_3/Ag/WO_3 photocatalysts for organic pollutant degradation, Environ Sci. Nano 4 (2017) 2175–2185, https://doi.org/10.1039/C7EN00713B.
[147] L. Jiang, X. Yuan, G. Zeng, J. Liang, X. Chen, H. Yu, H. Wang, Z. Wu, J. Zhang, T. Xiong, In-situ synthesis of direct solid-state dual Z-scheme WO_3/g-C_3N_4/Bi_2O_3 photocatalyst for the degradation of refractory pollutant, Appl. Catal. B Environ. 227 (2018) 376–385, https://doi.org/10.1016/j.apcatb.2018.01.042.
[148] L. Jiang, X. Yuan, G. Zeng, Z. Wu, J. Liang, X. Chen, L. Leng, H. Wang, H. Wang, Metal-free efficient photocatalyst for stable visible-light photocatalytic degradation of refractory pollutant, Appl. Catal. B Environ. 221 (2018) 715–725, https://doi.org/10.1016/j.apcatb.2017.09.059.
[149] Z. Wu, X. Yuan, G. Zeng, L. Jiang, H. Zhong, Y. Xie, H. Wang, X. Chen, H. Wang, Highly efficient photocatalytic activity and mechanism of Yb^{3+}/Tm^{3+} codoped In_2S_3 from ultraviolet to near infrared light towards chromium (VI) reduction and rhodamine B oxydative degradation, Appl. Catal. B Environ. 225 (2018) 8–21, https://doi.org/10.1016/j.apcatb.2017.11.040.
[150] X. Yuan, Z. Wu, G. Zeng, L. Jiang, J. Zhang, T. Xiong, H. Wang, D. Mo, Synthesis and boosting visible light photoactivity of Ag@AgI/$CdWO_4$ towards refractory organic pollutants degradation based on interfacial charge transfer, Appl. Surf. Sci. 454 (2018) 293–304, https://doi.org/10.1016/j.apsusc.2018.05.163.
[151] L. Jiang, X. Yuan, G. Zeng, J. Liang, Z. Wu, H. Wang, Construction of an all-solid-state Z-scheme photocatalyst based on graphite carbon nitride and its enhancement to catalytic activity Environ, Sci. Nano. 5 (2018) 599–615, https://doi.org/10.1039/C7EN01031A.
[152] K. Tamai, S. Hosokawa, H. Asakura, K. Teramura, T. Tanaka, Low-temperature NO_x trapping on alkali or alkaline earth metal modified TiO_2 photocatalyst, Catal. Today (2018), https://doi.org/10.1016/j.cattod.2018.07.045.
[153] L. Tian, Y. Zhao, S. He, M. Wei, X. Duan, Immobilized Cu–Cr layered double hydroxide films with visible-light responsive photocatalysis for organic pollutants, Chem. Eng. J. 184 (2012) 261–267, https://doi.org/10.1016/j.cej.2012.01.070.
[154] M. Shao, J. Han, M. Wei, D.G. Evans, X. Duan, The synthesis of hierarchical Zn–Ti layered double hydroxide for efficient visible-light photocatalysis, Chem. Eng. J. 168 (2011) 519–524, https://doi.org/10.1016/j.cej.2011.01.016.
[155] M. Xu, S. He, H. Chen, G. Cui, L. Zheng, B. Wang, M. Wei, TiO_{2-x}-modified Ni nanocatalyst with tunable metal–support interaction for water–gas shift reaction, ACS Catal. 7 (2017) 7600–7609, https://doi.org/10.1021/acscatal.7b01951.
[156] H. Wang, Y. Wu, T. Xiao, X. Yuan, G. Zeng, W. Tu, S. Wu, H.Y. Lee, Y.Z. Tan, J.W. Chew, Formation of quasi-core-shell In_2S_3/anatase TiO_2 @metallic $Ti_3C_2T_x$ hybrids with favorable charge transfer channels for excellent visible-light-photocatalytic performance, Appl. Catal. B Environ. 233 (2018) 213–225, https://doi.org/10.1016/j.apcatb.2018.04.012.
[157] H. Wang, X. Yuan, Y. Wu, G. Zeng, X. Chen, L. Leng, H. Li, Synthesis and applications of novel graphitic carbon nitride/metal-organic frameworks mesoporous photocatalyst for dyes removal, Appl. Catal. B Environ. 174–175 (2015) 445–454, https://doi.org/10.1016/j.apcatb.2015.03.037.
[158] D. Jiang, P. Xu, H. Wang, G. Zeng, D. Huang, M. Chen, C. Lai, C. Zhang, J. Wan, W. Xue, Strategies to improve metal organic frameworks photocatalyst's performance for degradation of organic pollutants, Coord. Chem. Rev. 376 (2018) 449–466, https://doi.org/10.1016/j.ccr.2018.08.005.
[159] R. Pang, K. Teramura, H. Asakura, S. Hosokawa, T. Tanaka, Highly selective photocatalytic conversion of CO_2 by water over Ag-loaded $SrNb_2O_6$ nanorods, Appl. Catal. B Environ. 218 (2017) 770–778, https://doi.org/10.1016/j.apcatb.2017.06.052.
[160] Z. Huang, K. Teramura, H. Asakura, S. Hosokawa, T. Tanaka, Flux method fabrication of potassium rare-earth tantalates for CO_2 photoreduction using H_2O as an electron donor, Catal. Today 300 (2018) 173–182, https://doi.org/10.1016/j.cattod.2017.03.043.
[161] Z. Huang, K. Teramura, H. Asakura, S. Hosokawa, T. Tanaka, Recent progress in photocatalytic conversion of carbon dioxide over gallium oxide and its nanocomposites, Curr. Opin. Chem., Eng. 20 (2018) 114–121, https://doi.org/10.1016/j.coche.2018.02.012.
[162] L. Zhou, M. Shao, J. Li, S. Jiang, M. Wei, X. Duan, Two-dimensional ultrathin arrays of CoP: electronic modulation toward high performance overall water splitting, Nano Energy 41 (2017) 583–590, https://doi.org/10.1016/j.nanoen.2017.10.009.
[163] C. Zhang, M. Shao, F. Ning, S. Xu, Z. Li, M. Wei, D.G. Evans, X. Duan, Au nanoparticles sensitized ZnO nanorod@nanoplatelet core–shell arrays for

enhanced photoelectrochemical water splitting, Nano Energy 12 (2015) 231–239, https://doi.org/10.1016/j.nanoen.2014.12.037.
[164] B. Li, Y. Zhao, S. Zhang, W. Gao, M. Wei, Visible-light-responsive photocatalysts toward water oxidation based on NiTi-Layered double hydroxide/reduced graphene oxide composite materials, ACS Appl. Mater. Interfaces 5 (2013) 10233–10239, https://doi.org/10.1021/am402995d.
[165] L. Wang, X. Liu, J. Luo, X. Duan, J. Crittenden, C. Liu, S. Zhang, Y. Pei, Y. Zeng, X. Duan, Self-optimization of the active site of molybdenum disulfide by an irreversible phase transition during photocatalytic hydrogen evolution, Angew. Chem. 129 (2017) 7718–7722, https://doi.org/10.1002/ange.201703066.
[166] Y. Li, K. Yin, L. Wang, X. Lu, Y. Zhang, Y. Liu, D. Yan, Y. Song, S. Luo, Engineering MoS_2 nanomesh with holes and lattice defects for highly active hydrogen evolution reaction, Appl. Catal. B Environ. 239 (2018) 537–544, https://doi.org/10.1016/j.apcatb.2018.05.080.
[167] Y. Xu, L. Wang, X. Liu, S. Zhang, C. Liu, D. Yan, Y. Zeng, Y. Pei, Y. Liu, S. Luo, Monolayer MoS_2 with S vacancies from interlayer spacing expanded counterparts for highly efficient electrochemical hydrogen production, J. Mater. Chem. A 4 (2016) 16524–16530, https://doi.org/10.1039/C6TA06534A.
[168] Y. Li, L. Wang, T. Cai, S. Zhang, Y. Liu, Y. Song, X. Dong, L. Hu, Glucose-assisted synthesize 1D/2D nearly vertical CdS/MoS_2 heterostructures for efficient photocatalytic hydrogen evolution, Chem. Eng. J. 321 (2017) 366–374, https://doi.org/10.1016/j.cej.2017.03.139.
[169] C. Liu, L. Wang, Y. Tang, S. Luo, Y. Liu, S. Zhang, Y. Zeng, Y. Xu, Vertical single or few-layer MoS_2 nanosheets rooting into TiO_2 nanofibers for highly efficient photocatalytic hydrogen evolution, Appl. Catal. B Environ 164 (2015) 1–9, https://doi.org/10.1016/j.apcatb.2014.08.046.
[170] H. Wang, Y. Wu, M. Feng, W. Tu, T. Xiao, T. Xiong, H. Ang, X. Yuan, J.W. Chew, Visible-light-driven removal of tetracycline antibiotics and reclamation of hydrogen energy from natural water matrices and wastewater by polymeric carbon nitride foam, Water Res. 144 (2018) 215–225, https://doi.org/10.1016/j.watres.2018.07.025.
[171] G. Zhou, Y. Shan, Y. Hu, X. Xu, L. Long, J. Zhang, J. Dai, J. Guo, J. Shen, S. Li, L. Liu, X. Wu, Half-metallic carbon nitride nanosheets with micro grid mode resonance structure for efficient photocatalytic hydrogen evolution, Nat. Commun. 9 (2018), https://doi.org/10.1038/s41467-018-05590-x.
[172] J. Ren, S. Ouyang, H. Xu, X. Meng, T. Wang, D. Wang, J. Ye, Targeting activation of CO_2 and H_2 over Ru-loaded ultrathin layered double hydroxides to achieve efficient photothermal CO_2 methanation in flow-type system, Adv. Energy Mater. 7 (2017) 1601657, https://doi.org/10.1002/aenm.201601657.
[173] C.G. Silva, Y. Bouizi, V. Fornés, H. García, Layered double hydroxides as highly efficient photocatalysts for visible light oxygen generation from water, J. Am. Chem. Soc. 131 (2009) 13833–13839, https://doi.org/10.1021/ja905467v.
[174] C. Wang, B. Ma, S. Xu, D. Li, S. He, Y. Zhao, J. Han, M. Wei, D.G. Evans, X. Duan, Visible-light-driven overall water splitting with a largely-enhanced efficiency over a Cu_2O@ZnCr-layered double hydroxide photocatalyst, Nano Energy 32 (2017) 463–469, https://doi.org/10.1016/j.nanoen.2017.01.010.
[175] R. Zhang, M. Shao, S. Xu, F. Ning, L. Zhou, M. Wei, Photo-assisted synthesis of zinc-iron layered double hydroxides/TiO_2 nanoarrays toward highly-efficient photoelectrochemical water splitting, Nano Energy 33 (2017) 21–28, https://doi.org/10.1016/j.nanoen.2017.01.020.
[176] C. Wang, B. Ma, X. Cao, S. He, J. Han, M. Wei, D.G. Evans, X. Duan, Bridge-type interface optimization on a dual-semiconductor heterostructure toward high performance overall water splitting, J. Mater. Chem. A 6 (2018) 7871–7876, https://doi.org/10.1039/C8TA02001A.
[177] L. Zhou, S. Jiang, Y. Liu, M. Shao, M. Wei, X. Duan, Ultrathin CoNiP@layered double hydroxides core–shell nanosheets arrays for largely enhanced overall water splitting, ACS Appl. Energy Mater. 1 (2018) 623–631, https://doi.org/10.1021/acsaem.7b00151.
[178] H. Zhao, J. Xu, L. Liu, G. Rao, C. Zhao, Y. Li, CO_2 photoreduction with water vapor by Ti-embedded MgAl layered double hydroxides, J. CO_2 Util. 15 (2016) 15–23, https://doi.org/10.1016/j.jcou.2016.04.004.
[179] M. Miyano, H. Zhang, M. Yoshiba, Y. Izumi, Selective photoconversion of carbon dioxide into methanol using layered double hydroxides at 0.40 MPa, Energy Technol. 5 (2017) 892–900, https://doi.org/10.1002/ente.201600578.
[180] D. Saliba, A. Ezzeddine, R. Sougrat, N.M. Khashab, M. Hmadeh, M. Al-Ghoul, Cadmium-aluminum layered double hydroxide microspheres for photocatalytic CO2 reduction, ChemSusChem 9 (2016) 800–805, https://doi.org/10.1002/cssc.201600088.
[181] S. Iguchi, K. Teramura, S. Hosokawa, T. Tanaka, Photocatalytic conversion of CO_2 in water using fluorinated layered double hydroxides as photocatalysts, Appl. Catal. Gen. 521 (2016) 160–167, https://doi.org/10.1016/j.apcata.2015.11.023.
[182] K. Teramura, S. Iguchi, Y. Mizuno, T. Shishido, T. Tanaka, Photocatalytic conversion of CO_2 in water over layered double hydroxides, Angew. Chem. 124 (2012) 8132–8135, https://doi.org/10.1002/ange.201201847.
[183] K. Wang, L. Zhang, Y. Su, D. Shao, S. Zeng, W. Wang, Photoreduction of carbon dioxide of atmospheric concentration to methane with water over CoAl-layered double hydroxide nanosheets, J. Mater. Chem. A 6 (2018) 8366–8373, https://doi.org/10.1039/C8TA01309H.
[184] Y. Tokudome, M. Fukui, S. Iguchi, Y. Hasegawa, K. Teramura, T. Tanaka, M. Takemoto, R. Katsura, M. Takahashi, A nanoLDH catalyst with high CO_2 adsorption capability for photo-catalytic reduction, J. Mater. Chem. A 6 (2018) 9684–9690, https://doi.org/10.1039/C8TA01621F.
[185] S. Iguchi, K. Teramura, S. Hosokawa, T. Tanaka, Photocatalytic conversion of CO_2 in an aqueous solution using various kinds of layered double hydroxides, Catal. Today 251 (2015) 140–144, https://doi.org/10.1016/j.cattod.2014.09.005.
[186] Y. Bang, S.J. Han, S. Kwon, V. Hiremath, I.K. Song, J.G. Seo, High temperature carbon dioxide capture on nano-structured MgO–Al_2O_3 and CaO–Al_2O_3 adsorbents: an experimental and theoretical study, J. Nanosci. Nanotechnol. 14 (2014) 8531–8538, https://doi.org/10.1166/jnn.2014.9954.
[187] Z.W. Seh, J. Kibsgaard, C.F. Dickens, I. Chorkendorff, J.K. Nørskov, T.F. Jaramillo, Combining theory and experiment in electrocatalysis: Insights into materials design, Science 355 (2017) eaad4998, https://doi.org/10.1126/science.aad4998.
[188] T. Ye, W. Huang, L. Zeng, M. Li, J. Shi, CeO_{2-x} platelet from monometallic cerium layered double hydroxides and its photocatalytic reduction of CO_2, Appl. Catal. B Environ. 210 (2017) 141–148, https://doi.org/10.1016/j.apcatb.2017.03.051.
[189] N. Ahmed, M. Morikawa, Y. Izumi, Photocatalytic conversion of carbon dioxide into methanol using optimized layered double hydroxide catalysts, Catal. Today 185 (2012) 263–269, https://doi.org/10.1016/j.cattod.2011.08.010.
[190] S. Iguchi, Y. Hasegawa, K. Teramura, S. Kidera, S. Kikkawa, S. Hosokawa, H. Asakura, T. Tanaka, Drastic improvement in the photocatalytic activity of Ga_2O_3 modified with Mg–Al layered double hydroxide for the conversion of CO_2 in water, Sustain Energy Fuels 1 (2017) 1740–1747, https://doi.org/10.1039/C7SE00204A.
[191] S. Kumar, M.A. Isaacs, R. Trofimovaite, L. Durndell, C.M.A. Parlett, R.E. Douthwaite, B. Coulson, M.C.R. Cockett, K. Wilson, A.F. Lee, P25@CoAl layered double hydroxide heterojunction nanocomposites for CO_2 photocatalytic reduction, Appl. Catal. B Environ. 209 (2017) 394–404, https://doi.org/10.1016/j.apcatb.2017.03.006.
[192] K. Li, B. Peng, T. Peng, Recent advances in heterogeneous photocatalytic co_2 conversion to solar fuels, ACS Catal. 6 (2016) 7485–7527, https://doi.org/10.1021/acscatal.6b02089.
[193] S.M. Xu, T. Pan, Y.B. Dou, H. Yan, S.T. Zhang, F.Y. Ning, W.Y. Shi, M. Wei, Theoretical and experimental study on $M^{II}M^{III}$-layered double hydroxides as efficient photocatalysts toward oxygen evolution from water, J. Phys. Chem. C 119 (2015) 18823–18834, https://doi.org/10.1021/acs.jpcc.5b01819.
[194] S.M. Xu, H. Yan, M. Wei, Band structure engineering of transition-metal-based layered double hydroxides toward photocatalytic oxygen evolution from water: a theoretical–experimental combination study, J. Phys. Chem. C 121 (2017) 2683–2695, https://doi.org/10.1021/acs.jpcc.6b10159.
[195] A. Crake, Metal-organic frameworks based materials for photocatalytic CO_2 reduction, Mater Sci. Technol. 33 (2017) 1737–1749, https://doi.org/10.1080/02670836.2017.1318250.
[196] H. Jiang, K. Katsumata, J. Hong, A. Yamaguchi, K. Nakata, C. Terashima, N. Matsushita, M. Miyauchi, A. Fujishima, Photocatalytic reduction of CO_2 on Cu_2O-loaded Zn-Cr layered double hydroxides, Appl. Catal. B Environ. 224 (2018) 783–790, https://doi.org/10.1016/j.apcatb.2017.11.011.
[197] K. Li, X. An, K.H. Park, M. Khraisheh, J. Tang, A critical review of CO_2 photoconversion: catalysts and reactors, Catal. Today 224 (2014) 3–12, https://doi.org/10.1016/j.cattod.2013.12.006.
[198] X. Li, J. Wen, J. Low, Y. Fang, J. Yu, Design and fabrication of semiconductor photocatalyst for photocatalytic reduction of CO_2 to solar fuel, Sci. China Mater. 57 (2014) 70–100, https://doi.org/10.1007/s40843-014-0003-1.
[199] D. Wang, Y. Yu, Z. Zhang, H. Fang, J. Chen, Z. He, S. Song, Ag/Ag_2SO_3 plasmonic catalysts with high activity and stability for CO_2 reduction with water vapor under visible light Environ, Sci. Pollut. Res. 23 (2016) 18369–18378, https://doi.org/10.1007/s11356-016-7032-3.
[200] J. Shi, I.U. Islam, W. Chen, F. Wang, Z. Xu, S. Xu, Y. Li, J. Lu, Two-dimensional ultrathin $Zn_xCd_{1-x}S$ nanosheet with exposed polar facet by using layered double hydroxide template for photocatalytic hydrogen generation, Int. J. HydrogenEnergy (2018), https://doi.org/10.1016/j.ijhydene.2018.08.208.
[201] M. Lv, H. Liu, Photocatalytic property and structural stability of CuAl-based layered double hydroxides, J. Solid State Chem. 227 (2015) 232–238, https://doi.org/10.1016/j.jssc.2015.04.010.
[202] S. Zhang, L. Wang, C. Liu, J. Luo, J. Crittenden, X. Liu, T. Cai, J. Yuan, Y. Pei, Y. Liu, Photocatalytic wastewater purification with simultaneous hydrogen production using MoS_2 QD-decorated hierarchical assembly of $ZnIn_2S_4$ on reduced graphene oxide photocatalyst, Water Res. 121 (2017) 11–19, https://doi.org/10.1016/j.watres.2017.05.013.
[203] S. Zhang, L. Wang, Y. Zeng, Y. Xu, Y. Tang, S. Luo, Y. Liu, C. Liu, CdS-nanoparticles-decorated perpendicular hybrid of MoS_2 and N-Doped graphene nanosheets for omnidirectional enhancement of photocatalytic hydrogen evolution, ChemCatChem 8 (2016) 2557–2564, https://doi.org/10.1002/cctc.201600388.
[204] S. Zhang, X. Liu, C. Liu, S. Luo, L. Wang, T. Cai, Y. Zeng, J. Yuan, W. Dong, Y. Pei, Y. Liu, MoS_2 quantum dot growth induced by S vacancies in a $ZnIn_2S_4$ monolayer: atomic-level heterostructure for photocatalytic hydrogen production, ACS Nano 12 (2018) 751–758, https://doi.org/10.1021/acsnano.7b07974.
[205] S. Iguchi, K. Teramura, S. Hosokawa, T. Tanaka, Effect of the chloride ion as a hole scavenger on the photocatalytic conversion of CO_2 in an aqueous solution over Ni–Al layered double hydroxides, Phys. Chem. Chem. Phys. 17 (2015) 17995–18003, https://doi.org/10.1039/C5CP02724A.
[206] M. Li, L. Zhang, X. Fan, M. Wu, M. Wang, R. Cheng, L. Zhang, H. Yao, J. Shi, Core-shell $LaPO_4$/g-C_3N_4 nanowires for highly active and selective CO_2

reduction, Appl. Catal. B Environ 201 (2017) 629–635, https://doi.org/10.1016/j.apcatb.2016.09.004.
[207] S. Kawamura, M.C. Puscasu, Y. Yoshida, Y. Izumi, G. Carja, Tailoring assemblies of plasmonic silver/gold and zinc–gallium layered double hydroxides for photocatalytic conversion of carbon dioxide using UV–visible light, Appl. Catal. Gen. 504 (2015) 238–247, https://doi.org/10.1016/j.apcata.2014.12.042.
[208] N. Ahmed, Y. Shibata, T. Taniguchi, Y. Izumi, Photocatalytic conversion of carbon dioxide into methanol using zinc–copper–M(III) (M=aluminum, gallium) layered double hydroxides, J. Catal. 279 (2011) 123–135, https://doi.org/10.1016/j.jcat.2011.01.004.
[209] Y. Zhao, G. Chen, T. Bian, C. Zhou, G.I.N. Waterhouse, L.Z. Wu, C.H. Tung, L.J. Smith, D. O'Hare, T. Zhang, Defect-rich ultrathin ZnAl-layered double hydroxide nanosheets for efficient photoreduction of CO_2 to CO with water, Adv. Mater. 27 (2015) 7824–7831, https://doi.org/10.1002/adma.201503730.
[210] M. Morikawa, Y. Ogura, N. Ahmed, S. Kawamura, G. Mikami, S. Okamoto, Y. Izumi, Photocatalytic conversion of carbon dioxide into methanol in reverse fuel cells with tungsten oxide and layered double hydroxide photocatalysts for solar fuel generation, Catal. Sci Technol. 4 (2014) 1644–1651, https://doi.org/10.1039/C3CY00959A.
[211] C. Zhao, L. Liu, G. Rao, H. Zhao, L. Wang, J. Xu, Y. Li, Synthesis of novel MgAl layered double oxide grafted TiO_2 cuboids and their photocatalytic activity on CO_2 reduction with water vapor, Catal. Sci. Technol. 5 (2015) 3288–3295, https://doi.org/10.1039/C5CY00216H.
[212] S. Kumar, L.J. Durndell, J.C. Manayil, M.A. Isaacs, C.M.A. Parlett, S. Karthikeyan, R.E. Douthwaite, B. Coulson, K. Wilson, A.F. Lee, Delaminated CoAl-layered double hydroxide@TiO_2 heterojunction nanocomposites for photocatalytic reduction of CO_2, Part. Part. Syst. Charact. 35 (2018) 1700317, https://doi.org/10.1002/ppsc.201700317.
[213] W. Fang, Y. Deng, L. Tang, G. Zeng, Y. Zhou, X. Xie, J. Wang, Y. Wang, J. Wang, Synthesis of Pd/Au bimetallic nanoparticle-loaded ultrathin graphitic carbon nitride nanosheets for highly efficient catalytic reduction of p-nitrophenol, J. Colloid Interface Sci. 490 (2017) 834–843, https://doi.org/10.1016/j.jcis.2016.12.017.
[214] K. Katsumata, K. Sakai, K. Ikeda, G. Carja, N. Matsushita, K. Okada, Preparation and photocatalytic reduction of CO_2 on noble metal (Pt, Pd, Au) loaded Zn–Cr layered double hydroxides, Mater. Lett. 107 (2013) 138–140, https://doi.org/10.1016/j.matlet.2013.05.132.
[215] H.R. Cho, Y.M. Kwon, Y.J. Lee, Y.A. Park, H.G. Ji, J.H. Lee, Morphological control of gold nanoparticles on exfoliated layers of layered double hydroxide: a reusable hybrid catalyst for the reduction of p-nitrophenol, Appl. Clay Sci. 156 (2018) 187–194, https://doi.org/10.1016/j.clay.2018.02.012.
[216] S. Tonda, W.K. Jo, Plasmonic Ag nanoparticles decorated NiAl-layered double hydroxide/graphitic carbon nitride nanocomposites for efficient visible-light-driven photocatalytic removal of aqueous organic pollutants, Catal. Today 315 (2018) 213–222, https://doi.org/10.1016/j.cattod.2017.12.019.
[217] Y. Wang, H. Ji, W. Peng, L. Liu, F. Gao, M. Li, Gold nanoparticle-coated Ni/Al layered double hydroxides on glassy carbon electrode for enhanced methanol electro-oxidation, Int. J. Hydrogen Energy 37 (2012) 9324–9329, https://doi.org/10.1016/j.ijhydene.2012.03.024.
[218] S. Zhao, K. Li, S. Jiang, J. Li, Pd–Co based spinel oxides derived from pd nanoparticles immobilized on layered double hydroxides for toluene combustion, Appl. Catal. B Environ. 181 (2016) 236–248, https://doi.org/10.1016/j.apcatb.2015.08.001.
[219] L. Anton Wein, H. Zhang, K. Urushidate, M. Miyano, Y. Izumi, Optimized photoreduction of CO_2 exclusively into methanol utilizing liberated reaction space in layered double hydroxides comprising zinc, copper, and gallium, Appl. Surf. Sci. 447 (2018) 687–696, https://doi.org/10.1016/j.apsusc.2018.04.046.
[220] D. Chen, Y. Li, J. Zhang, W. Li, J. Zhou, L. Shao, G. Qian, Efficient removal of dyes by a novel magnetic Fe_3O_4/ZnCr-layered double hydroxide adsorbent from heavy metal wastewater, J. Hazard. Mater. 243 (2012) 152–160, https://doi.org/10.1016/j.jhazmat.2012.10.014.
[221] G. Barik, E. Padhan, B. Dash, K. Sarangi, T. Subbaiah, Preparation of layered nickel aluminium double hydroxide from waste solution of nickel, Miner. Eng. 69 (2014) 107–112, https://doi.org/10.1016/j.mineng.2014.07.015.
[222] M.R. Mahmoud, M.A. Soliman, G.M. Rashad, Performance appraisal of foam separation technology for removal of Co(II)-EDTA complexes intercalated into in-situ formed Mg-Al layered double hydroxide from radioactive liquid waste, Chem. Eng. J. 326 (2017) 781–793, https://doi.org/10.1016/j.cej.2017.06.035.
[223] B. Sadeghalvad, A. Azadmehr, A. Hezarkhani, Sulfate decontamination from groundwater by metal layered double hydroxides functionalized high phosphorus iron ore waste as a new green adsorbent: experimental and modeling, Ecol. Eng. 106 (2017) 219–230, https://doi.org/10.1016/j.ecoleng.2017.05.047.
[224] A. Gil, E. Arrieta, M.A. Vicente, S.A. Korili, Synthesis and CO_2 adsorption properties of hydrotalcite-like compounds prepared from aluminum saline slag wastes, Chem. Eng. J. 334 (2018) 1341–1350, https://doi.org/10.1016/j.cej.2017.11.100.
[225] W. Bing, L. Zheng, S. He, D. Rao, M. Xu, L. Zheng, B. Wang, Y. Wang, M. Wei, Insights on active sites of caal-hydrotalcite as a high-performance solid base catalyst toward aldol condensation, ACS Catal. 8 (2018) 656–664, https://doi.org/10.1021/acscatal.7b03022.
[226] J. Wu, Z. Ren, S. Du, L. Kong, B. Liu, W. Xi, J. Zhu, H. Fu, A highly active oxygen evolution electrocatalyst: ultrathin CoNi double hydroxide/CoO nanosheets synthesized via interface-directed assembly, Nano Res. 9 (2016) 713–725, https://doi.org/10.1007/s12274-015-0950-4.
[227] H. Yang, S. Luo, Y. Bao, Y. Luo, J. Jin, J. Ma, In situ growth of ultrathin Ni–Fe LDH nanosheets for high performance oxygen evolution reaction, Inorg. Chem. Front. 4 (2017) 1173–1181, https://doi.org/10.1039/C7QI00167C.
[228] Y. Izumi, Recent advances in the photocatalytic conversion of carbon dioxide to fuels with water and/or hydrogen using solar energy and beyond, Coord. Chem. Rev. 257 (2013) 171–186, https://doi.org/10.1016/j.ccr.2012.04.018.